

Brushes and Proteins

Thesis committee

Thesis supervisors

Prof. dr. M.A. Cohen Stuart
Professor of Physical Chemistry and Colloid Science
Wageningen University

Prof. dr. ir. W. Norde
Emeritus professor Bionanotechnology
Wageningen University

Other members

Prof. dr. K.U. Loos, University of Groningen
Prof. dr. C. Werner, Technische Universität Dresden, Germany
Prof. dr. J.T. Zuilhof, Wageningen University
Dr. ir. R. Tuinier, DSM Research, Geleen

This research was conducted under the auspices of Graduate School VLAG.

Brushes and Proteins

Wouter Theodoor Engelbert Bosker

Thesis

submitted in fulfilment of the requirements for the degree of doctor

at Wageningen University

by the authority of the Rector Magnificus

Prof. dr. M.J. Kropff

in the presence of the

Thesis Committee appointed by the Academic Board

to be defended in public

on Wednesday 18 May 2011

at 4 p.m. in the Aula.

ISBN 978-90-8585-917-8

Aan mijn vader en mijn moeder

Contents

Dankwoord	xi
Chapter 1. General Introduction	1
1.1. Biofouling	1
1.2. Protein Adsorption	4
1.3. Polymer Brushes	5
1.4. Polymer Brushes and Protein Adsorption	6
1.5. Outline of this Thesis	8
Part I. PEO Brushes	11
Chapter 2. BSA Adsorption on Bimodal PEO Brushes	13
2.1. Introduction	14
2.2. Materials and Methods	18
2.2.1. Preparation of the Brushes	18
2.2.2. Reflectometry	20
2.3. Results and Discussion	20
2.3.1. Preparation and Characterization of Brushes	20
2.3.2. Reflectometry	26
2.4. Conclusions	30
2.5. Appendix	31
2.5.1. Ternary Adsorption Theory	31
2.5.2. Contact-angle Measurements	32
2.5.3. LB Deposition	32
Part II. Polysaccharide Brushes	35
Chapter 3. Polystyrene–Polysaccharide Diblock Copolymers	37
3.1. Introduction	38
3.2. Experimental	39
3.2.1. Synthesis	39

3.2.2. Interfacial Pressure	40
3.3. Results and Discussion	41
3.3.1. Synthesis	41
3.3.2. Interfacial Pressure	43
3.4. Conclusions	52
Chapter 4. Polystyrene-b-Dextran by Epoxide–Amine Coupling	55
4.1. Introduction	56
4.2. Experimental	57
4.2.1. Materials and Methods	57
4.2.2. Synthesis Procedures	57
4.2.3. Interfacial Behaviour	60
4.2.4. AFM	61
4.3. Results and Discussion	61
4.3.1. Synthesis	61
4.3.2. Interfacial Behaviour	69
4.3.3. AFM	79
4.4. Conclusions	81
Chapter 5. Sweet Brushes and Dirty Proteins	83
5.1. Introduction	84
5.2. Materials and Methods	87
5.2.1. Materials	87
5.2.2. Preparation of the Brushes	87
5.2.3. Ellipsometry	89
5.2.4. Contact-angle Measurements	90
5.2.5. AFM	90
5.2.6. Reflectometry	90
5.3. Results and Discussion	90
5.3.1. Characterization of Dextran Brushes	90
5.3.2. Protein Adsorption	93
5.4. Conclusions	99
Part III. General Discussion	101
Chapter 6. General Discussion	103
6.1. Langmuir-Blodgett Deposition and (Quasi-) 2D Aggregation	103
6.2. Brushes and Proteins	110

Bibliography	115
Summary	127
Samenvatting	131
Eiwitten	131
Borstels	133
Borstels en Eiwitten	135
List of Publications	137
Levensloop	139
Overview of Training Activities	141

Dankwoord

Tot mijn grote vreugde heb ik mijn proefschrift afgerond. Het is de weergave van het onderzoek dat ik heb uitgevoerd bij het Laboratorium voor Fysische chemie en Kolloïdkunde (Fysko) aan de Universiteit Wageningen. Ik heb de afgelopen jaren van vele mensen hulp gehad en ik wil iedereen die mij op wat voor manier dan ook heeft geholpen heel hartelijk bedanken. Zonder jullie hulp had ik mijn onderzoek en proefschrift niet kunnen voltooien.

Ik wil een aantal mensen in het bijzonder noemen. Allereerst Martien en Willem, mijn promotoren. Zij hebben mij begeleid bij het uitvoeren van het onderzoek, bij het schrijven van mijn artikelen en proefschrift en bij mijn presentaties. Ik heb veel van hun geleerd, met name hoe je goed onderzoek doet. Zij hebben mij ook de tijd gegeven om mijn proefschrift af te maken in mijn eigen tempo. Hartelijk dank voor alles! Ik dank de promotie commissieleden Katja Loos, Carsten Werner, Han Zuilhof en Remco Tuinier voor het plaatsnemen in de commissie en voor hun kostbare tijd die zij aan mijn proefschrift hebben besteed.

Veel dank ook gaat uit naar Josie, de secretaresse van Fysko. Ze heeft me geholpen op momenten dat het nodig was. Maar ik herinner me vooral de leuke gesprekken die we hebben gehad.

Dank aan Dick Gage voor de introductie in het polymeerborstel maken en eiwit adsorptie meten met reflectometrie. De fijne kneepjes van reflectometrie leerde ik van Remco, alsmede het gebruik van allerlei andere apparatuur. Altijd bereid om te helpen of mee te denken over praktische problemen.....en ook zijn gereedschapskist kwam vaak van pas. Bedankt voor alles. Ben en Mara bedank ik voor hun hulp bij de chemicaliën en alle andere spullen die ik nodig had voor mijn onderzoek.

Gedurende vrijwel mijn hele onderzoeksperiode heb ik samengewerkt met Petya, aan PEO borstels. Het was een erg leuke en leerzame samenwerking. Bijzonder was ons gezamenlijke bezoek aan St. Petersburg, zijn geboortestad. Ik dank Frans Leermakers voor de boeiende discussies en inzichten, bijvoorbeeld over de aggregatie van blok copolymeren aan het lucht–water grensvlak. Dank gaat uit

naar Gerard voor zijn hulp bij hoofdstuk 4. Ik bedank Jasper voor zijn hulp bij LaTeX.

Met plezier heb ik samengewerkt met een aantal studenten, tijdens hun Bachelor of Masters onderzoek (dat daarmee onderdeel uitmaakt van mijn promotieonderzoek). Allereerst Petya, vervolgens Katja, Janneke en Martijn. Hun inzet en enthousiasme hebben mij zeer bruikbare data en conclusies opgeleverd en hun kritische vragen waren voor mij leerzaam. Ik bedank ook mijn kamergenoten bij Fysko, waarmee ik met plezier de kamer heb gedeeld: Anton, Sonja, Jos, Bas, Petya en Richard. Verder wil ik alle mensen van Fysko bedanken. Fysko is een bijzondere plek om te werken, niet alleen door het hoge niveau van onderzoek, maar ook door de ontspannen sfeer, dat mede wordt bepaald door de koffie- en lunchpauzes, het labuitje, de jaarlijkse fietstocht en natuurlijk het voetballen op vrijdagmiddag. Jullie hebben mijn tijd tot een onvergetelijke tijd gemaakt.

Ik heb de afgelopen jaren ook samengewerkt met een aantal mensen van buiten de Universiteit Wageningen. Om dextraanborstels te kunnen maken is samengewerkt met Ted Slaghek en Johan Timmermans van TNO Voeding. Zij zijn experts op het gebied van koolhydraatchemie en hebben geholpen de benodigde blok copolymeren te maken. Ik bedank hun hartelijk voor hun hulp en tijd. Ons overleg was altijd levendig en ik heb veel geleerd over koolhydraten. Veel dank gaat uit naar Karoly Ágoston (voor hoofdstuk 3) en Eugen Sisu (voor hoofdstuk 4), die de eigenlijke syntheses van de dextraan copolymeren hebben uitgevoerd, onder leiding van Ted en Johan. Zonder jullie inzet was het niet gelukt dextraanborstels te maken en daarmee de belangrijkste onderzoeksvraag te beantwoorden. Paulo Pinheiro vroeg me mee te helpen aan een verbetering van de meetmethode voor zware metalen. Dat was een leuk zijproject. Paulo, bedankt voor de leuke samenwerking. Onder leiding van Ad van Well van de TU Delft zijn Neutronen Reflectie experimenten uitgevoerd bij ISIS in Engeland. Het heeft veelbelovende resultaten opgeleverd. Ik bedank Ad hartelijk voor de plezierige samenwerking.

Ik wil graag al mijn huisgenoten in de woongroep Het Balderhuis in Utrecht bedanken voor de leuke tijd die we hebben gehad in ons huis. Vooral het samen eten was altijd erg gezellig. Berno, Jean-Paul, Maaike, Lammie, Erica, Iwan, Marjolein, Paul, Kommerien, Daphne, Jelle, Siebe, Frouk, Patrick, Linda, Hannah (ook voor de hulp bij de Engelse vertaling van de stellingen), Julianne, Chiel, Bas en Boudewijn.

De vrienden om mij heen wil ik bedanken voor de leuke dingen die we hebben gedaan en hopelijk nog gaan doen, voor hun hulp en steun.....en gewoon omdat

jullie er zijn: Jörgen, Annemarie, Paul, Ilonca, Robert, Lyndall, Guido, Ingeborg, Daniël, Marian, Martijn, Anne, Jelle, Daphne, Roy, Dorothy, Mark, Mariska, Mark, Ellen, Maarten, Mari, Gerben en Anke.

Als laatste wil ik mijn familie bedanken voor alles: Gerda, Willem Peter, Anne, Eva, mijn zus Jacqueline en mijn vader. Wat zij voor mij betekenen, daar zijn geen woorden voor.

CHAPTER 1

General Introduction

'Brushes and Proteins', that's in brief what this thesis is about. The prevention of protein adsorption at solid surfaces by applying a polymer brush. Special attention is drawn to the use of polysaccharides to prepare brushes. Research hardly ever starts from scratch. In most cases it is a continuation of previous work, most often developments take place where 'different lines of thought meet'. The present thesis is in line with the earlier work of Edwin Currie ('Brushes and Soap'³⁵) and Wiebe de Vos ('Brushes and Particles'¹⁶³) on polymer brush – colloid interaction, performed in our laboratory, as well as the work of Katja Loos ('Hybridmaterialien mit Amylose durch enzymatische *grafting from* polymerization'¹⁰⁶) on polystyrene–amylose block copolymers. In this introduction the main characteristics of polymer brushes and protein adsorption will be presented, along with the motivation for the research described in this thesis.

1.1. Biofouling

The motivation of this thesis is related to biofilm formation: 'Cells immobilized at a substratum and frequently embedded in an organic polymer matrix of microbial origin'.⁵³ This bioadhesion is 'one of the most relevant colloidal and interfacial phenomenon in life sciences'.¹²⁵ Extensive discussions of biofilms can be found in the books 'Biofilms' by Characklis and Marshall⁵³ and 'Colloids and Interfaces in Life Sciences' by Norde,¹²⁵ as well as the publications of Gristina,⁷¹ Busscher^{21,22,68,69} and Von Eiff.⁵² Biofilm formation is a common phenomenon in biological systems where it often is of vital importance, *e.g.* the adherence of blood platelets to injured blood vessels. Biofilms serve beneficial purposes in the natural environment, for example, removal of dissolved contaminants from water. Most of the cell adhesion events concern bacteria. In natural environments about 99% of bacterial mass exists at surfaces, which seems to imply that the association with surfaces is beneficial for them.

In contrast, undesirable biofilm formation may result in unsatisfactory equipment performance (water purification and food processing equipment) or reduced equipment lifetime (corrosion). This is referred to as 'Biofouling'. Biofouling is of

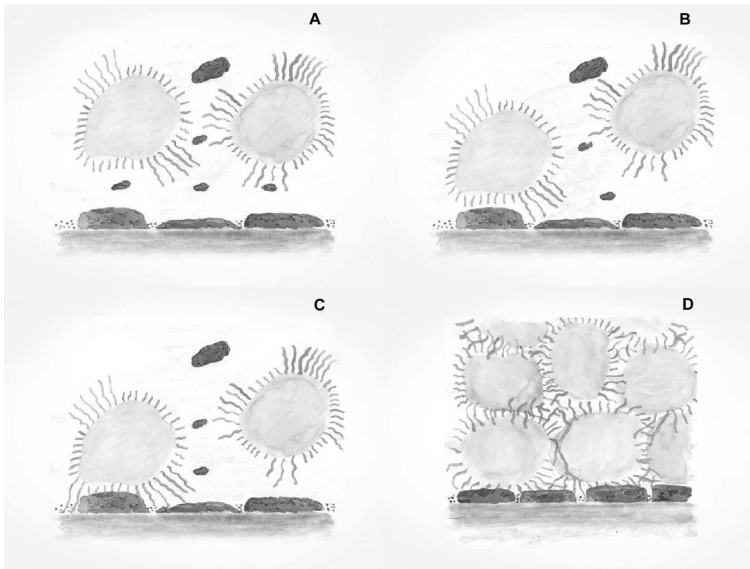


FIGURE 1.1. General procedure of biofilm formation at a solid surface in contact with a biofluid containing proteins and cells: (A) Adsorption of proteins (conditioning film), (B) initial cell adhesion, (C) cell attachment and (D) growth into a mature biofilm. Cartoons were kindly provided by Willem Norde.

utmost importance to medicine and dentistry. Bacterial adhesion may cause dental caries and severe infections on biomaterials used for implants like artificial organs, voice prostheses, heart valves, joint replacements, and so on, as well as contact lenses, hemodialysis membranes, catheters, etc. The biomaterial-centered infections are recurrent and notoriously resistant to antibiotics and the host immune system. Infections almost always result in secondary operation, at the expense of considerable costs and patient's suffering. In the end, even amputation or death may follow.

The only promising remedy against infections seems to be the prevention of the formation of a bacterial film at the biomaterial surface. Besides, improvement of the compatibility and tissue integration of biomaterials diminishes infections. A first way of prevention is hospital hygiene. Hospital hygiene is of great importance to prevent adhesion of micro-organisms during surgery. Secondly, physical-chemical modification of the biomaterial surface or biomimetic materials can result

in inhibition of adherence of micro-organisms at the surface. Necessarily, the mechanism of biofouling needs to be known in order to develop effective biomaterials.

Although bioadhesion is complicated and biofilms may have different appearances, there is a common sequence of events in biofilm formation. In figure 1.1 the general course of events in biofilm formation in an aqueous environment is pictured. A solid surface is in contact with a biofluid containing a mixture of organic molecules, particularly proteins, and cells. Very quickly, within seconds, proteins adsorb at the surface (figure 1.1A). Proteins are much smaller than cells and occur in much higher concentrations, therefore they reach the surface well before cells arrive. Initially, small proteins adsorb (having the highest diffusion coefficient). Subsequently, they are replaced by proteins having a higher affinity for the surface (in general proteins of higher molecular weight). As a result, a conditioning film of proteins is formed (figure 1.1A). In the second step initial cell adhesion takes place (figure 1.1B). Because biological cells respond specifically to proteins, the composition of the conditioning film influences the successive cell adhesion. Cells are transported towards the surface through diffusion, convection, sedimentation or active movement. For the initial cell adhesion a distinction can be made between non-specific and specific cell-substratum interactions. The non-specific interactions are long range, acting from a few up to a few tens of nm, and of physical-chemical nature (Van de Waals forces and electrostatic interaction). The adhesion in this state is regarded as reversible. Specific interactions arise when the cell is more close to the surface (less than a few nm up to direct contact). They are called 'specific' because they originate from strongly localized groups at the cell and the conditioning film that allow specific recognition, but the interactions themselves are also of physical-chemical nature (ion pairing, hydrogen bonding, hydrophobic interaction/dehydration). As a consequence of the specific interactions, the cell gets irreversible attached to the surface. Additionally, various kinds of bacteria have (long) thin microfilaments on their surface that may facilitate adhesion. After initial adhesion, cell attachment is strengthened through excretion of exopolymers and unfolding of cell surface structures (figure 1.1C). Eventually, adhered cells start growing and proliferate to colonize the surface (figure 1.1D).

The objective of this thesis is focused on the first step of biofilm formation, the conditioning film of proteins. The aim is prevention of protein adsorption at a solid surface by attaching a polymer brush to the surface, thereby restraining the development of a biofilm. Before the antifouling aspects of polymer brushes

are discussed, some basic characteristics of protein adsorption at an interface are reviewed.

1.2. Protein Adsorption

This short introduction on the principles of protein adsorption refers to the books of Andrade⁷ and Norde.¹²⁵ 'Proteins rule life'.¹²⁵ They are omnipresent, occurring in all living species, but also diverse, each having its specific metabolic function. Proteins have the natural tendency to adsorb at interfaces, *e.g.* solid-liquid, liquid-liquid as well as liquid-air interfaces. Among the biopolymers proteins are the most surface active. Protein adsorption is often advantageous. In biotechnical applications proteins are adsorbed on purpose, for example immobilized enzymes in biosensors and bioreactors. However, in many cases protein adsorption has an adverse effect. Being the first step in the formation of an unwanted biofilm at the surface, it needs to be prevented. Another problem related to protein adsorption is thrombosis, taking place at the blood vessel wall or at the surface of a biomedical implant.

Dissolved proteins exposed to an interface can undergo the following consecutive processes: A) transport towards the surface, B) adsorption at the interface, C) structural rearrangements of the adsorbed molecule (relaxation), D) desorption from the interface, E) transport away from the surface and F) possible restructuring of the desorbed molecule. The different steps proceed at different time scales: initial adsorption takes place within seconds, whereas conformational changes can last up to several hours, in some cases even days. Usually, adsorption-induced structural changes lead to decreased biological activity. Protein adsorption is a non-equilibrium process: it is time dependent, meta-stable states are present, relaxation of adsorbed proteins occurs as well as hysteresis. Furthermore, in most cases the adsorption is irreversible, because proteins are polymers, having multiple contacts with the surface. Only at the initial stage desorption may readily occur. And in the case of mixtures of proteins, the small proteins that adsorb first (having the highest diffusion coefficient) can be replaced by proteins having a higher affinity for the surface (in general proteins with a higher molecular weight). Structural rearrangements strengthen the irreversibility, because the change in tertiary and secondary structure of the protein optimizes the contact with the surface. Hence, proteins are hard to remove from the interface. In the context of biofouling, the best strategy is therefore to prevent proteins to adsorb at all.

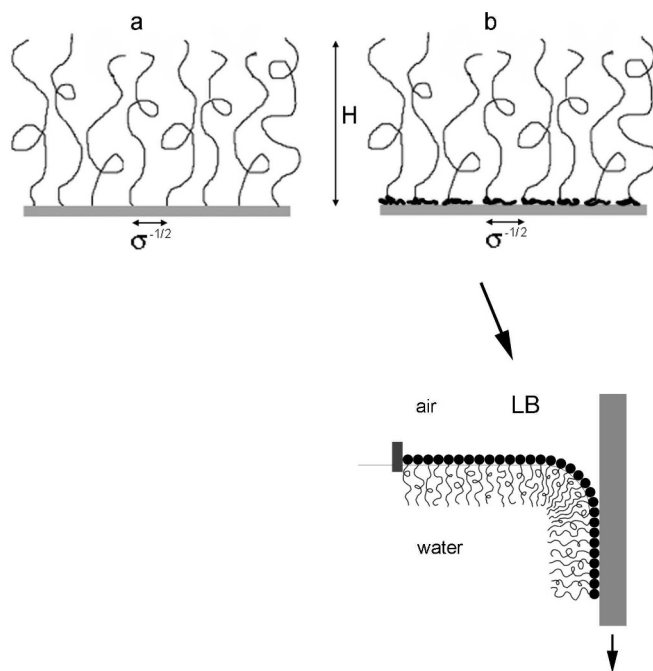


FIGURE 1.2. Cartoons of a polymer brush. Two ways of preparation: (a) chemical grafting and (b) grafting through adsorption of block copolymer, for instance by Langmuir-Blodgett deposition (LB). For explanation of symbols, see text.

From a physical-chemical point of view, four driving forces for adsorption of (globular) proteins can be identified: 1) interaction between electrical double layers, 2) dispersion (London–Van der Waals) interaction, 3) changes in the state of hydration and 4) rearrangements in the protein structure. Influencing these driving forces can reduce or prevent proteins to adsorb.

1.3. Polymer Brushes

This short overview of the main aspects of polymer brushes refers to parts of the review of Currie *et al.* on tethered polymer chains³⁷ and citations therein. A polymer brush consists of polymer chains end-attached to an interface at such a grafting density that the chains stretch out into the solvent, normal to the interface. In figure 1.2 cartoons of a polymer brush are depicted. Polymer brushes

have been studied since the end of the 1970's, first theoretically, followed by various experimental approaches. Both neutral and, more recently, polyelectrolyte brushes have been investigated, from a scientific as well as from an application point of view. Mixed brushes, comprised of different polymers, also showed interesting properties. Here we restrict ourselves to neutral brushes.

The main parameters that characterize a neutral brush are the polymer chain length (N), the grafting density (σ) and the solvent quality (expressed by the χ parameter). The thickness or height of the brush (H) is a function of these parameters. According to the theoretical models, in a good solvent H scales as: $H \sim N\sigma^{1/3}$. In figure 1.2 the brush height and the grafting density (indicated as the distance between the chains $\sigma^{-1/2}$) are shown. Polymer brushes have many applications, *e.g.* stabilizing colloids, lubrication, modifying wetting and controlling adsorption of (bio)colloids such as proteins at surfaces. In general, two ways of preparing polymer brushes at a solid surface can be distinguished: chemical grafting (figure 1.2a) and grafting through adsorption of diblock or triblock copolymers (figure 1.2b), where one polymer block serves as an anchor for the polymer brush at the surface. This second method is used in this thesis, in particular by employing the Langmuir-Blodgett (LB) deposition technique (see figure 1.2 LB). In this technique a monolayer of amphiphilic diblock copolymer is spread at an air-water interface in a Langmuir trough, compressed to a desired grafting density and subsequently transferred to a solid substrate. With LB well-defined brushes can be prepared with control of the grafting density and chain length, as demonstrated for poly(ethylene oxide) (PEO) and poly(acrylic acid) brushes.

1.4. Polymer Brushes and Protein Adsorption

From numerous studies over the past decades, it was concluded that coating surfaces with non-charged polymers minimizes protein adsorption. One can use, for example, polysaccharides like dextran and agarose but also synthetic polymers like PEO and poly(acryl amide). Especially, PEO *brushes* proved to be successful. The main effect of this polymer brush is preventing the protein molecules to reach the solid surface, thereby directly diminishing the driving forces for adsorption which were mentioned in the section Protein Adsorption. A substantial amount of research was performed on the antifouling characteristics of neutral brushes, mostly PEO brushes, both theoretically^{39, 72, 75, 90, 91, 118, 156} and experimentally.^{39, 51, 93, 118, 126, 145} From this research the parameters determining the protein resistance of brushes can be concluded. At first, the polymer chain length

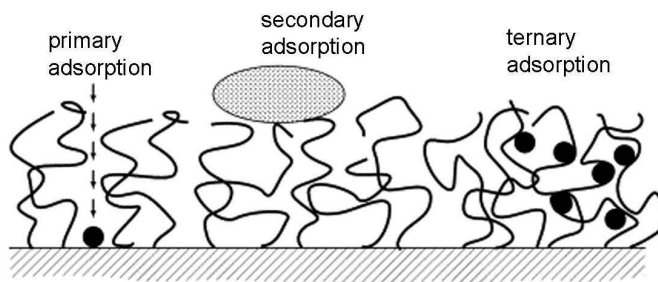


FIGURE 1.3. Different mechanisms for particle deposition at polymer brushes: primary, secondary, and ternary adsorption (from Currie *et al.*³⁷).

(N), the grafting density (σ) and the solvent quality for the polymer. Furthermore, the polymer forming the brush needs to be non-charged to prevent electrostatic interaction with the charged proteins. In addition, the size of the protein molecule, the interaction of the protein with the surface, as well as the interaction of the protein with the monomers in the brush are decisive. Research showed that the main parameter determining the adsorbed amount of protein is the grafting density. The reasons why PEO is primarily used for antifouling brushes are its flexibility, large excluded volume in water and its (believed) exclusion of proteins, as well as its nontoxicity.

Mindful of the parameters determining the antifouling capacity of polymer brushes mentioned above, the following three mechanisms for particle deposition (like protein adsorption) can be identified, see figure 1.3.³⁷ *Primary adsorption* occurs when the diameter of the protein is (much) smaller than the distance between the grafted polymers in the brush. The protein can penetrate the brush without deforming it and, when there is no attraction between the protein and the polymer chains, the protein can adsorb at the solid surface. In case of *secondary adsorption*, the protein is (much) bigger than the separation distance between the chains and can only adsorb at the edge of the brush. Penetration of the brush would result in compression of polymer chains in the brush, at the cost of increased osmotic pressure and loss of conformational entropy. Consequently, a repulsive force from the brush will prevent this penetration. *Ternary adsorption* results from an attraction between the proteins and the polymer chains in the brush. The diameter of the protein, relative to the grafting density, is such that the protein can diffuse into the brush, where it gets trapped due to binding with the chains.

Currie and coworkers³⁹ presented experimental evidence by performing adsorption studies with Bovine Serum Albumin (BSA) at PEO brushes of variable grafting density. At low σ a maximum in the adsorbed amount was observed, exceeding the adsorption at a bare surface, that could only be explained by an attraction between the BSA and EO monomers. Similar adsorption experiments by Gage *et al.*¹²⁶ with human blood plasma at PEO brushes showed an accumulation of plasma proteins in the brush at low σ because of ternary adsorption.

Besides protein adsorption studies, polymer brushes have also been tested for their cell anti-adhesion properties, especially for bacteria.^{62,129,140} The brushes are generally anti-adhesive, although the extent depends on the type of bacteria and the polymer used. Recently, even *in vivo* experiments testing the biofilm formation at brush-coated surfaces have been performed, with promising results.^{122,142}

Almost all research on antifouling brushes was concentrated on synthetic polymers. However, natural polymers like polysaccharides might be more successful to prepare nonfouling surfaces with. In nature, oligosaccharides are found at the exterior of living cells, having the function to explicitly bind necessary proteins and cells, while preventing non-specific adsorption. Furthermore, polysaccharides are natural polymers and may therefore be more appropriate for use in biomedical applications. Hence, the main research in this thesis is about the manufacturing of polysaccharide brushes at a solid surface and protein adsorption experiments with these brushes. There are a few previous studies on the preparation of polysaccharide brushes. Amylose brushes at silica particles were synthesized by Loos^{106,109} and Breitingner,¹⁶ by an enzymatic *grafting from* method, with a possible use in liquid chromatography. Recently, van der Vlist¹⁶¹ grafted amylopectine-like brushes to silica surfaces for supposed antifouling purposes, using an enzymatic tandem polymerization related to the procedure of Loos. Apart from that, de Smet covalently attached saccharide-terminated alkene monolayers on silicon surfaces for potential applications like biosensors and field effect transistors.^{148,149} Voit makes 'sweet dendrimers', neutral mono- and oligosaccharide terminated dendrimers, for medical use.^{9,95}

1.5. Outline of this Thesis

This thesis contains three parts. In the first part, chapter 2, the protein resistance of PEO brushes is discussed. Ternary adsorption for long PEO chains at low grafting density is highlighted by suppressing (possible) primary adsorption. This suppression of primary adsorption is accomplished by applying a bimodal

PEO brush, consisting of a dense layer of short PEO chains near the surface and long PEO chains of variable grafting density. Preparation of these bimodal PEO brushes and protein adsorption studies are presented.

The second part, comprising chapters 3 to 5, is about polysaccharide brushes, in particular dextran brushes. In order to prepare polysaccharide brushes using LB deposition, polystyrene–polysaccharide diblock copolymers needed to be synthesized. A synthesis method related to the work of Loos was chosen.¹⁰⁶ The synthesis and interfacial behaviour of these block copolymers are described in chapters 3 and 4. In both chapters different block coupling methods were used in an attempt to synthesize polystyrene–dextran copolymers with a long dextran block. In chapter 5 adsorption experiments are reported with different proteins at dextran brushes with variable grafting densities, prepared with the block copolymers from chapters 3 and 4. Results are compared to adsorption studies with PEO brushes.

The third part of this thesis is the General Discussion. It reflects on the use of the LB deposition method to prepare brushes and the behaviour at the air–water interface of the amphiphilic diblock copolymers used. Moreover, some general remarks are made on the theories and experimental results in polymer brush antifouling studies.

Part I

PEO Brushes

CHAPTER 2

BSA Adsorption on Bimodal PEO Brushes

Published in: *J. Colloid Interface Sci.*, 286 (2005), 496–503

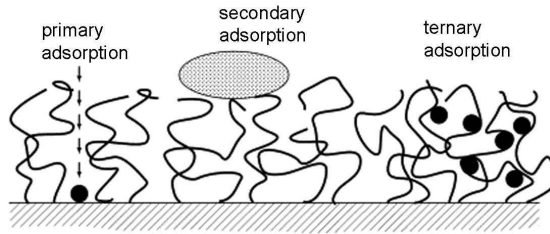


FIGURE 2.1. Different mechanisms for particle deposition at polymer brushes: primary, secondary, and ternary adsorption (from Currie *et al.*³⁷).

2.1. Introduction

Brushes of Poly(ethylene oxide) (PEO) chains have been widely used as antifouling agents.^{37,39,103,118} The formation of an unintended biofilm at a surface may cause many problems, *e.g.*, in medical applications (artificial implants, catheters, contact lenses), in the food industry (contamination of process equipment), in water purification plants and on ship hulls. The formation of a biofilm starts with the adsorption of proteins at a surface, followed by deposition of biological cells, bacteria or other micro-organisms.^{49,110} Research has shown that covering a (hydrophobic) surface with a PEO brush can be effective in preventing or retarding the adsorption of proteins at the surface^{37,103,118} and suppressing deposition of biological cells and bacteria.^{92,129,141}

PEO is a water-soluble, flexible, neutral polymer, which has a large excluded volume in water.¹²⁰ PEO brushes consist of PEO chains that are end-grafted to a surface and stretch out into a solution (water). The main brush parameters determining the extent of particle deposition (*e.g.*, protein adsorption or cell adhesion), are the grafting density (σ) (the number of polymer chains per unit area), the brush height (H) and the interactions between the particles and PEO chains. The brush height is a function of the grafting density and the number of EO units (N) in the polymer chains, and in a good solvent scales as $H \sim N\sigma^{1/3}$.^{6,36,64} Other factors that influence the extent of particle deposition are the particle size and the particle–surface interactions. Three different ways of particle deposition can be distinguished, following the terminology used in reference³⁷ and illustrated in figure 2.1.

The term ‘primary adsorption’ is used when the particle is smaller than the separation distance between the PEO chains, allowing diffusion into the brush

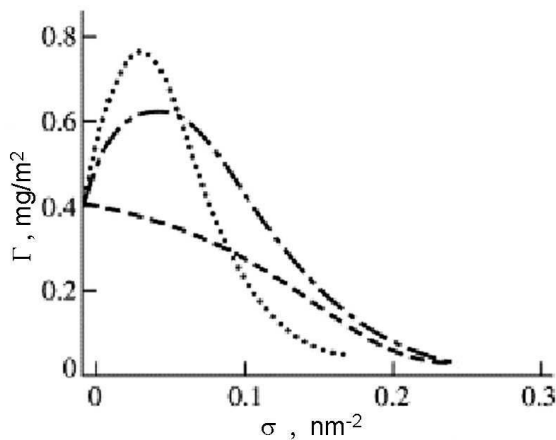


FIGURE 2.2. BSA adsorption on PEO brushes with different chain lengths: $N = 700$ (\cdots), 445 ($- \cdot -$), and 148 ($--$) (from Currie and coworkers³⁹).

and adsorption at the surface. In the case of 'secondary adsorption', the particle is bigger than the distance between the PEO chains, so it cannot enter the brush, but it may adsorb at the brush-solvent interface. Finally, one refers to 'ternary adsorption' when the particle can diffuse into the brush where it is 'captured'. Currie *et al.* have observed that the adsorbed amount (Γ) of BSA (bovine serum albumin) at a PEO brush as a function of the grafting density, displays a maximum at low grafting density for long PEO chains ($N > 148$); see figure 2.2.³⁹ This maximum is explained by the ternary adsorption mechanism, which implies an attraction between the BSA and PEO. At low grafting densities the BSA molecules can diffuse into the brush and adsorb at the PEO chains. With increasing grafting density it becomes more difficult for BSA to penetrate the brush, due to increasing excluded volume interactions. Therefore the adsorbed amount decreases at higher grafting densities. Self-consistent-field calculations (nSCF) confirm the observed maximum, assuming an effective segmental adsorption energy of -0.05 kT per EO unit.³⁹ The fact that only long PEO chains ($N > 148$) have a maximum at low grafting densities, implies that it cannot be due to secondary adsorption, because secondary adsorption decreases with increasing chain length.⁷² However, there might be a contribution of primary adsorption to the observed maximum. The BSA molecules can diffuse into the brush at low grafting densities, possibly all the way to the surface, where they adsorb.

Short PEO chains ($N \leq 148$) do not show a maximum at low grafting densities, because they do not offer enough adsorption sites to enhance protein adsorption.^{37,39} A maximum at low grafting density was also observed for adsorption of human blood plasma proteins onto PEO brushes ($N=700$), at 25°C and 37°C,¹²⁶ indicating attraction between the blood plasma proteins and PEO. Again, a contribution of primary adsorption could not be excluded from these experiments.

The interaction between PEO and proteins is generally considered to be repulsive.¹²⁰ However, research by Sheth and co-workers, using surface force measurements between the protein streptavidin and a PEO brush, both bound to mica, provided evidence of subtle attraction between the protein and PEO.^{51,145} Moreover, Abbott and coworkers provided evidence of subtle attraction between PEO coils and BSA in an aqueous two-phase system.² A quantitative model using an attractive interaction energy of about 0.05 kT per EO unit was sufficient to describe the interactions between BSA and PEO coils.

Sheth and co-workers (qualitatively) explained the attraction between PEO and streptavidin with a change in conformation of the EO segments from a protein-repellent polar conformation to a protein-attractive apolar conformation.⁵¹ The change of polar to apolar conformation may be induced by compressing the PEO layer or raising the temperature. Research by Kreuzer and Grunze on self-assembled monolayers (SAMs) of ethylene oxide (EO) terminated alkane thiolates revealed similar results.^{76,167} When the EO moieties are in the crystalline helical or amorphous conformation, the SAMs are protein repellent. When the EOs in the SAM are in the all-*trans* form, proteins adsorb at the SAMs. The protein resistance is explained by the structure of the water layer at the SAMs: water adsorbs much more strongly onto the helical or amorphous EO conformation than onto the all-*trans* EO conformation. The authors claim that this stable water film prevents proteins from adsorbing at the SAMs in the helical or amorphous conformation; the less stable water film at the all-*trans* EOs results in protein adsorption. However, this is not yet proven.

All these researches show that the antifouling capacity of PEO brushes cannot be explained by excluded volume interactions and PEO-protein repulsion alone. At least conformational changes of the PEO chains, depending on the environmental conditions, have to be taken into account, which may lead to PEO-protein attraction. Relating to this, the ternary adsorption at PEO brushes at low grafting densities might be induced by the penetrating protein forcing the PEO chains

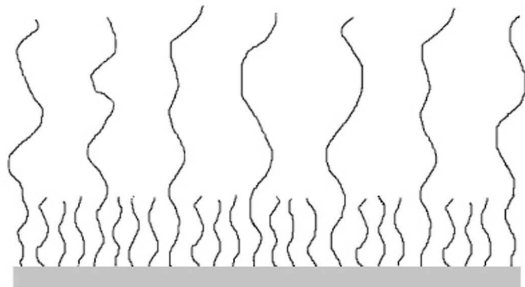


FIGURE 2.3. Cartoon of a bimodal brush consisting of PEO_{48} and PEO_{770} chains (length of short and long chains not to scale).

to change conformation, thereby forming more apolar, protein adsorbing EO moieties.

The objective of this investigation is to test the antifouling properties of bimodal PEO brushes by measuring the adsorption of BSA at such brushes. Our aim is to highlight the ternary adsorption for long PEO chains at low grafting density by suppressing (possible) primary adsorption. The bimodal brushes consist of long ($N=770$) and short ($N=48$) PEO chains, schematically pictured in figure 2.3. In our experiments the long PEO/short PEO ratio is varied, keeping the total grafting density constant. In this way the proximity of the surface is covered with a dense PEO layer, which should prevent primary adsorption and thereby reduce the total adsorbed amount. The structure of bimodal PEO brushes has been investigated using NR and SCF calculations with three different PEO chain lengths at different ratios of long and short chains and at different grafting densities.^{40,41} The results show distinct regions of short chains (close to the surface) and long chains (protruding through the proximal layer into the water).

We determined the adsorbed amount of BSA as a function of the grafting density of the long chains in the brush. The adsorption data for the bimodal brushes are compared with those for monomodal brushes (with $N=770$) to demonstrate a possible contribution of primary adsorption to the maximum in the adsorption curve for monomodal brushes. Before the bimodal brush experiments were performed, BSA adsorption onto short ($N=48$) PEO brushes with varying σ was

studied to ascertain the grafting density yielding minimal BSA adsorption at short PEO brushes. This σ -value is used for the total grafting density of the bimodal brushes.

The adsorption is measured by optical reflectometry, an *in situ* method to determine the adsorbed amount at a solid surface.^{45,46} The brushes are prepared by means of deposition of polystyrene(PS)-b-PEO copolymers at a PS surface, using the Langmuir-Blodgett (LB) technique:¹³⁹ first a PEO brush is prepared at the air–water interface and then transferred to the solid surface. The PS part of the copolymer serves as an anchor for the PEO chain at the surface through hydrophobic interaction between the PS surface and the PS block.⁸⁶ This method provides well-defined, homogeneous, and reproducible polymer brushes at solid surfaces with tunable grafting densities.^{37,39,126} To establish the 'brush-regime' for the mixtures of long and short PS-b-PEO copolymers, interfacial pressure (Π) vs. area (A) isotherms of the Langmuir films at the air–water interface were determined.^{11,112} Results are compared to $\Pi - A$ isotherms of monomodal brushes ($N=48$ and $N=770$). The brushes produced with LB are characterized using ellipsometry and contact-angle measurements.

2.2. Materials and Methods

2.2.1. Preparation of the Brushes

The adsorption of BSA on the PEO brushes was measured using optical reflectometry. Therefore reflecting silicon wafers were used (Wafernet GmbH, Si(100), with a SiO₂-layer of 2-3 nm), cut in slides of 1 cm \times 6 cm. These wafers were first coated with a PS film after which the (bimodal) PEO brush was transferred from an air–water interface to the PS-coated wafer, using the LB deposition. The coating with polystyrene was performed in two steps. First, vinyl-terminated PS (M_w (weight-average molecular mass) = 2100 Da, $M_w/M_n = 1.11$ (M_n is number-average molecular mass, M_w/M_n indicates polydispersity)), Polymer Source Inc.), was covalently bound to the silica layer of the wafer.¹¹³ The covalently bound PS serves as an anchor for an additional layer of PS ($M_w = 870$ kDa, $M_w/M_n = 1.05$, Polymer Source Inc.) that was applied by spin-coating, using a 13 g/l PS solution in toluene.³⁸ In this way a stable PS layer of approximately 70 nm, as measured by ellipsometry, was achieved. This layer thickness is required in the optical reflectometry experiments to get the optimum sensitivity.⁴⁶

For the preparation of the (bimodal) brushes using LB, PS-b-PEO copolymers of different PEO chain lengths were utilized, i.e., PS₂₉-b-PEO₄₈ ($M_w =$

3000(PS)-2100(PEO) Da, $M_w/M_n = 1.05$, Polymer Source Inc.) and PS₃₇-b-PEO₇₇₀ ($M_w = 3800$ (PS)-34000(PEO) Da, $M_w/M_n = 1.05$, Polymer Source Inc.). These copolymers were dissolved in chloroform at different mixing ratios, with a total weight concentration of 0.50 g/l. All solvents used were pro analysis grade (Sigma-Aldrich).

First, $\Pi - A$ isotherms at room temperature were determined, for long and short PS-b-PEO copolymer and solutions of different mixing ratios of long and short PS-b-PEO. A measured volume of solution (in the range of 80-120 μ l) was spread with a micro syringe on a clean air-water interface in a Teflon Langmuir trough, containing ultra pure water (Seralpur Pro 90C, conductivity $< 0.055 \mu$ S/cm, pH 6) and equipped with a platinum Wilhelmy plate to measure the interfacial tension (γ). After evaporation of the chloroform, the copolymer film was compressed and expanded, at a speed of 50 mm²/s, in a number of successive cycles, with 5 minutes waiting time between compressions and expansions, and the $\Pi - A$ isotherms were recorded. The interfacial pressure (Π) is the difference between the interfacial tension of the water (γ_w), measured prior to the addition of the copolymer, and the interfacial tension of the monolayer of the copolymer at the air-water interface (γ_p): $\Pi = \gamma_w - \gamma_p$. From these $\Pi - A$ isotherms the 'brush regime' was established, as that range where $\Pi \sim A^{-5/3}$.^{11,112}

For the LB transfer, a procedure similar to that for the 'brush regime' determination was followed. However, in the second compression the copolymer film was set to the desired grafting density within the 'brush regime'. A PS-coated wafer was dipped through the copolymer film, while the interfacial pressure was kept constant, transferring the copolymer chains to the wafer. The transfer ratios (ratios of area change of copolymer film to area of dipped wafer) obtained for the different wafers were approximately unity, indicating good transfer.¹³⁹ The grafting density for each wafer was calculated from the amount of copolymer added to the air-water interface and the area of the (compressed) monolayer in the Langmuir trough at the start of LB transfer. To enhance the attachment of the PS-b-PEO chains after deposition, the wafers were annealed for 5 min. at 95°C (at the glass transition temperature of the PS) in an oven, allowing diffusion of the PS-block of the copolymer into the PS sublayer. After cooling the PS layer becomes glassy again and the block copolymers are irreversibly attached to the surface.

The brushes were characterized by measuring the thickness of the transferred PS-b-PEO layer with ellipsometry (Sentech Instruments GmbH). The ellipsometry measurements were performed at three different spots on the wafer, in air (implying

that the PEO brush is collapsed). This gives a measure for the amount of PS-b-PEO transferred to the wafer in LB. Furthermore, advancing contact angles of a sessile drop of ultra pure water were measured on the PEO brushes (in air) at room temperature, using a Krüss microscope. For each wafer, six to eight contact angles were captured and averaged. For comparison, the contact angle on a wafer with a PS layer was measured.

2.2.2. Reflectometry

We used an optical reflectometry setup described in detail by Dijt *et al.*⁴⁶ This setup contains a He-Ne laser (monochromatic light, $\lambda = 632.8$ nm) with linearly polarized light. The change in polarization upon reflection is measured, by simultaneously detecting the parallel (R_p) and perpendicular (R_s) reflectivity, resulting in a signal $S = R_p/R_s$. For each wafer the system was first calibrated with flowing phosphate buffer to obtain a stable baseline signal (S_0). At t_0 the adsorption is started by introducing a BSA solution in the cell, by stagnation point flow, and measuring the change in signal (ΔS) in real time. Detector sampling time is 1 s; the flow of BSA solution is set at 1 ml/min. The adsorbed amount (Γ) can be calculated from the change in signal (ΔS) and a sensitivity factor (Q), which depends on the refractive index and thickness of the layers on the silicon wafer: $\Gamma = Q(\Delta S/S_0)$, $\Delta S = S - S_0$. Silicon wafers coated with a PS layer of approximately 70 nm were used. BSA (Sigma, A3912, minimum 96%, $M_w = 66$ kDa) is a heart-shaped protein with pI 4.7.²⁶ Its dimensions in solution (pH 4.5 – 8.0) can be approximated by a triangle with sides of 8.0 nm and a depth of 3.0 nm.²⁶ BSA solutions of 50 mg/l in phosphate buffer of pH 7.00 (Merck, $I = 0.148$ mol/l) were used, so the average charge of BSA is negative in the adsorption experiments. All experiments were performed at room temperature. The occurrence of desorption was checked by switching from BSA solution to buffer solution after a plateau value for the adsorbed amount was reached. Desorption will result in a decrease of the reflectometry signal. The reflectometry measurements were performed in duplicate or triplicate; the data shown are average values.

2.3. Results and Discussion

2.3.1. Preparation and Characterization of Brushes

Interfacial Pressure–Area Isotherms. Monomodal brush ($N=770$)

The Π – A isotherms of the PEO₇₇₀ monolayer at the air–water interface are presented in figure 2.4. Π – σ^{-1} curves, presented in figure 2.4 as well, are constructed

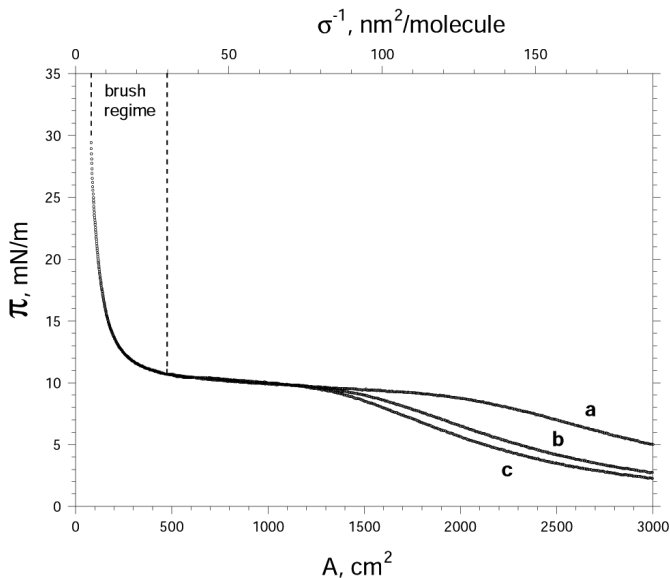


FIGURE 2.4. $\Pi - A$ and $\Pi - \sigma^{-1}$ isotherms for $\text{PS}_{37}\text{-b-PEO}_{770}$ at room temperature. Three successive compression/expansion curves are shown: first compression (**a**), first expansion and second compression (**b**), and second expansion and third compression (**c**). Compression/expansion speed is $50 \text{ mm}^2/\text{s}$. Waiting time in between compressions and expansions is 5 min. Brush regime is indicated.

from the $\Pi - A$ isotherms and the amount of copolymer molecules supplied to the air-water interface. The $\Pi - \sigma^{-1}$ isotherms are similar to those previously reported by Bijsterbosch *et al.*¹¹ and Fauré and coworkers.⁵⁵ The curves show three distinct regions: at large molecular area (i.e., low σ) the interfacial pressure increases only slightly upon compression until it levels off to a Π -value of approximately 10 mN/m at intermediate σ . Upon further compression a steep rise occurs in the interfacial pressure at low molecular area. This isotherm shape is interpreted in the following way:^{11,112} when the area per molecule is large, the copolymer molecules spread onto the surface, and both hydrophobic PS and hydrophilic PEO units are located at the interface. Surface micelles are formed via self-assembly as described by Israelachvili⁸⁷ and by Eisenberg *et al.*³²⁻³⁴ for different amphiphilic block copolymers, including PS-b-PEO. With the decrease in area, the PS-b-PEO molecules start to interact and PEO partly desorbs from the air-water interface (loops and tails are formed), which is reflected in the rise in pressure. Then, at

an interfacial pressure of approximately 10 mN/m, the PEO part starts to desorb completely into the water phase and continues to do so over a considerable range of σ -values, whereby Π only slightly increases ('plateau regime'). The plateau value of 10 mN/m corresponds to the interfacial pressure of a saturated surface of a PEO solution.²³ Both numerical and experimental isotherms show a continuous increase in Π with a decreasing area per molecule in the 'plateau regime', indicating a continuous adsorption-desorption transition.³⁶ As soon as all PEO is desorbed, the PEO chains are essentially end-grafted at the air-water interface by the PS block. Upon further compression the PEO chains have to stretch out from the surface into the solution, i.e., a polymer brush is formed. This compression results in a sharp increase of Π . The region of sharp increase of Π is called the 'brush regime' ($\sigma^{-1} < 30nm^2$, indicated in figure 2.4). In the 'brush regime' the surface pressure is considered to consist of two contributions: a constant pressure $\Pi_{plateau}$ (of 10 mN/m) resulting from a monolayer of adsorbed EO segments of constant density and an increasing surface pressure Π_b due to the formation of a brush.³⁶ In this region $\Pi_b \sim \sigma^{5/3}$. The shape of the $\Pi - \sigma^{-1}$ isotherm as found by SCF calculations is fully consistent with this scenario.³⁶

In figure 2.4, the compression and expansion isotherms coincide. Only at large area (low σ -value) do the curves differ (**a-c**), probably due to relaxation of the copolymer layer after a compression/expansion cycle.

Monomodal brush ($N=48$)

In contrast to the isotherms in figure 2.4, the $\Pi - A$ (and $\Pi - \sigma^{-1}$) isotherms for the short copolymer in figure 2.5 are rather complicated. Four cycles are shown. The curves of the second to fourth compression (**b**) coincide and are shifted to grafting densities lower than those for the first compression isotherm (**a**). The shape of the compression isotherms is similar to that of the isotherms for PS₃₇-b-PEO₇₇₀ (however, without a 'plateau regime'). In contrast, the expansion curves do not coincide with the compression curves and exhibit a dip at low area per molecule (**c**). With increasing number of compression/expansion cycles the dip becomes less pronounced (**c**, **1-4**). This kind of hysteresis behaviour has previously been reported in literature for short PS-b-PEO copolymers (PS₁₇-b-PEO₄₈ and PS₃₈-b-PEO₉₀),^{66,67} but a satisfactory explanation of that effect has not yet been given. The hysteresis suggests that upon compression some kind of 2D-aggregation of the PS₂₉-b-PEO₄₈ occurs. For the purpose of preparing PEO brushes the obtained $\Pi - \sigma^{-1}$ isotherms are sufficient.

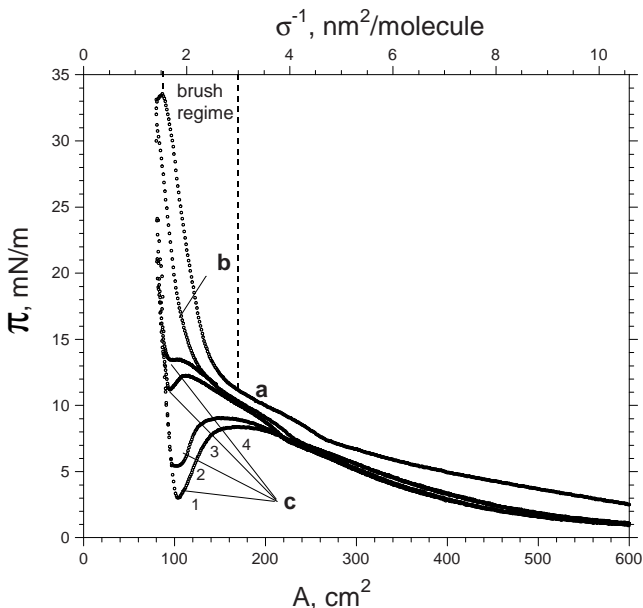


FIGURE 2.5. $\Pi - A$ and $\Pi - \sigma^{-1}$ isotherms for $\text{PS}_{29}\text{-b-PEO}_{48}$ at room temperature. Four successive compression/expansion curves are shown: first compression (**a**), second to fourth compression (**b**), and expansions (**c**, **1-4**). Compression/expansion speed is $50 \text{ mm}^2/\text{s}$. Waiting time in between compressions and expansions is 5 min. Brush regime is indicated.

Bimodal brushes

As for the short-chain brush (figure 2.5), we observed a dip in the interfacial pressure of bimodal brushes upon expansion (figure 2.6), but it was less pronounced, and gradually vanished with increasing ratio of $\text{PS}_{37}\text{-b-PEO}_{770}$ to $\text{PS}_{29}\text{-b-PEO}_{48}$ (from **a** to **c**). This indicates that the length of the PEO block relative to that of the PS block and the average density of the short-chain copolymer which is reached in compression, are important factors for the observed hysteresis phenomenon. For the purpose of preparing bimodal brushes at a solid surface, the obtained isotherms are adequate.

Langmuir-Blodgett. In view of the foregoing, some precautions were taken to minimize a possible (adverse) influence of the $\Pi(\sigma)$ hysteresis on the preparation of a well-defined brush on the solid surface. First, LB deposition was carried out only after the layer was compressed, expanded, and compressed again to a required

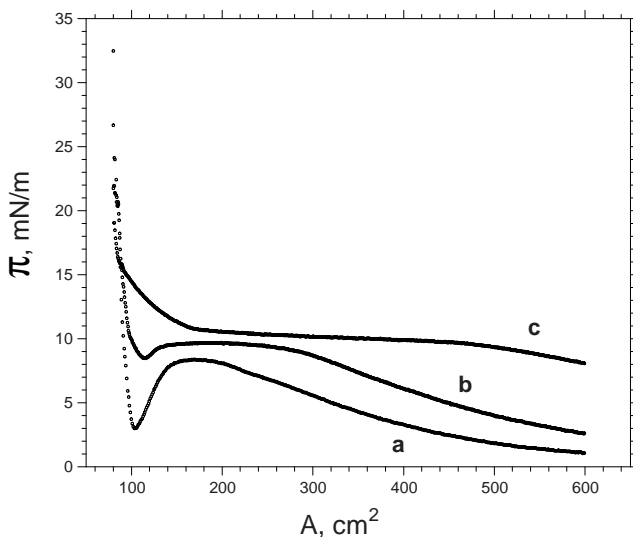


FIGURE 2.6. $\Pi - A$ isotherms for bimodal brushes and monomodal $\text{PS}_{29}\text{-b-PEO}_{48}$ at room temperature. Only first expansion curves are shown: monomodal $\text{PS}_{29}\text{-b-PEO}_{48}$ (a), bimodal with $\text{PS}_{29}\text{-b-PEO}_{48}$ to $\text{PS}_{37}\text{-b-PEO}_{770}$ weight ratio 5:1 (b), and bimodal with $\text{PS}_{29}\text{-b-PEO}_{48}$ to $\text{PS}_{37}\text{-b-PEO}_{770}$ weight ratio 1:1 (c). Compression/expansion speed is $50 \text{ mm}^2/\text{s}$. Waiting time in between compression and expansion is 5 min.

value of surface pressure (corresponding to a desired grafting density). The other precaution was to avoid too high interfacial pressure values, so that there would be minimal hysteresis in compression/expansion regimes. Furthermore, after the second compression to the desired σ the monolayer was left to relax until a constant surface pressure was reached, enabling controlled LB transfer. Preparation of short-chain brushes at σ values below 0.12 nm^{-2} did not succeed in complete transfer, so no adsorption data were obtained below $\sigma = 0.12 \text{ nm}^{-2}$.

Characterization of the Brushes. Ellipsometry yielded PS-b-PEO layer thicknesses ranging between 0.5 and 6.0 nm, the thicker layers being measured for higher values of σ and long-chain brushes. In this way, ellipsometry confirmed a successful transfer of PS-b-PEO copolymer. The (advancing) contact angles for the bimodal brushes are presented in figure 2.7A as a function of σ_{770} , together with the (advancing) contact angles for the long chain monomodal brush. The advancing contact angles for PEO_{48} brushes are shown in figure 2.7B. The contact angles of

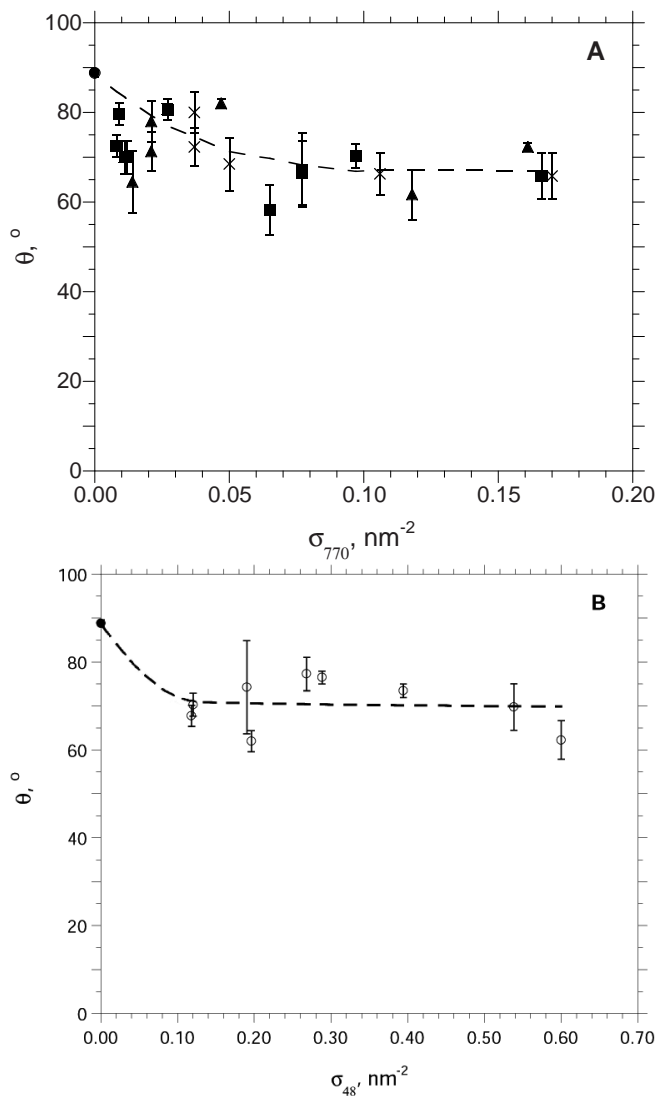


FIGURE 2.7. Advancing contact angle of water on bimodal PEO brush and monomodal PEO₇₇₀ brush (A) and monomodal PEO₄₈ brush (B). Average measured values are shown, including calculated error bars and trend lines: PS (●), bimodal brush $\sigma_{\text{total}} = 0.30 \text{ nm}^{-2}$ (■), bimodal brush $\sigma_{\text{total}} = 0.50 \text{ nm}^{-2}$ (▲), monomodal PEO₇₇₀ brush (×), and monomodal PEO₄₈ brush (○).

all the brushes are lower than the measured values on a pure PS film ($88.8^\circ \pm 0.8^\circ$), confirming the presence of a PEO layer. In case of the bimodal and long monomodal brushes (figure 2.7A) the contact angle decreases with increasing σ_{770} , because the number of (water-soluble) long PEO chains per unit surface area increases. However, at high σ -values the contact angle leveled off to $65\text{--}70^\circ$, which is higher than we anticipated, considering the increasing amount of PEO at the interface with increasing σ . Equilibrium contact-angle measurements by Gombotz *et al.* on covalently bound PEO films (side-grafted) at a poly(ethylene terephthalate) surface showed values ranging from 25° to 55° .⁶⁵ Roosjen and coworkers prepared PEO brushes by chemical grafting of vinyl-terminated PEO₂₂₀ on glass and silica.¹⁴¹ Advancing and receding contact angles of water were determined at PEO brushes with a grafting density of about 0.6 nm^{-2} . Reported advancing contact angles are 48° on PEO-coated glass and 36° on PEO-coated silica. Again, finite contact angles were obtained. The advancing contact angle for PEO₄₈ (figure 2.7B) also leveled off with increasing grafting density, to approximately 70° . It can be concluded that a PEO brush possesses a finite contact angle for water, even at high grafting densities (see appendix).

2.3.2. Reflectometry

Adsorption of BSA results in an increase of the reflectometry signal ΔS . In real time this signal gradually levels off to a plateau value (steady-state adsorption), which, for most brushes, was reached within 90 min. At high grafting densities the adsorption is very slow and a true plateau value could not be reached; the signal at 90 min is used as an approximate saturation value. As an example a few reflectometry experiments of BSA adsorption at long PEO brushes are displayed in figure 2.8. Γ values, calculated from the change in signal ΔS , vs. sampling time are displayed. After reaching the plateau value, the protein solution was replaced by a pure buffer solution and the reflectometer signal was monitored up to 7 h. For none of the brushes could any protein desorption be detected.

Monomodal PEO Brush

Results of reflectometry of BSA adsorption on monomodal PEO brushes with $N = 48$ and $N = 770$ are presented in figure 2.9. For $N = 48$ there is a gradual decrease of adsorbed amount as a function of grafting density. This result is consistent with other observations for 'short' PEO chains, *e.g.*, McPherson and coworkers¹¹⁸ (lysozyme, $N_{PEO} = 75, 98$ and 128) and Currie *et al.*³⁹ (BSA, $N_{PEO} = 148$). At high grafting density ($\sigma = 0.60\text{nm}^{-2}$) the adsorbed amount is reduced by 90%, to approximately 0.10 mg/m^2 .

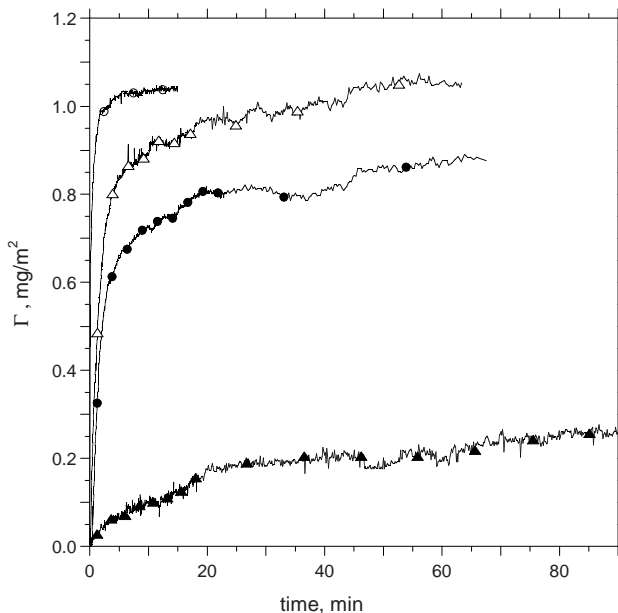


FIGURE 2.8. Examples of a few reflectometry experiments of BSA adsorption at PEO₇₇₀ brushes: $\sigma = 0.00 \text{ nm}^{-2}$ (PS) (\circ), $\sigma = 0.06 \text{ nm}^{-2}$ (Δ), $\sigma = 0.08 \text{ nm}^{-2}$ (\bullet), and $\sigma = 0.17 \text{ nm}^{-2}$ (\blacktriangle).

BSA adsorption on the long-chain PEO₇₇₀ brushes shows a similar behaviour as observed by Currie *et al.*:³⁹ at low σ the adsorption is enhanced, probably as a result of ternary adsorption and at higher σ the adsorption gradually decreases, due to increasing excluded volume interactions between BSA and PEO chains.

The errors for the adsorption values in figure 2.9 are considerable, especially at low grafting densities. In reflectometry each measurement is performed at one single spot of the wafer and duplicate experiments are performed with different wafers. This might account for the observed variations in the adsorbed amount. The accuracy of the average adsorption values would increase if more wafers were used. Nevertheless, our data provide unambiguous trends for $\Gamma(\sigma)$.

Bimodal PEO Brush

Based on the BSA adsorption on PEO₄₈ brushes two types of bimodal brushes were prepared, with total grafting densities σ_{total} ($= \sigma_{48} + \sigma_{770}$) of 0.30 and 0.50 nm^{-2} respectively. Hence, they have a dense layer of PEO close to the PS surface with σ_{total} of 0.30 or 0.50 nm^{-2} . $\sigma_{\text{total}} = 0.60 \text{ nm}^{-2}$ was not attainable due to a too high Π in the Langmuir trough.

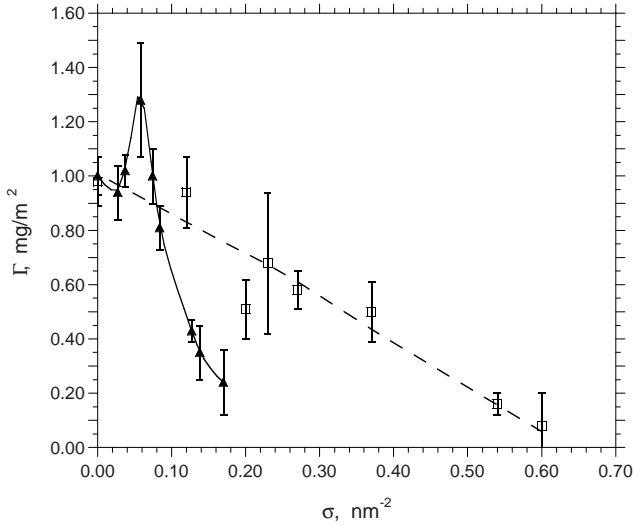


FIGURE 2.9. BSA adsorption onto PEO₄₈ and PEO₇₇₀ monomodal brushes as a function of the grafting density. Average measured values are shown, including calculated error bars and trend lines: PEO₇₇₀ (—▲—) and PEO₄₈ (—□—).

From figure 2.9 it can be concluded that for the PEO₄₈ brushes the adsorbed amount at $\sigma = 0.30 \text{ nm}^{-2}$ is 0.55 mg/m^2 and at $\sigma = 0.50 \text{ nm}^{-2}$ it is 0.20 mg/m^2 . Based on this, one expects for the bimodal brushes with $\sigma_{\text{total}} = 0.50 \text{ nm}^{-2}$ strongly suppressed primary adsorption ($\leq 20\%$). For the bimodal brushes with $\sigma_{\text{total}} = 0.30 \text{ nm}^{-2}$ the primary adsorption will be $\leq 55\%$.

Figure 2.10 displays the BSA adsorption on bimodal PEO brushes as a function of the grafting density of the long PEO chain (σ_{770}) for the two total grafting densities, together with data for the monomodal PEO₇₇₀ brush. The adsorption data for the bimodal brushes are very similar to those for the monomodal PEO₇₇₀ brushes. In both cases there is a maximum at low grafting densities and a gradual decrease at higher grafting densities. Also, the maximum adsorption values are very similar, although the maximum for the bimodal brushes is shifted to a lower grafting density ($0.03\text{-}0.05 \text{ nm}^{-2}$) compared to the monomodal brush (0.06 nm^{-2}). This can be due to extended stretching of the long chains of the bimodal brush at low grafting density, imposed by the dense short-chain layer near the surface as described by Currie and co-workers.^{40,41} It would yield more sites at the long chains available for adsorption and therefore more ternary adsorption at lower

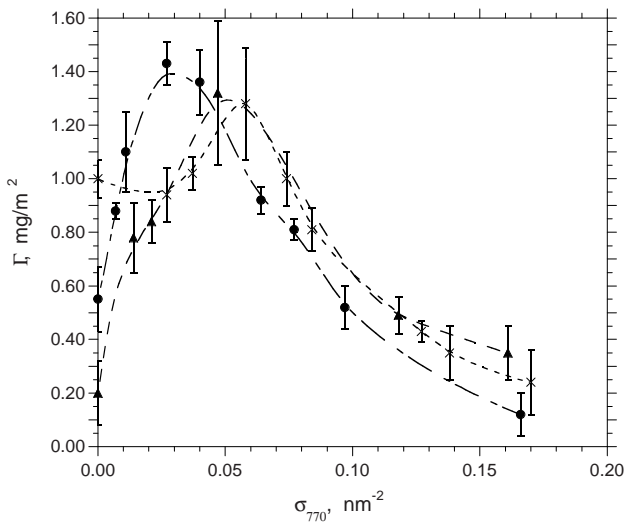


FIGURE 2.10. BSA adsorption onto bimodal brushes for two different total grafting density. Data for monomodal PEO₇₇₀ brush are shown for comparison. Average measured values are shown, including calculated error bars and trend lines: bimodal brush $\sigma_{\text{total}} = 0.30 \text{ nm}^{-2}$ (—●—), bimodal brush $\sigma_{\text{total}} = 0.50 \text{ nm}^{-2}$ (—▲—), and monomodal PEO₇₇₀ brush (- -×- -).

grafting density, compared to the monomodal PEO₇₇₀ brush. This corresponds to the observed increasing maximum with increasing chain length of PEO (increasing number of adsorption sites), both experimental as with SCF calculations,³⁹ as well as the observed shift of the maximum to lower grafting density (increasing osmotic penalty with increasing chain length).³⁹

From the similar maximum values for BSA adsorption at the bimodal and monomodal PEO₇₇₀ brushes it can be concluded that the contribution of primary adsorption to the total adsorption of BSA on PEO₇₇₀ brushes is negligible. If there were primary adsorption at low σ , then this primary adsorption would be suppressed by the dense PEO₄₈ layer at the surface in case of the bimodal brushes. Accordingly, the adsorption curves for the bimodal brushes in figure 2.10 should display (much) less adsorption at the maximum than the adsorption curve for the monomodal brush. This is not the case. This suggests the following scenario: at low grafting densities the BSA can penetrate the brush, but it presumably does not reach the PS surface. The observed maximum can only be explained with

adsorption at the long PEO chains (ternary adsorption). Because no desorption was detected during 7 h of washing with buffer, the BSA is not kinetically 'trapped' in the grafted PEO layer and the attraction between BSA and PEO is substantial.

Probably a preferred orientation of the BSA molecules is required to allow them to penetrate the brush. BSA is a heart-shaped protein which can be approximated to a triangle with sides of 8.0 nm and a depth of 3.0 nm.²⁶ At low σ_{770} ($\approx 0.05 \text{ nm}^{-2}$), where the maximum adsorbed amount is observed, the area between the PEO chains ($= 1/\sigma \approx 20 \text{ nm}^2$) is comparable to the area occupied by a BSA molecule in an end-on orientation (24.0 nm^2). Furthermore, from light-scattering and electron spin resonance data a hydrodynamic radius of 2.64 nm has been inferred for BSA.²⁶ The cross-sectional area of a BSA molecule calculated from the hydrodynamic radius is 21.9 nm^2 , again comparable to the area between PEO chains at the observed maximum. This suggests that the BSA penetrates the brush in an end-on orientation, where it is 'captured' inside eventually. The adsorption at the PEO chains might be due to conformational changes of the EO units, caused by the penetrating protein. This conformational change results in more apolar/protein adsorbing EO moieties. At higher grafting densities the brush becomes more dense, inhibiting the penetration of BSA, due to excluded volume interactions between the (long) PEO chains and the BSA, a 'squeezing out' effect anticipated in ref.³⁹

Atomic Force Microscopy (AFM) (images not shown) of bimodal brushes revealed the possible existence of domains with an excess of long respectively short PEO chains, in contrast to monomodal brushes which provide homogeneous brushes.^{37,41,55} This inhomogeneity of the bimodal brushes might contribute to the observed shift of the maximum to lower σ . Moreover it may cause variation in the adsorbed amount between different wafers with brushes of the same (average) grafting density.

2.4. Conclusions

Bimodal brushes consisting of PEO₄₈ and PEO₇₇₀ demonstrated similar BSA adsorption behaviour as monomodal PEO₇₇₀ brushes: a maximum in the low grafting density regime and a subsequential gradual decrease at higher grafting densities. The maximum in BSA adsorption at low grafting density is ascribed to ternary adsorption, because the contribution of primary adsorption can be neglected and no desorption could be detected, indicating an attraction between

the BSA and PEO chains. This supports the conclusions made by Currie *et al.* based on experimental data and SCF calculations.³⁹

The possible inhomogeneity of the bimodal brushes is still under investigation. The observed hysteresis phenomena of the interfacial pressure will be analyzed in more detail in the General Discussion. The length of the PEO block relative to that of the PS block and the average density of the short-chain copolymer seem to be the important parameters.

Acknowledgement

I thank Petya Iakovlev for the pleasant collaboration over the past years. He has done a lot of work on the interfacial behaviour of PS-b-PEO and BSA adsorption on PEO brushes. I am very grateful for that and also for our fruitful discussions.

2.5. Appendix

Since the publication of this chapter in the *J. Colloid Interface Sci.* in 2005 a number of research results were published that are relevant to the content of this chapter. The main features will be mentioned here, together with the consequences for the preparation of bimodal PEO brushes and the adsorption of BSA at these brushes.

2.5.1. Ternary Adsorption Theory

Halperin and coworkers⁷³ studied the primary versus ternary adsorption of proteins onto PEO brushes using a scaling theory, in the weak adsorption limit. The protein adsorption is considered a reversible process and the focus is on the equilibrium situation. In their discussion they use the simple Alexander model for brushes.⁶ They compared the expressions for the adsorption isotherms with experimental data. One of their conclusions is that BSA adsorption at long PEO brushes (as an example they use $N=770$) can be described by pure ternary adsorption and that a maximum in the adsorbed amount is observed as function of the grafting density. They used the data of BSA adsorption at PEO₇₇₀ brushes presented in this chapter (fig 2.9) to fit their scaling expressions. According to Halperin *et al.* the measured Γ values incorporate contributions due to primary adsorption, however for these long PEO chains the ternary adsorption is dominant. More recently Halperin *et al.*⁷⁴ analyzed the ternary protein adsorption onto brushes using a SCF theory and comparing two ternary adsorption modes:

weak, due to nonspecific weak attraction between polymer segments and the surface of the protein (*e.g.* BSA) and strong, due to strong binding of polymer segments to specific protein sites as it occurs in antibodies. Again, a maximum in Γ is exhibited as function of σ , for both weak and strong attraction. Furthermore, the concentration profile of adsorbed proteins displays a maximum at some distance away from the solid surface that shifts outwards as σ increases. These conclusions confirm the ternary adsorption mechanism proposed in this chapter. Although there are some different assumptions between the scaling theory and SCF theory of Halperin *et al.* and the nSCF theory of Currie and coworkers, they yield similar results, *e.g.* the observed maximum and an attractive interaction energy between BSA and PEO of 0.05 kT per EO unit that can describe the ternary adsorption.

2.5.2. Contact-angle Measurements

Water contact-angle measurements were used to characterize the PEO brushes, as a means of determining the presence of PEO at the solid surface and to indicate the grafting density of PEO. The results were presented in figure 2.7. It shows that at high σ -values the contact angle leveled off to 65–70°, thus, the PEO brush possesses a finite contact angle for water. Cohen Stuart *et al.*³⁰ explained this, using SCF calculations and experiments for water contact angles at PEO brushes, as being typical behaviour for wetting of a polymer brush by a good solvent. Grafted chains adsorb at the solvent–air interface, forming a bridge between the solid surface and the solvent–air interface, thereby preventing the droplet to spread. Therefore, even at high grafting densities of a hydrophilic polymer, a finite contact angle of water is observed. Consequently, the use of contact-angle measurements to determine the grafting density of a polymer brush at a solid surface is erroneous. An accurate way *e.g.* is to calculate σ from the measured layer thickness in a dry state with ellipsometry.

2.5.3. LB Deposition

The most important discovery concerning our BSA adsorption on bimodal PEO brushes study was made by de Vos.¹⁶⁴ He studied the production of PEO brushes via LB deposition on PS surfaces applying PS-b-PEO with various PEO chain lengths, similar to the method described in this chapter. He observed an incomplete transfer of the PS-b-PEO copolymers to the PS-coated surface by determining the transferred amount with ellipsometry. The extent of transfer proved to be dependent on the ratio of the PEO to PS chain length of the copolymer.

For PS₃₆-b-PEO₁₄₈ the mass transfer is 94%, for PS₃₆-b-PEO₃₇₀ the transferred amount is 57%, while for the longest PEO chain length, PS₃₇-b-PEO₇₇₀, a transfer of 19% is obtained. This reduced mass transfer is attributed to a competition for the PS surface between the PEO block and the PS block, since both PS and PEO can adsorb at a PS surface. Adsorbed PEO blocks act as a kinetic barrier for the adsorption of a PS block. The longer the PEO compared to the PS chain, the less chance the PS block has of strongly attaching to the PS interface, the less the transferred amount. Additional research by de Vos demonstrated that applying the Langmuir-Schaefer (LS, horizontal) deposition resulted in much higher mass transfers compared to the LB method.

The consequence of this discovery is that the PEO brushes described in this chapter are much diluter than anticipated. The grafting densities of the prepared brushes have to be corrected. The σ of the monomodal PEO₇₇₀ brushes is corrected with 19%, because the same PS₃₇-b-PEO₇₇₀ copolymer was used as de Vos.¹⁶⁴ For the monomodal PEO₄₈ brushes the PS and PEO block are of comparable size (PS₂₉-b-PEO₄₈) and in addition, the PEO block is much smaller than the smallest studied by de Vos (PS₃₆-b-PEO₁₄₈), that showed 94% transfer. Therefore a 100% transfer is assumed for the monomodal PEO₄₈ brushes and no correction of σ is needed. Considering no data are available on the transfer efficiency of the LB deposition of bimodal brushes of PEO₇₇₀ and PEO₄₈ chains, we assume the transfer of the long chains of the bimodal brush (PS₃₇-b-PEO₇₇₀) to be equal to that of the monomodal PEO₇₇₀ brush, i.e. 19%. It is likely that the large PEO chains of the bimodal brush (partly) adsorb at the PS surface, in a similar way as the PEO chains of the monomodal PEO₇₇₀ brush. The adsorbed PEO forms a barrier for the PS₂₉-b-PEO₄₈ chains to reach the PS surface, hence, the transfer of PS₂₉-b-PEO₄₈ in the bimodal brush is less than 100%. The exact values of the transfer of long and short chains in the bimodal brush need to be studied.

The implications for the adsorption of BSA at the monomodal and bimodal brushes are as follows. The data for BSA adsorption at monomodal PEO₄₈ in figure 2.9 do not change, the $\Gamma(\sigma)$ curve for monomodal PEO₇₇₀ in figure 2.9 shifts to much lower σ (figure not shown). The corrections of the adsorption data of figure 2.10, for both bimodal PEO brushes and monomodal PEO₇₇₀, are presented in figure 2.11. It clearly shows the considerable shift of the curves to lower σ , compared to figure 2.10. Explaining the corrected data is not straightforward. The brushes used in the adsorption experiments proved to be very dilute ($\sigma_{770} \leq 0.03 \text{ nm}^{-2}$), in such a way that part of the grafted PEO₇₇₀ layers used is in

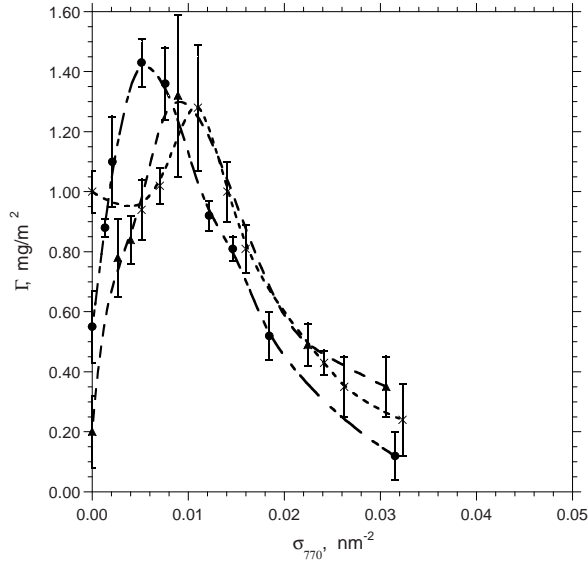


FIGURE 2.11. Corrected BSA adsorption data onto bimodal brushes for two different total grafting density. Data for monomodal PEO₇₇₀ brush are shown for comparison. Corrections of σ_{LB} based on the research by de Vos¹⁶⁴ (see text). Average measured values are shown, including calculated error bars and trend lines: bimodal brush $\sigma_{total} = '0.30' \text{ nm}^{-2}$ (—●—), bimodal brush $\sigma_{total} = '0.50' \text{ nm}^{-2}$ (—▲—), and monomodal PEO₇₇₀ brush (- -x- -).

the mushroom regime. It is most certain that adsorbed BSA can penetrate the PEO layers and some of it might even reach the PS surface. In case of monomodal PEO₇₇₀ it can adsorb at the surface, in case of the bimodal brushes it might adsorb at the PS surface as well, because the grafting density of the PEO₄₈ at the surface is lower than anticipated. Consequently, primary adsorption (reasonably) did occur in the reflectometry experiments. However, after correction of the reflectometry data, still a maximum in the adsorbed amount is observed as function of the grafting density, for monomodal and bimodal brushes, with a maximum exceeding the adsorption value at a bare PS surface. This phenomena can only be explained by a ternary adsorption mechanism. Therefore, the main conclusion of this chapter is maintained.

Part II

Polysaccharide Brushes

CHAPTER 3

Polystyrene–Polysaccharide Diblock Copolymers

Published in: *Macromolecules*, 36 (2003), 1982–1987

3.1. Introduction

Biofouling is the undesired accumulation of biological substances at surfaces and occurs on solids exposed to biological fluids such as blood, urine, saliva, tear fluid, milk, fruit juices and seawater. It is usually initiated by protein adsorption and causes many problems in medical applications (such as implants), food technology (pollution of processing equipment), and water processing. Research has shown that coating surfaces with hydrophilic polymer brushes can prevent or reduce protein adsorption and hence retard biofouling.^{103,118} So far, these brushes usually consist of flexible, synthetic polymers, often based on poly(ethylene oxide) (PEO). In biological systems the use of natural polymers may be preferred and polysaccharides seem to be the most plausible candidate. In nature polysaccharides can be found in extra-cellular polymer layers and in the glycocalyx of biomembranes, having the function to prevent non-specific adsorption of for example proteins.^{5,80}

Polymer brushes can be prepared by physical adsorption or by chemical grafting. Physical adsorption can be performed either from a polymer solution or by using the Langmuir-Blodgett technique.¹¹²

The object of the research presented here was (1) to synthesize and characterize linear polystyrene-polysaccharide diblock copolymers and (2) to study the interfacial behaviour of these copolymers at the air-water interface. The copolymers will be used in future research to prepare polysaccharide brushes at a solid surface, with the Langmuir-Blodgett technique, and subsequently to perform protein adsorption experiments. The polystyrene (PS) block of the copolymers serves as an anchor for the polysaccharide block at the air-water interface. Moreover, the PS block will be the adsorbing part of the copolymer when brushes are prepared at a solid surface.

Copolymers can be synthesized in different ways. One possibility is to couple different small oligomers and then to grow the chains by polymerization, *e.g.* Kobayashi.⁹⁸ Another route is to first synthesize one of the blocks, then couple it to another type of monomer and polymerize the second block, for example Loos¹⁰⁸ and Ziegast.¹⁷⁵ A third way is to polymerize blocks separately and then perform a coupling reaction between them, *e.g.* Xie.¹⁷¹ In the present study the last approach (coupling of prefabricated blocks) was used to couple polysaccharides to amino-terminated PS. In the context of a comparative study different polysaccharides were used (dextrans and maltodextrins) with various chain lengths. Dextrans (mainly) consist of $\alpha(1 \rightarrow 6)$ -linked glucosyl units, maltodextrins of $\alpha(1 \rightarrow 4)$ -linked glucosyl units.

The copolymers were analyzed using IR spectroscopy. To characterize the interfacial behaviour and investigate the possible application as brush material, a monolayer of these polymers was spread on an air–water surface in a Langmuir trough. PS does not dissolve in water and serves as an anchor for the polysaccharide chain, preventing the copolymer from dissolving in the water phase. The interfacial pressure as a function of the surface area was measured during sequential compressions and expansions.

3.2. Experimental

3.2.1. Synthesis

All solvents were purified by conventional methods. Dextrans (weight-average molecular mass (M_w) 1500 Da, 6000 Da, 9500 Da and 15000–20000 Da (Fluka)), and maltodextrins (Paselli MD 20, number-average molecular mass (M_n) approximately 850 Da and Paselli MD 6, M_n about 2800 Da (AVEBE)) were used without further purification. The Paselli-type maltodextrins are characterized by the DE value, the dextrose equivalent (20 and 6, respectively). This DE value corresponds to a number-average molar mass ($M_n = (100/DE) * M_{glycosyl} (= 162Da)$). Maltoheptaose, a maltodextrin, (M_n 1150 Da) was kindly provided by Lorant Janossy (Institute of Biochemistry, University of Debrecen, Hungary). Glucose (Merck) was used to test the reaction. Amino-terminated PS (M_w 12300 Da, $M_w/M_n = 1.02$, (M_w/M_n is a measure of polydispersity)) was purchased from Polymer Source Inc., and used without further purification. IR spectra were recorded on a Bio-Rad spectrometer using Win-IR software.

The coupling reaction was performed under the following general conditions: 20 mg sodium cyanoborohydride (NaCNBH_3), as reducing agent, was added to a mixture of amino-terminated PS and polysaccharide dissolved in the appropriate solvent (*N,N*-dimethylformamide (DMF) or DMF/water). The reaction mixture was stirred for 7 days at 60 °C, and NaCNBH_3 (20 mg) was added every day. Subsequently the mixture was cooled to room temperature and diluted with water (100 ml) to form a precipitate. The precipitate was filtered and washed several times with cold water to remove the excess polysaccharide. Afterwards the precipitate was dried in a vacuum desiccator (with P_2O_5) to obtain the copolymer as a white powder.

In table 3.1 the reaction mixtures and yields of the coupling reaction of the different polysaccharides are summarized. The yield, in wt%, is based on the mass of polystyrene derivative before and after reaction.

<i>Polysaccharide</i>	<i>Molar mass [Da]</i>	<i>Polysaccharide [g]</i>	<i>PS [mg]</i>	<i>Solvent</i>	<i>Yield^a [wt%]</i>
Glucose	180	2.0	100	DMF (10 ml)	95
Maltodextrin MD20	850 (M_n)	1.0	100	DMF (25 ml)	90
Maltoheptaose	1150 (M_n)	2.0	200	DMF (35 ml)	90
Maltodextrin MD6	2800 (M_n)	4.0	100	DMF/water 30/1 (31 ml)	85
Dextran	1500 (M_w)	1.2	100	DMF/water 30/1 (31 ml)	80
Dextran	6000 (M_w)	4.8	100	DMF/water 50/3 (53 ml)	75

^a Yield (in wt%) is based on the mass of polystyrene derivative before and after reaction.

TABLE 3.1. Reaction mixtures and reaction yield of the polysaccharides.

3.2.2. Interfacial Pressure

The interfacial pressure (Π) versus area (A) isotherms of PS-b-Dextrans and PS-b-Maltodextrins at the air–water surface were determined in a Teflon Langmuir trough with a computer-controlled barrier. The interfacial pressure was measured continuously using a platinum Wilhelmy plate. Ultra pure water (specific conductivity $< 0.05 \mu\text{S}/\text{m}$, pH 6) was used for the water phase and chloroform (Sigma) was used as spreading solvent. The concentration of the copolymer solutions ranged between 0.25 and 1.00 g/l, depending on the solubility of the copolymer. A small amount (100 to 400 μl) of the copolymer solution was spread drop wise with a micro syringe. After allowing the chloroform to evaporate (5 minutes), the Π - A measurement was started. The copolymer monolayer was compressed from 600 to 80 cm^2 . The compression speed was 30 mm^2/s , unless mentioned otherwise. The measurements were performed at constant room temperature. Several successive compression and expansion cycles were performed with varying time intervals between expansion and compression. Reproducibility of the interfacial pressure isotherms was verified by performing experiments in duplicate. Π - A isotherms of the two separate polymer blocks (PS and the different polysaccharides) were recorded for comparison with the isotherms of the copolymers. The PS used ($M_w = 13700$ Da, without amino end group) was purchased from Aldrich. The Trurnit method was applied for spreading of the water-soluble polysaccharides with ultra pure water as spreading solvent.¹⁶⁰ The obtained isotherms are presented as interfacial pressure (Π) versus area per molecule (σ^{-1}) isotherms (σ is the polymer grafting density). The area per molecule (σ^{-1}) was calculated from the amount of copolymer added to the air–water interface ($V \times C$, V is the volume added, C is the copolymer concentration) and the area (A) of the (compressed) monolayer in the Langmuir trough: $\sigma^{-1} = \frac{A \times M}{V \times C \times N_{Av}}$ (M is the molar mass of the copolymer,

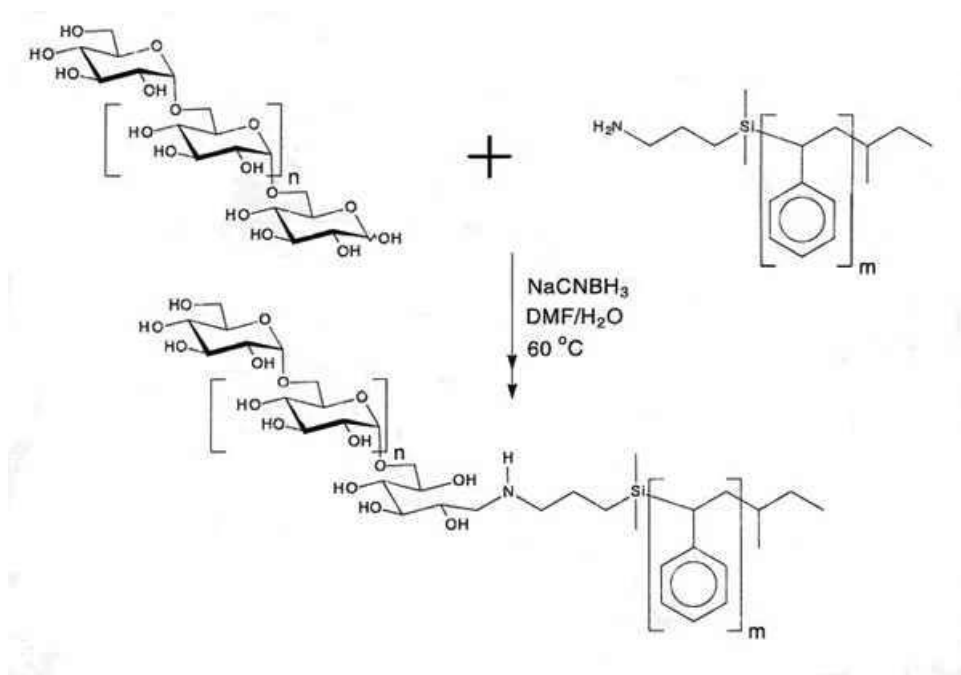


FIGURE 3.1. Synthesis of polystyrene–dextran block copolymer: amino-terminated polystyrene reacts with dextran, in the aldehyde end group isomer (not shown), with sodium cyanoborohdride as reducing agent ($n=7$ or 35 , $m = 120$).

N_{Av} is Avogadro's number). The glycerol used in the hysteresis experiment was obtained from J.T. Baker.

3.3. Results and Discussion

3.3.1. Synthesis

The synthesis strategy was based on a coupling reaction between a polysaccharide and amino-terminated PS.^{107,108} In figure 3.1 the coupling reaction is illustrated for dextrans and amino-terminated PS. Conventional reductive amination was chosen to couple the two blocks, with sodium cyanoborohydride as a reducing agent.¹⁵ Polysaccharides have two structural isomers, one containing a glucosyl end group and the other containing an aldehyde end group. The isomer containing the aldehyde end group reacts with the amino-terminated PS. Each polysaccharide chain contains only one aldehyde end group. Consequently, each

polysaccharide chain reacts with only one amino-terminated PS chain, resulting in only linear diblock copolymers. The different polysaccharides used varied in linkage type and molecular weight. Glucosyl $\alpha(1 \rightarrow 4)$ -linked maltodextrins and $\alpha(1 \rightarrow 6)$ -linked dextrans were investigated.

To test the reaction, glucose was coupled to the polystyrene, dissolved in DMF. Subsequently the maltodextrins and dextrans, mentioned in table 3.1, were coupled to the polystyrene. The coupling reactions were performed in DMF in the case of Maltodextrin(850) and Maltodextrin(1150) or in DMF/water mixtures in the case of Maltodextrin(2800), Dextran(1500) and Dextran(6000). The choice of reaction solvent(s) proved to be very critical with respect to the solubility of the reacting polymers and consequently the conversion. Adding water isolated the synthesized copolymers. A white precipitate was formed, which was purified by extensive washing and filtering, to remove remaining unreacted polysaccharide. Afterwards, the precipitate was dried in a vacuum desiccator and characterized by IR spectroscopy. The synthesized copolymers were used for interfacial pressure measurements without further purification. To achieve high conversion of the amino-terminated PS, large excesses (50-100 eqv.) of polysaccharides were used combined with a long reaction time (7 days). The yield of reaction was 75 to 95 wt% (see table 3.1). During purification of the precipitate, some of the copolymer is lost, which contributes to yields of less than 100%. The presence of uncoupled amino-terminated PS in the products can be excluded, because of a ninhydrin test performed on the products showing negative results (no presence of primary amine).

Figure 3.2 shows the IR spectra of the carefully dried starting compounds and the product obtained upon coupling PS with Dextran(6000). The broad peak between 3600 and 3100 cm^{-1} for dextran in figure 3.2 illustrates the OH vibration of the OH groups of dextran. The sharp peaks at 1500 to 1600 cm^{-1} for PS indicate the C=C vibrations of the aromatic ring. Both peaks can be found in the copolymer (PS(12300)-b-Dextran(6000)), indicating the presence of OH groups and aromatic rings in the formed product. Because of the intensive washing, the presence of remaining uncoupled polysaccharide is unlikely. Hence, it can be concluded from the IR spectra that the coupling reaction between PS and dextran was successful. IR spectra of the other synthesized copolymers exhibit similar results (data not shown).

Attempts to couple longer dextrans (M_w 9500 Da and M_w 15000-20000 Da) with the same PS and using the same method and several different solvent systems were

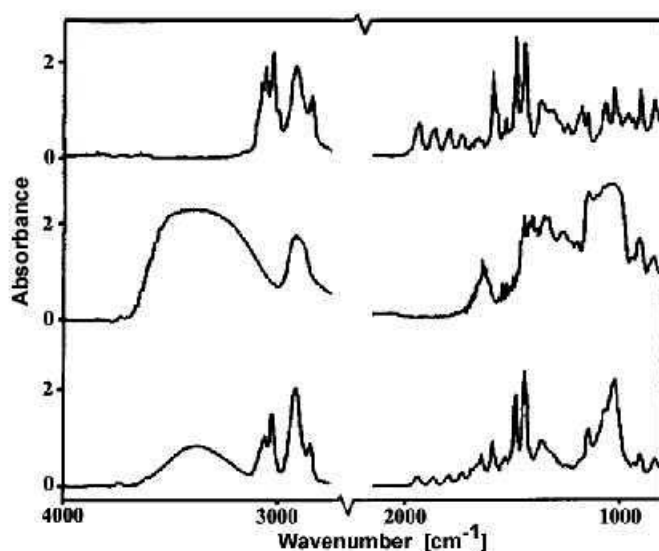


FIGURE 3.2. Transmission IR spectra (KBr, 700-4000 cm^{-1} region) of amino-terminated polystyrene (top), Dextran(6000) (middle) and PS(12300)-b-Dextran(6000) (bottom).

not successful (data not shown). For the synthesis of these longer copolymers a different approach is required.

3.3.2. Interfacial Pressure

Interfacial Pressure Isotherms and Scaling Relationships. All isotherms were recorded in duplicate and proved to be reproducible. Figures 3.3 and 3.4 display the interfacial pressure (Π) of the individual polysaccharides and PS as a function of the area per molecule (σ^{-1}). The interfacial pressure of the polysaccharides levels off at low σ^{-1} , the value being dependent on the length of the polysaccharide: $< 0.7 \text{ nm}^2/\text{molecule}$ for Dextran(6000) down to $< 0.05 \text{ nm}^2/\text{molecule}$ for glucose (see figure 3.3). It indicates that at this compression level the polysaccharides are pushed into solution. The leveling off starts at almost identical values of Π for all the polysaccharides, i.e. 16 mN/m . Hence, the saturated interfacial pressure of a monolayer of the polysaccharides used is approximately 16 mN/m .

PS can be compressed up to high interfacial pressures (see figure 3.4). PS is not forced into solution at pressures $\leq 30 \text{ mN/m}$, which is plausible because of the insolubility of PS in water. As PS has no hydrophilic group, the surface pressure measured is not a true surface pressure but an apparent one, originating

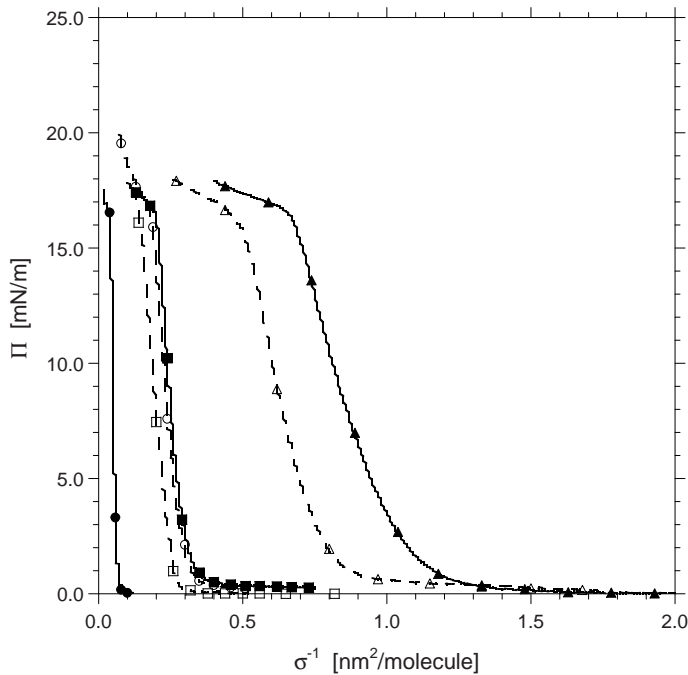


FIGURE 3.3. Interfacial pressure - area per molecule isotherms for various polysaccharides at room temperature. Glucose (—●—), Maltodextrin(850) (···○···), Maltodextrin(1500) (—□—), Maltodextrin(2800) (···△···), Dextran(1500) (—■—) and Dextran(6000) (—▲—).

from a mechanical resistance (during compression) instead of a decrease in surface tension.¹⁰⁰ The $\Pi - \sigma^{-1}$ curves of PS also demonstrates that there is a difference between successive compression/expansion cycles. This will be further discussed in section 3.2.2.

Figure 3.5 gives the interfacial pressure isotherms of PS(12300)-b-Dextran(6000). The first compression isotherm exhibits a pattern generally observed for monolayers of amphiphilic block copolymers.^{11,36,112,114} At large area per molecule the polysaccharide block is adsorbed at the air-water interface (**a** in figure 3.5). The PS block is in the collapsed state. Upon compression the molecules are forced into contact and the interfacial pressure starts to increase. The increasing pressure leads to desorption of dextran from the surface (**b**), 'loops' and 'tails' are formed.⁵⁶ The onset of the interfacial pressure increase, at $12.0 \text{ nm}^2/\text{molecule}$ is indicated by σ_o^{-1} in figure 3.5.

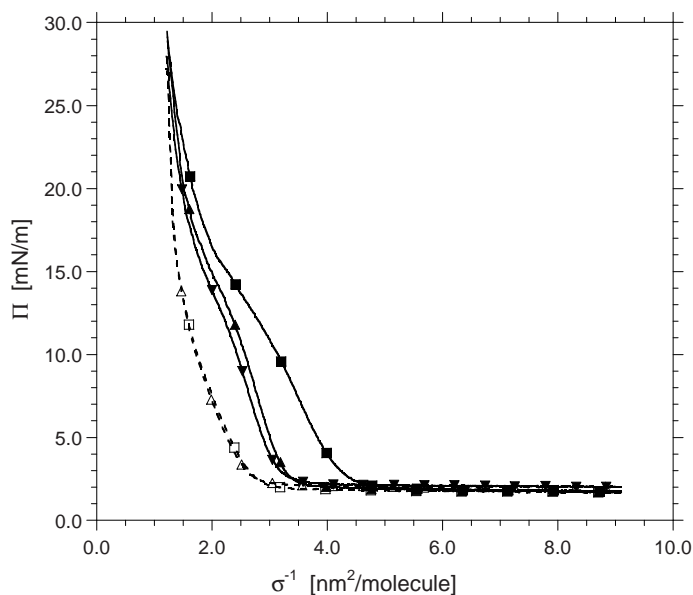


FIGURE 3.4. Interfacial pressure – area per molecule isotherms for PS(13700) at room temperature. Successive compression and expansion curves: first compression (—■—), first expansion (—□—), second compression (—▲—), second expansion (—△—) and third compression (—▼—).

Between 8.0 and 5.5 nm²/molecule the interfacial pressure increases very gradually and assumes a quasi-plateau value of 11-16 mN/m. In this region the dextran chains stretch out into the water phase to form a polymer brush (c). The main contribution to the interfacial pressure in this region results from the interacting dextran chains in the air–water surface, corresponding to the saturated interfacial pressure of dextran (16 mN/m, see figure 3.3). The PS block of the copolymer, at the air–water interface, prevents the dextran chains from dissolving in the water phase. At approximately 5.5 nm²/molecule all dextran chains are desorbed from the interface. Additional compression causes a sharp increase of the interfacial pressure, due to the repulsive interactions between the dextran chains in the polymer brush (d). At $\Pi = 45$ mN/m the monolayer collapses at an area of nearly 3 nm²/molecule (e). The different conformations of the copolymer at the interface are drawn schematically in figure 3.6, corresponding to a – e in figure 3.5.

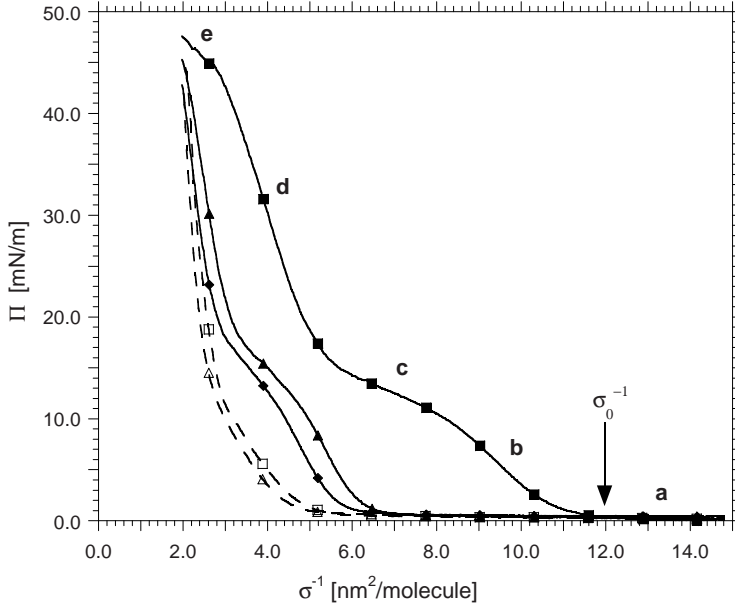


FIGURE 3.5. Interfacial pressure–area per molecule isotherms for PS(12300)-b-Dextran(6000) at room temperature. Successive compression and expansion curves: first compression (—■—), first expansion (—□—), second compression (—▲—), second expansion (—△—) and third compression (—◆—).

The expansion isotherms and the second and third compression isotherm do not coincide with the first compression isotherm, indicating that during compression/expansion equilibrium is not attained. This hysteresis will be discussed in more detail in section 3.2.2.

For a polymer brush in a good solvent the conformation is determined by a balance between the segment-segment excluded volume interactions, causing the chains to stretch, and the entropic cost of this stretching, causing the chains to contract. Polymer brush models describe the relation between the interfacial pressure of a brush (Π_b), the chain length (N) and the grafting density (σ). According to the Alexander–de Gennes model the pressure scales as $\Pi_b \sim N\sigma^{11/6}$.^{6,64} Analytical and numerical self-consistent-field (SCF) models predict a scaling of $\Pi_b \sim N\sigma^{5/3}$.^{36,119,174} In figure 3.7 the first compression isotherm of the Dextran(6000) brush is plotted as $\ln \Pi_b$ versus $\ln \sigma^{-1}$ for the brush regime (region **d** in figure 3.5). $\Pi_b = \Pi - \Pi_{\text{plateau}}$, Π_{plateau} is the saturated interfacial pressure of a

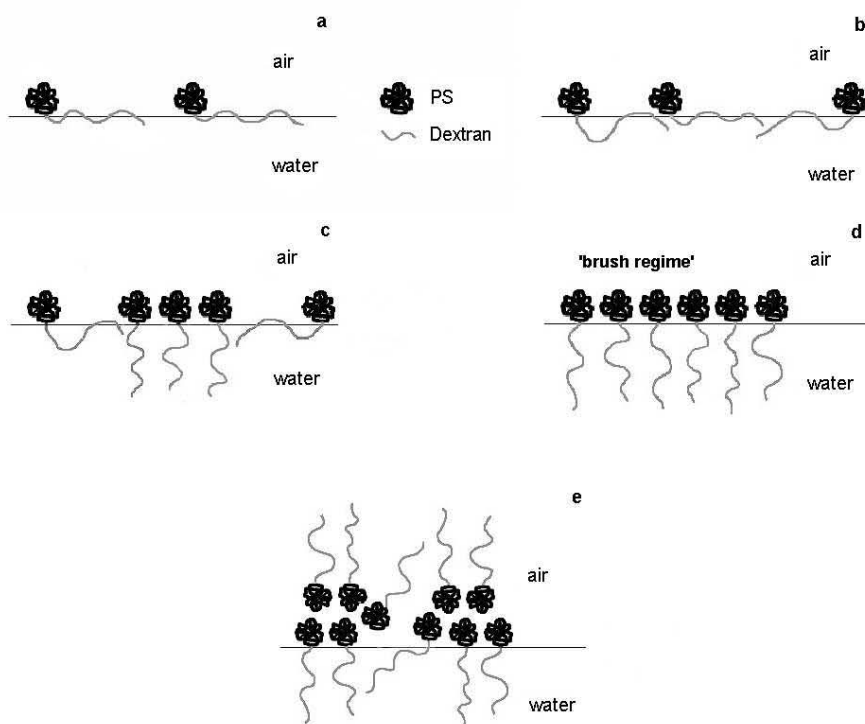


FIGURE 3.6. Conformations of PS-b-Dextran at the air–water interface: adsorbed at the interface (a), desorption from the interface (b), polymer brush formation (c), compression of the polymer brush (d), and collapse of the monolayer (e).

Dextran(6000) monolayer, with a value of 16.0 mN/m, as mentioned before. Lines corresponding to power laws of $11/6$ and $5/3$ are drawn for comparison. Figure 3.7 demonstrates that for sufficiently dense brushes the scaling behaviour approaches predicted power laws, even though the dextran chain is relatively short. The scaling exponent at high grafting densities is approximately 2.2, somewhat higher than predicted by the polymer brush models. Variation of Π_{plateau} between 11.0 and 17.0 mN/m showed only a slight change in the scaling exponent of Π_b (data not shown). Corrections, by assuming 25 wt% unreacted PS and consequently lower grafting densities, results in a scaling exponent of about 1.8, which is in good agreement with the predicted power laws. However, 25 wt% unreacted PS is over-estimated. The yield of less than 100% is also caused by loss of copolymer during purification (see section 3.1). To verify whether the polymer brush models are

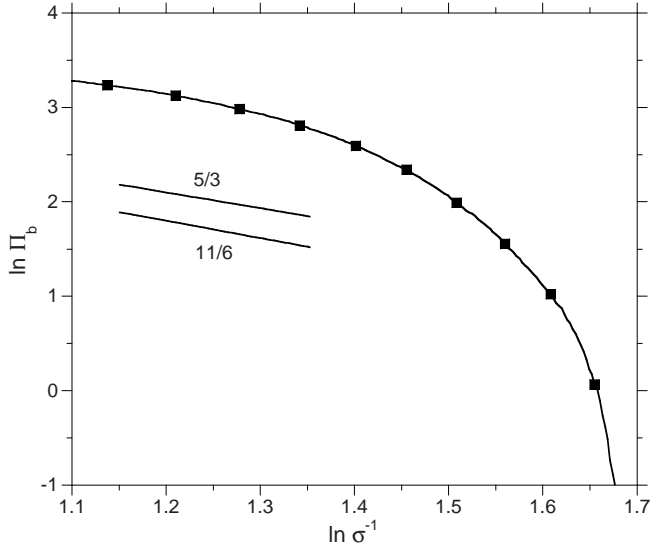


FIGURE 3.7. Interfacial pressure of Dextran(6000) brush (Π_b) vs area per molecule (σ^{-1}). Experimental ($-\blacksquare-$), Alexander-de Gennes model (scaling exponent 11/6) and SCF model (scaling exponent 5/3).

<i>PS-b-polysaccharide</i>	Π_{plateau} [mN/m]	σ_o^{-1} [nm ² /molecule]
PS(12300)-b-Glucose	16 ^a	8.2
PS(12300)-b-Maltodextrin(850)	18 ^a	6.5
PS(12300)-b-Maltodextrin(1150)	17 ^a	6.2
PS(12300)-b-Maltodextrin(2800)	17 ^a	5.9
PS(12300)-b-Dextran(1500)	16	8.0
PS(12300)-b-Dextran(6000)	16	12.0

^a The values of Π_{plateau} for PS(12300)-b-Glucose and the PS(12300)-b-Maltodextrins are average values of Π in the semi plateau region.

TABLE 3.2. Π_{plateau} and σ_o^{-1} values of different PS-b-polysaccharides determined from interfacial pressure isotherms.

applicable for polysaccharide brushes, a broader range of copolymers with longer polysaccharides is needed.

The other synthesized copolymers, PS(12300)-b-Dextran(1500) and the PS(12300)-b-Maltodextrins, show interfacial pressure isotherms similar to those of PS(12300)-b-Dextran(6000), including hysteresis. However, the values of σ_o^{-1} are different, as shown in table 3.2. The Π_{plateau} -values seem to be rather constant, indicating

a uniform saturated interfacial pressure for the different polysaccharides. Moreover, the semi plateau regime of PS(12300)-b-Dextran(1500) is smaller than that of PS(12300)-b-Dextran(6000) and the PS(12300)-b-Maltodextrins do not have pronounced plateau behaviour at all; the Π_{plateau} values of the PS(12300)-b-Maltodextrins in table 3.2 are average values of Π in the semi plateau region. These differences are in accordance with previous research on amphiphilic block copolymers with varying hydrophilic block lengths (*e.g.* PS-b-PEO by Bijsterbosch *et al.*¹¹). Considering the range of the semi plateau regime, it was associated with the length of the hydrophilic block of the copolymer: the longer the hydrophilic block length, the more time it takes to completely desorb the polymer chain from the air–water surface upon compression, and the broader the semi plateau regime.

The differences between the σ_o^{-1} -values in table 3.2 are due to differences in polysaccharide type and chain length: for longer polysaccharides the onset of the interfacial pressure increase starts at higher values of σ^{-1} , because larger molecules start to interact at larger area per molecule.

Hysteresis; Chain Interactions and Time Dependency

Compression of PS-b-PEO₇₇₀ copolymer at the air–water interface shows no hysteresis¹¹ (see figure 2.4, chapter 2). PEO is a very flexible polymer and accordingly adsorbs and desorbs rapidly at the surface.¹²⁰ In case of PS-b-polysaccharide copolymers hysteresis is observed in the interfacial pressure isotherms. This may be due to loss of copolymer from the monolayer, or it may be an intrinsic property of the monolayer itself.¹¹² To discriminate between these two possibilities, compression/expansion cycles were performed with PS(12300)-b-Dextran(6000), where time intervals in between cycles as well as the compression rates were varied. The time interval, the time between completion of the expansion and start of the compression, ranged from 0 to 900 minutes. The compression rate was varied from 5 to 100 mm²/s. The difference between the onset area values (σ_o^{-1}) of the first and second compression isotherm ($\Delta\sigma_o^{-1}$) can be considered a measure for the hysteresis.

The values of $\Delta\sigma_o^{-1}$ are presented as function of the time interval in figure 3.8. Figure 3.9 displays the $\Delta\sigma_o^{-1}$ -values as function of the compression rate. When the time interval is increased or the compression rate decreased, the hysteresis diminishes ($\Delta\sigma_o^{-1}$ decreases). This is also reflected in a less dramatic drop of Π upon expansion (data not shown). It suggests that, during expansion and compression, the dextran chains need some time to adsorb and desorb, respectively,

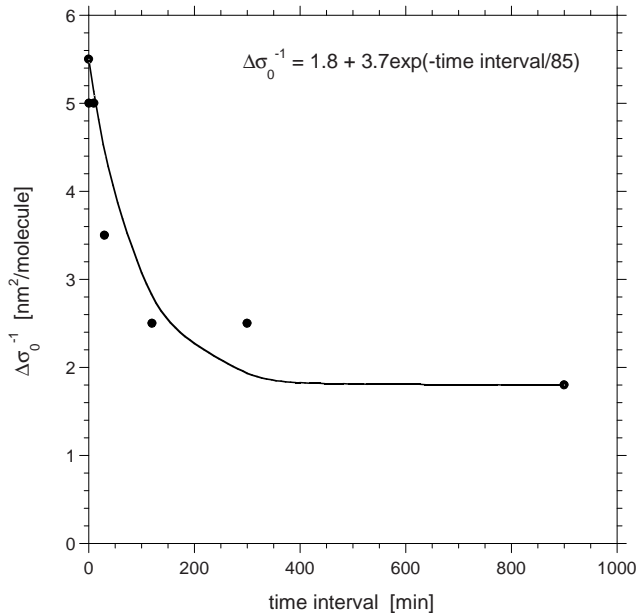


FIGURE 3.8. Influence of time interval (between expansion and compression) on hysteresis in the interfacial pressure isotherm of PS(12300)-b-Dextran(6000): experimental (●) and exponential curve fit (—), with relaxation time of 85 min. ($\Delta\sigma_o^{-1}$, see text).

from the air–water interface and adapt to a more favourable conformation. Fitting of the data in figure 3.8 to an exponential relaxation function results in a relaxation time of 85 minutes (indicated in figure 3.8). Apart from the time dependency of the hysteresis, the results in both figure 3.8 and 3.9 show a time independent hysteresis of $\Delta\sigma_o^{-1} \approx 1.5 - 1.8 \text{ nm}^2/\text{molecule}$. This indicates a permanent change in the structure of the copolymer or loss of copolymer during the experiment. The latter is less likely, because of the (large) PS block keeping the copolymer at the air–water surface.

To explain the behaviour of monolayers of PS-b-Dextrans and PS-b-Maltodextrins upon compression and expansion we consider the mutual interactions between the PS chains and the polysaccharide chains and the interaction of the polysaccharide chains with water. Dextrans and maltodextrins are rather stiff molecules compared to flexible molecules like PEO; desorption from and adsorption at the air–water surface is therefore presumably slow in comparison with PEO. This

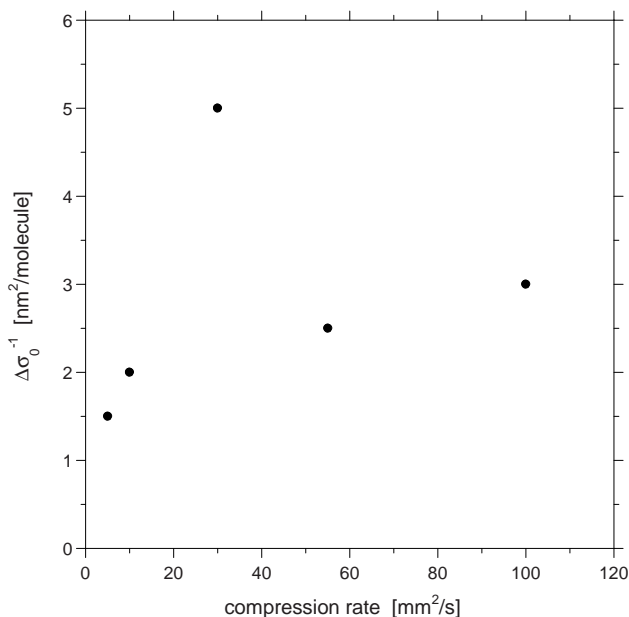


FIGURE 3.9. Influence of compression rate on hysteresis in the interfacial pressure isotherm of PS(12300)-b-Dextran(6000) (■) ($\Delta\sigma_0^{-1}$, see text).

probably leads to the observed hysteresis in the interfacial pressure isotherm (figure 3.5). Furthermore, the hydroxyl groups of the polysaccharide chains may form H-bonds between neighbouring glucosyl units of the same chain or neighbouring polysaccharide chains.²⁷ In addition, H-bonds can be formed with water molecules, where water molecules can be shared by hydroxyl groups of adjacent polysaccharide chains.²⁷ These H-bonds contribute to the stiffness of the chains and support aggregate formation. Upon expansion these aggregates break up only slowly, because it requires activation energy.

Kumaki demonstrated that monolayers of PS at an air–water interface may also aggregate.¹⁰⁰ Upon compression the PS particles tend to rearrange and form aggregates, which do not, or only partially, break up during expansion. This causes a shift of the second and following compression cycles towards lower values of σ^{-1} , which can also be seen in figure 3.4.

As judged from figure 3.5 the influence of the interactions between the polysaccharide chains dominate the interfacial pressure behaviour of the block copolymers. This is illustrated by the extent of hysteresis between PS (figure 3.4) and

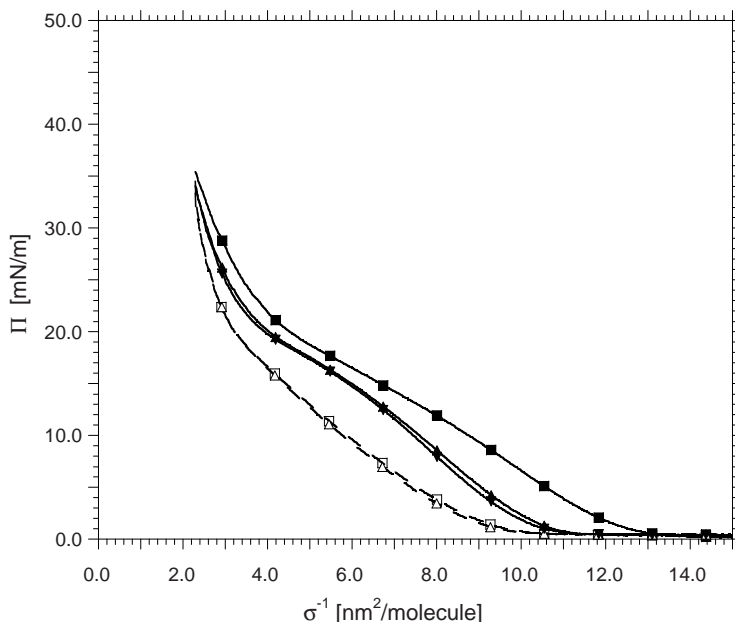


FIGURE 3.10. Interfacial pressure–area per molecule isotherms for PS(12300)-b-Dextran(6000) with 2.5 wt% glycerol in water phase, at room temperature. Successive compression and expansion curves: first compression (—■—), first expansion (---□---), second compression (—▲—), second expansion (---△---) and third compression (—◆—).

PS(12300)-b-Dextran(6000) (figure 3.5). In figure 3.10 another set of interfacial pressure isotherms is presented for PS(12300)-b-Dextran(6000) with 2.5 wt% glycerol added to the water phase. Glycerol is known to form H-bonds with carbohydrates, thereby preventing the formation of intra- and inter-molecular H-bonds in carbohydrates, and hence, serves as a plasticizer in carbohydrate-based materials.¹⁵⁰ A small amount of 2.5wt% glycerol in the water phase reduces the hysteresis considerably. This gives support to the hypothesis that the hysteresis is due to H-bonds between polysaccharide chains, in addition to the slow adsorption and desorption of the polysaccharide chains. Adding 2.5wt% glycerol to the water phase has no significant influence on the interfacial pressure of ‘pure’ water.

3.4. Conclusions

Linear diblock copolymers of polystyrene and dextrans, respectively maltodextrins, were synthesized successfully. Yields of 75 to 95 wt% were achieved. IR

spectroscopy confirmed the coupling of amino-terminated PS and the different polysaccharides. Moreover, the interfacial behaviour of a monolayer of the synthesized copolymers points to a successful coupling. The interfacial pressure pattern of the copolymers is typical for amphiphilic compounds and is clearly different from those of the individual PS and polysaccharides. The copolymers demonstrate interfacial pressure hysteresis between consecutive compression and expansion cycles of a monolayer. This is due to slow adsorption/desorption of the polysaccharide chains at the air–water surface and the formation of aggregates of copolymer at the interface. Both the PS chains and the polysaccharide chains can aggregate. However polysaccharide aggregation, due to H-bonds between adjacent chains, seems to be predominantly responsible for the observed hysteresis. Increasing the time interval between expansions and compressions or reducing the compression rate reduces the extent of hysteresis. The relaxation time for the hysteresis is 85 minutes.

The synthesis method here described proved to be unsuccessful for the coupling of long polysaccharides ($M_w > 6000$ Da). A different synthesis approach is needed for longer polysaccharides, which will be the focus of future research, together with the preparation of polymer brushes (LB films) of the different PS-b-polysaccharides and protein adsorption experiments on the polymer brushes.

Acknowledgement

The syntheses of the PS-b-polysaccharide copolymers described in this chapter were performed by Karoly Ágoston. I thank him for all the work he has done on the syntheses and also for the pleasant collaboration. Ted Slaghek and Johan Timmermans from TNO Food are thanked for their contributions and discussions concerning the synthesis of polysaccharide block copolymers.

CHAPTER 4

Polystyrene-b-Dextran by Epoxide–Amine Coupling

4.1. Introduction

In the previous chapter the synthesis and interfacial behaviour of different polystyrene (PS) - polysaccharide diblock copolymers were described, including PS(12300) - b - Dextran(6000) (block copolymer of PS with weight-average molecular mass (M_w) of 12300 Da and dextran with M_w of 6000 Da). A block coupling method, based on reductive amination of dextran with amine-terminated PS, as described by Loos,^{106–108} was used. The block copolymers are applied to prepare dextran brushes, that are used in protein adsorption studies. Our purpose is to investigate the influence of the dextran block length on the protein adsorption. However, with the method used in chapter 3, synthesis of PS-b-Dextran with dextran $M_w > 6000$ Da proved to be unsuccessful. We therefore synthesized PS-b-Dextran in a different way. The synthesis and interfacial behaviour of these block copolymers are described in this chapter. As in chapter 3, a block coupling method was chosen, to be able to control the block length of PS and dextran. Though, this time 1,6-diaminohexane (DAH) was used as a spacer between the PS and dextran block, to increase the effectiveness of the coupling reaction. First, DAH was coupled to dextran through reductive amination. Because a large excess of DAH was used, a high yield of DAH-dextran is obtained. Next, the DAH-dextran was coupled to epoxide-terminated PS. The reaction of an amine with an epoxide is very efficient.⁷⁸ Because of the two-step reaction procedure the overall reaction efficiency was expected to be high. Low molecular weight maltodextrins were used to test the coupling mechanism with the DAH spacer.

The products were characterized with NMR and IR spectroscopy. Moreover, interfacial behaviour at the air-water interface was used to identify typical behaviour for amphiphilic block copolymers, thereby providing more definitive proof of the coupling.

The epoxide-terminated PS used here has a M_w of 2100 Da, different from the PS M_w in the previous chapter. The influence of the PS block length on the interfacial behaviour of the PS-b-Dextran copolymers will be demonstrated. The homogeneity of the PS-b-Dextran layer at different grafting densities was investigated with Atomic Force Microscopy (AFM). The AFM images were recorded using Langmuir-Blodgett (LB) depositions of PS-b-Dextran monolayers transferred to a PS coated silicon wafer.

4.2. Experimental

4.2.1. Materials and Methods

Dextran (M_w 6000 Da, $M_w/M_n = 1.65$, Fluka (M_n is number-average molecular mass, M_w/M_n indicates polydispersity) and M_w 8500-11500 ('10000'), Sigma), maltodextrins (Paselli MD20, M_n approximately 850 and Paselli MD6, M_n about 2800, AVEBE) and vinyl-terminated polystyrene (M_w 2100 Da, $M_w/M_n = 1.11$, Polymer Source Inc.). 1,6-Diaminohexane (DAH), sodium cyanoborohydride, oxone, tetrahydrothiopyran-4-one (THTP), ethylenediamine tetraacetic acid(EDTA), tetrabutylammonium hydrogen sulphate (TBAHS) and the solvents acetic acid (AcOH), dioxane, dimethylformamide (DMF), dimethylsulphoxide (DMSO), ammonia and ethyl acetate - all purchased from Aldrich. Solvents from Aldrich were used without further purification (except for DMSO). Dialysis membrane (MWCO=1000 and MWCO=3500) was purchased from Spectrum, cationic exchange resin (Amberlite IR-120) and molecular sieve 3 Å from Aldrich. $^1\text{H-NMR}$ (200 MHz) and $^{13}\text{C-NMR}$ (50 MHz) spectra were obtained with a DPX 200 spectrometer (Bruker) and the IR spectra were recorded on a Vector 22 FTIR spectrometer (Bruker). Silicon wafers (Si(100)), with 2-3 nm SiO_2 (Wafernet GmbH).

4.2.2. Synthesis Procedures

Synthesis of DAH-linked Polysaccharides. The reaction was carried out under the following conditions, using Maltodextrin(850) as an example: a 50 ml round-bottom flask equipped with a Teflon-coated magnetic stirrer and reflux cooler was charged with 1.44g (12.4 mMol) of DAH, 0.6g (9.6 mMol) of sodium cyanoborohydride, 0.35 ml of acetic acid and 10 ml of DMF and the mixture was slowly heated for 3 hours to reach 85 °C. During this period 1.02 g (1.2 mMol) of Maltodextrin(850) was added in small portions. The reaction mixture was maintained at 85 °C for 24 hours. After cooling the reaction mixture to room temperature, 100 ml of p-xylene was added and then the solutes were concentrated by vacuum distillation (bath temperature no more than 45 °C). The obtained product was dissolved in 50 ml of water and the component precipitated with 200 ml of absolute ethanol. The precipitate was filtered and repeatedly washed with small portions of absolute ethanol and acetone. The obtained powder was dissolved in 75 ml of deionized water and passed through a strong cationic exchange column (2 cm diameter x 50 cm length, packed with Amberlite IR-120). The unreacted polysaccharide (150 mg) was washed off with water. The DAH-linked polysaccharide was eluted with a 10% ammonia solution. The eluate was concentrated under reduced

pressure to give 910 mg of a slightly yellow powder which was expected to be the DAH-linked Maltodextrin(850). From this amount of product, it can be calculated that 80% of the Maltodextrin(850) was coupled to DAH (yield = 80 Mol%).

DAH-linked Maltodextrin(850) ^{13}C -NMR (D_2O , ppm): 102.141 (C1, anomeric), 79.274, 75.857, 75.375, 75.271, 74.235, 74.050, 64.705, 62.961 (C2-C6 from maltodextrin), 41.954 (maltodextrin-NH-CH₂(CH₂)₄CH₂-NH₂), 28.987 (maltodextrin-NH-CH₂CH₂(CH₂)₂CH₂CH₂-NH₂), 28.133 (maltodextrin-NH-(CH₂)₂(CH₂)₂(CH₂)₂-NH₂)

DAH-linked Maltodextrin(2800) ^{13}C -NMR (D_2O , ppm): 101.151 (C1, anomeric), 75.848, 73.850, 72.629, 71.960, 67.960 (C2-C6 from maltodextrin), 41.774 (maltodextrin-NH-CH₂(CH₂)₄CH₂-NH₂), 28.966 (maltodextrin-NH-CH₂CH₂(CH₂)₂CH₂CH₂-NH₂), 27.583 (maltodextrin-NH-(CH₂)₂(CH₂)₂(CH₂)₂-NH₂)

DAH-linked Dextran(6000) ^{13}C -NMR (DMSO, ^6d , ppm): 98.008 (C1, anomeric), 73.707, 72.134, 70.717, 68.575, 65.838 (C2-C6 from dextran), 39.638 (dextran-NH-CH₂(CH₂)₄CH₂-NH₂), 26.810 (dextran-NH-CH₂CH₂(CH₂)₂CH₂CH₂-NH₂), 25.551 (dextran-NH-(CH₂)₂(CH₂)₂(CH₂)₂-NH₂)

DAH-linked Dextran(10000) ^{13}C -NMR (DMSO, ^6d , ppm): 102.498 (C1, anomeric), 78.142, 76.342, 74.908, 74.365, 70.181 (C2-C6 from dextran)

Note: in the case of Maltodextrin(2800), Dextran(6000) and Dextran(10000) DMSO was used as solvent instead of DMF. The solvent and the unreacted reagents were removed by dialysis against water, using dialysis membranes (MWCO = 1000 and MWCO = 3500). The aqueous solutions obtained after dialysis were concentrated by vacuum distillation and then passed through a strong cationic exchange column. Unreacted polysaccharide was removed with water. The product was eluted with 10% ammonia solution and finally concentrated under reduced pressure to give DAH-linked maltodextrin or dextran.

Synthesis of Epoxide-terminated Polystyrene. To a 50 ml round-bottom flask with a Teflon-coated magnetic stirrer, 375 mg (0.196mMol) of vinyl-terminated PS, 25 mg (0.23 mMol) of THTP, 100 mg (0.294 mMol) of TBAHS, 5 ml of aqueous EDTA $4 \cdot 10^{-4}$ M solution and 10 ml of dioxane was added. After 3-4 hour of intense

stirring at room temperature (dissolving the vinyl-terminated PS), a mixture of 1g (1.63 mMol) of oxone and 0.450 g (5.35 mMol) of sodium bicarbonate was added in small portions over a period of 3 hr at room temperature. Thereafter the reaction mixture was stirred for 2 more hours at room temperature until evolution of gas bubbles was no longer observed. The content of the flask was diluted with 50 ml water, transferred to a separating funnel and extracted repeatedly with 100 ml of ethyl acetate. The pooled organic layers were washed with 50 ml of salt water, dried over anhydrous magnesium sulphate, filtered and concentrated under reduced pressure. The yield was 315 mg (as a mixture of vinyl-terminated PS (40 Mol%) and epoxide-terminated PS (60 Mol%)).

$^1\text{H-NMR}$ (CDCl_3 , ppm): 6.2-7.2 (Broad peak, C_6H_5 , C_6H_4 , H_B), 5.90 (dd, H_A or H_B), 5.40 (dd, H_A or H_B), 3.85-4.2 (H_b), 3.31 (dd, H_a or H_b), 2.91 (dd, H_a or H_b), 1.25-2.0 (broad peak, $(-\text{CH}_2-\text{CH}(\text{Ph}))_p-\text{CH}_2\text{CH}_2\text{O}-$)

Coupling of DAH-linked Dextran with Epoxide-terminated Polystyrene. In a 25 ml round bottom flask with magnetic stirrer, 2.6 g of DAH-linked dextran 6000 (dried in a vacuum oven for one week at 75 °C) was dissolved in 5 ml DMSO (distilled over CaH_2 and kept over a molecular sieve 3 Å) at 60 °C. When the reaction mixture turned clear, a solution of 200 mg of epoxide-terminated PS (60 Mol%), dissolved in 3 ml of anhydrous THF, was added drop by drop, under argon, during one day. The reaction mixture was stirred for 5 days at 60 °C. Subsequently the mixture was cooled to 30 °C and diluted with 50 ml of DMSO. The obtained solution was dialysed against deionized water, using a dialysis membrane (MWCO=3500). After two days the dialysed solution was filtered over a G5 sintered glass funnel and a white precipitate was obtained. The precipitate was washed several times with cold water to remove the excess polysaccharide. Subsequently, the precipitate was dried in a vacuum oven at 50 °C for 48 hours. To remove unreacted vinyl-terminated PS, the precipitate was suspended in chloroform and sonicated in an ultrasonic bath at room temperature for 24 hours. The precipitate was filtered and dried over P_2O_5 in a vacuum desiccator to obtain the copolymer as a slightly yellow powder. The yield was 88 mg (11 Mol%) PS(2100)-b-Dextran(6000). The yield for PS(2100)-b-Dextran(10000) was 53 mg (5 Mol%).

PS(2100)-b-Dextran(6000): $^1\text{H-NMR}$ (DMSO, ^6d , 80 °C, ppm): 6.4 - 7.4 (broad peak, C_6H_5 , C_6H_4), 4.80 (d, $\text{H}_{\text{anomeric}}$ from $(\text{C}_6\text{H}_{10}\text{O}_5)_n$), 3.1 - 3.9 (H_2 - H_6 from $(\text{C}_6\text{H}_{10}\text{O}_5)_n$), 1.2 - 2.1 (broad peak, from $(-\text{CH}_2-\text{CH}(\text{Ph}))_p-\text{CH}_2\text{CH}_2\text{O}-$)

and DAH linker (-NH(CH₂)₆NH-)

PS(2100)-b-Dextran(10000): ¹H-NMR, (DMSO, ⁶d, 80 °C, ppm): 6.5-7.2 (broad peak, C₆H₅, C₆H₄), 4.8 - 4.9 (d, H_{anomeric} from (C₆H₁₀O₅)_n), 3.2 - 4.7 (H₂ - H₆ from (C₆H₁₀O₅)_n), 1.2 - 1.8 (broad peak from (-CH₂-CH(Ph)-)_p-CHOHCH₂- and DAH linker (-NH(CH₂)₆NH-))

4.2.3. Interfacial Behaviour

Π versus σ⁻¹ Isotherms. The procedure to obtain the interfacial pressure (Π) versus area per molecule (σ⁻¹) isotherms at room temperature for PS(2100)-b-Dextran(6000) and PS(2100) - b - Dextran(10000) is similar to the procedure for PS(12300) - b - Dextran(6000) described in chapter 3, except for the use of chloroform as spreading solvent, because the newly synthesized copolymers did not dissolve in chloroform. Instead, the PS(2100)-b-Dextran copolymers were dissolved in DMSO (distilled over CaH₂ and kept over a molecular sieve 3 Å) at 70 °C at a concentration of 0.49 g/l under vigorous stirring. Because DMSO is miscible with water, the Trunitt method was used to bring the block copolymer on the air-water interface.¹⁶⁰ After 10 minutes, to allow for dissolution of DMSO in the water phase, compression/expansion cycles of the copolymer film were started at a speed of 30 mm²/s, while recording Π. Reproducibility of the isotherms was tested by performing experiments in duplicate.

Langmuir-Blodgett Deposition. The homogeneity of the PS-b-Dextran monolayers was studied with tapping mode AFM. To this end, a compressed PS-b-Dextran copolymer monolayer was transferred from the air-water interface to a PS-coated silicon wafer, using the Langmuir-Blodgett (LB) deposition technique,^{13,14,139} as previously described for PS-b-PEO copolymers^{39,126} (also see chapter 2). It turned out that the Π versus σ⁻¹ isotherms do not behave in a reversible, time-independent manner, as expected for an equilibrium situation, *i.e.* a time-dependent hysteresis is observed. Therefore, in the LB deposition, at each σ the freshly added PS-b-Dextran monolayer was compressed once and left to relax at the desired grafting density. After relaxation, two PS-coated wafers, put side by side (to produce duplicates), were vertically inserted through the copolymer film into the sub phase while keeping Π constant, thereby transferring the monolayer to the wafers. A dipping 'speed' of 1 mm²/s was used. Subsequently the wafers were heated for 10 min. at 120 °C (that is beyond the glass transition temperature of PS) in an oven, allowing diffusion of the PS-block of the copolymer into the PS sublayer. After

cooling to room temperature, the PS layer becomes glassy. This treatment results in block copolymers that are irreversibly attached to the surface.

4.2.4. AFM

Tapping mode AFM was applied to investigate the structure of the PS-b-Dextran monolayers in water, prepared with LB deposition on PS-coated silicon wafers as described in the previous section. A Nanoscope III, Veeco Instruments Inc. was used, equipped with a fluid cell filled with ultra pure water (Seralpur Pro 90C, conductivity $< 0.055 \mu\text{S}/\text{cm}$, pH 6). Veeco TESP silicon cantilevers were used with length of $125 \mu\text{m}$ and tip radius of 10 nm. $1 \times 1 \text{ cm}^2$ pieces were cut from the LB wafers, placed in the fluid cell and covered with ultra pure water. The surface was scanned in tapping mode at a scan rate of 0.5–1 Hz and with a cantilever driving frequency of 130 kHz. 3D AFM images are obtained, as well as a cross section perpendicular to the scanning direction. To test the smoothness of the spincoated PS layer, contact mode AFM in air was performed. For that Veeco DNP silicon nitride cantilevers were used with a tip radius of 20 nm and a scan rate of 2 Hz.

4.3. Results and Discussion

4.3.1. Synthesis

DAH-linked Polysaccharides.

Our goal was to develop methods and procedures that could specifically be adapted for the synthesis and purification of PS-b-Dextran using DAH-linked polysaccharides with high molecular weight (6000, 10000 and higher) and epoxide-terminated PS. First we discuss the synthesis of DAH-linked polysaccharides. As model compounds for high molecular weight dextrans, Maltodextrin(850) and Maltodextrin(2800) were chosen. Maltodextrin is composed of $\alpha(1 \rightarrow 4)$ -linked glucosyl units, dextran of $\alpha(1 \rightarrow 6)$ -linked glucosyl units. To create a new C-N bond between a carbohydrate (in the open-chain aldehyde form) and a diamine, the reductive amination reaction was chosen with sodium cyanoborohydride as reducing agent,¹⁵ see figure 4.1.

Although the reaction works best in the pH range of 6 to 8, the reaction has also shown to proceed successfully at a pH as low as 4 and as high as 10.¹³¹ A series of UV labels was linked with oligosaccharides by reductive amination with yields that vary from good to excellent: 2-aminopyridine,⁸² p-aminobenzoic

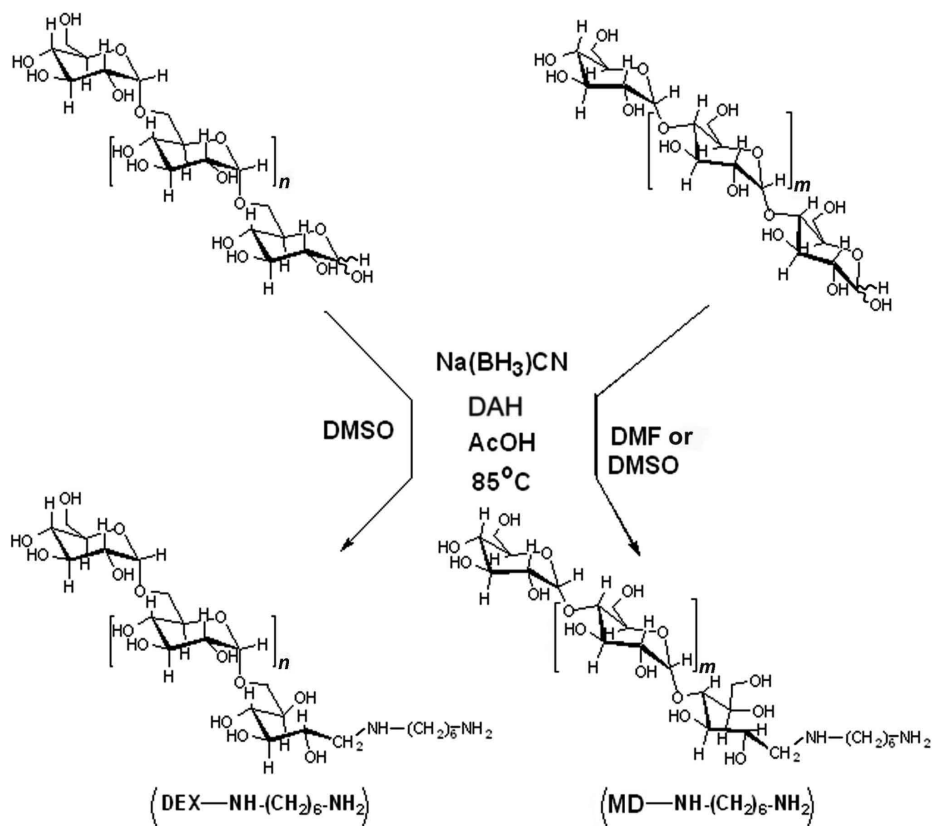


FIGURE 4.1. Synthesis of DAH-linked polysaccharides: reductive amination of maltodextrin (MD) ($m=3$ or 15) and dextran (DEX) ($n=35$ or 60) with DAH and sodium cyanoborohydride as reducing agent.

Polysaccharide	Polysacch. [g]	DAH [g]	Molar ratio polysacch.:DAH	$\text{Na}(\text{BH}_3)\text{CN}$ [g]	Solvent/AcOH [ml]/[ml]	Yield [Mol%]
Maltodextrin(850)	1.02	1.44	1:10	0.60	A 10/0.35	80
Maltodextrin(2800)	3.00	3.00	1:24	1.60	B 5/0.73	85
Dextran(6000)	3.00	3.60	1:62	2.40	B 8/0.88	78
Dextran(10000)	3.00	3.60	1:103	2.40	B 10/1.2	63

A = DMF, **B** = DMSO.

TABLE 4.1. Reaction mixtures and reaction yields of the DAH-link reaction.

acid,⁷⁰ 4-aminobenzonitrile,¹⁴³ 8-aminonaphtalene-1,3,6-trisulfonic acid,¹⁵⁴ and 3-(4-carboxybenzoyl)-2-quinoline carboxyaldehyde.¹⁰⁵ We have modified the procedure of Williams (commonly used for short oligosaccharides or branched oligosaccharides) to apply to polymeric carbohydrate.¹⁵⁷ To achieve high conversion of

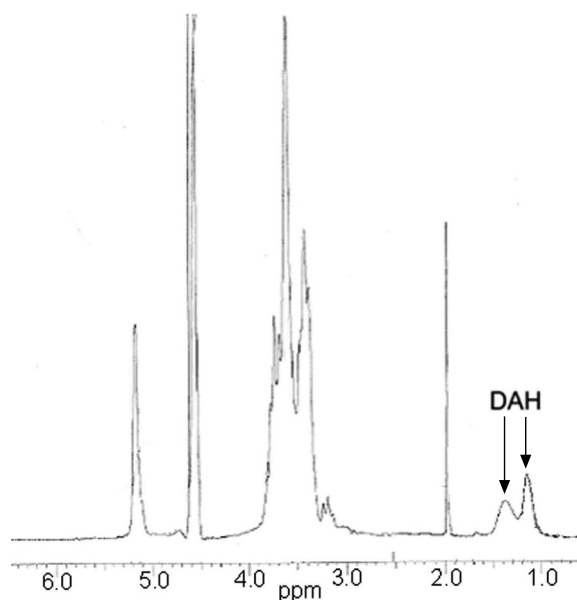


FIGURE 4.2. ^1H -NMR of DAH-linked Maltodextrin(2800) in D_2O at $25\text{ }^\circ\text{C}$.

polysaccharides, a large excess of DAH was used (also to avoid the formation of diblock polysaccharide as a result of double reductive amination on the same molecule of DAH). The conditions for obtaining DAH-linked polysaccharides are presented in table 4.1. The molar ratios polysacch.:DAH in table 4.1 indicate the large excess of DAH used.

The obtained DAH-linked polysaccharides were separated from uncoupled polysaccharides by ion-exchange chromatography. A ninhydrin test of the aqueous solution of purified DAH-linked polysaccharides gave a positive result (presence of amine groups) and inspection by TLC showed no unreacted DAH. From this we concluded that the products were pure enough for investigation by NMR spectroscopy and for further use in the coupling with epoxide-terminated PS.

^{13}C -NMR spectra show three signals between 25 and 42 ppm (except for DAH-linked Dextran(10000)) that correspond to aliphatic carbons from DAH, confirming a successful reductive amination reaction. In case of DAH-linked Dextran(10000) no ^{13}C -NMR-peaks from DAH-aliphatic carbons could be detected, probably due to the large excess of carbons present from the Dextran(10000). The ^1H -NMR spectra verify a successful reaction, for all polysaccharides. As an

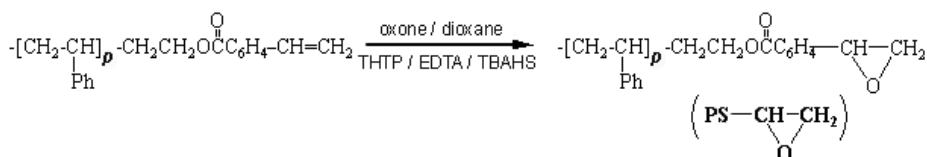


FIGURE 4.3. Epoxidation of the double bond of vinyl-terminated PS (p=18) with oxone, in phase transfer catalyst conditions.

example the $^1\text{H-NMR}$ spectrum for DAH-linked Maltodextrin(2800) is shown in figure 4.2: the region 4.5-5.3 ppm points to the presence of anomeric protons from glucose units, the region 3.0-3.9 ppm corresponds to H2-H6 of glucose units and the region 1.0-1.5 ppm corresponds to aliphatic protons of the DAH-linker. Furthermore, electrospray ionization quadrupole time-of-flight tandem mass spectrometry verified the successful coupling of DAH with the maltodextrins and Dextran(6000) (data published elsewhere).¹⁴⁷

Epoxide-terminated Polystyrene. The epoxidation of vinyl-terminated PS has so far not been reported in literature. In contrast, the epoxidation of the double bond of styrene is well documented. There are several oxidizing agents that can be used for this: m-chloroperbenzoic acid with or without N-methyl-morpholine-N-oxide in dichloromethane,^{153,173} H_2O_2 in acetonitrile (*in situ* generation of peroxy-carboximidic acid) with MnSO_4 as catalyst,^{101,159} NaIO_4 in acetonitrile/water,¹⁵⁸ NaClO in the presence of catalytic or stoichiometric amounts of bromide⁹⁶ and trichloroisocyanic acid followed by treatment of the resulting chlorohydrin with aqueous KOH in ether/pentane.¹⁷⁰ The best result for epoxidation of styrene (70 Mol%, quantitative yield) was obtained using dioxirane, a powerful and environmentally safe oxidant that can be generated *in situ* from ketones and oxone ($2\text{KHSO}_5\cdot\text{KHSO}_4\cdot\text{K}_2\text{SO}_4$).³

This last approach was applied to vinyl-terminated PS, essentially using the method of Wong,¹⁷² as depicted in figure 4.3. The following modifications were applied (see figure 4.3): first, instead of acetonitrile, dioxane was used as solvent, in order to improve the solubility of the polymer. Second, in order to facilitate the access of oxidizing reagent in organic media, TBAHS was utilized as phase transfer catalyst. The best yield obtained was 60 Mol%. Other attempts using any of the epoxidizing reagents mentioned above failed in obtaining higher conversions. However, the relatively low yield of 60 Mol% is not surprising, in fact corresponding to reaction efficacies found in literature.^{3,172} The efficacy of epoxidation by dioxirane

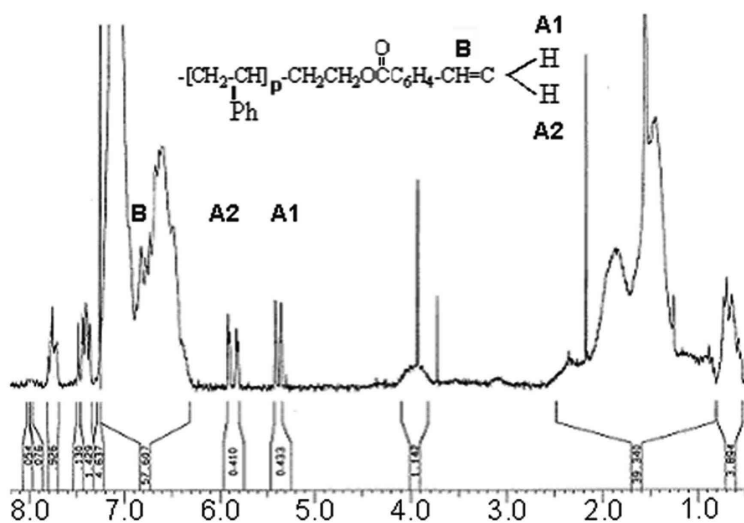


FIGURE 4.4. $^1\text{H-NMR}$ spectrum of vinyl-terminated PS obtained in CDCl_3 at 25°C .

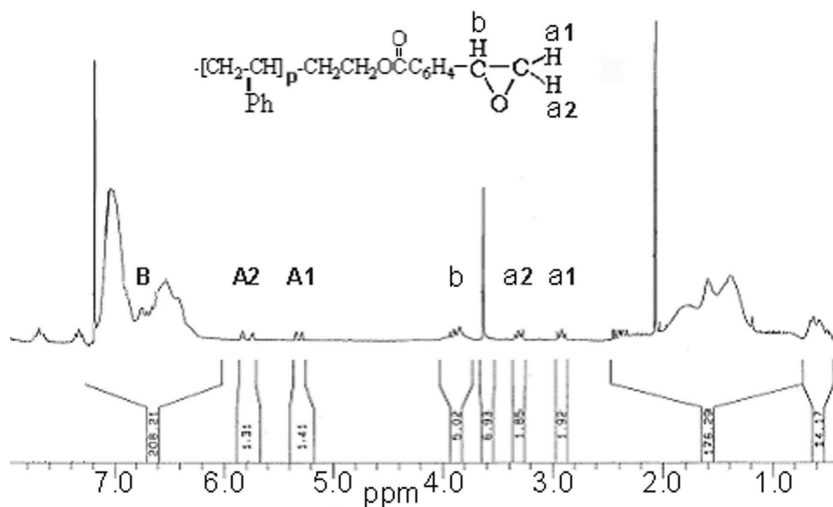


FIGURE 4.5. $^1\text{H-NMR}$ spectrum of the oxidation product of vinyl-terminated PS obtained in CDCl_3 at 25°C .

is strongly dependent on the substrate that is being oxidized. For example, the conversion of 1-dodecene is 43 Mol%.³ Likely, unwanted side-reactions occur.

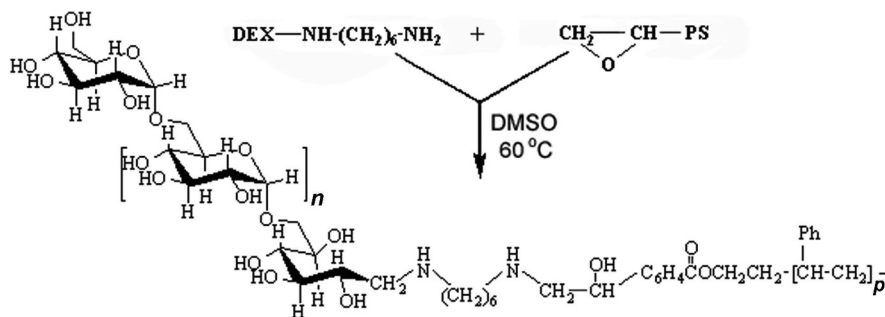


FIGURE 4.6. Coupling reaction: Synthesis of PS-b-Dextran copolymer from epoxide-terminated PS ($p=18$) with DAH-linked Dextran ($n=35$ or 60).

The epoxidation yield (60 Mol%) was evaluated by ¹H-NMR spectra of epoxide-terminated PS (product) and vinyl-terminated PS (starting compound), from the ratio of integrated areas of vinylic geminal protons, as can be seen from figure 4.4 and figure 4.5. This is possible due to the fact that the chemical shifts of the vinylic geminal protons of vinyl- and epoxide-terminated PS are located at different spectral regions: H_{A1} and H_{A2} between 5.2-6.0 ppm (figure 4.4), H_{a1} and H_{a2} between 2.8-3.4 ppm (figure 4.5). The peaks at 2.9 and 3.3 ppm were assigned to geminal protons from the epoxide compound in agreement with data in literature: 2.79 and 3.13 ppm for geminal protons in styrene epoxide.¹⁷⁰ The obtained modified polymer was used, without any further purification, for the coupling reaction with DAH-linked dextrans. The unreacted vinyl-terminated PS in the epoxidation product is washed out after the coupling reaction.

Coupling Reaction. An epoxide will react with an amine in a ring-opening process⁷⁸ (see figure 4.6). The reaction requires moderate alkaline pH conditions. The coupling reaction of epoxide-terminated PS and DAH-linked Dextran(6000) and Dextran(10000) was performed in DMSO at 60 °C to ensure the solubility of the reacting polymers (see figure 4.6). The NH₂ of DAH-linked dextran can react to both the C1 and C2 of the epoxide, C1 being more reactive, thereby forming a β-hydroxy group on the epoxy compound⁷⁸ (illustrated in figure 4.6). To achieve high conversion of epoxide-terminated PS, excess of DAH-linked dextran was used (molar ratio 4.5:1) combined with a long reaction time (5 days). To remove the

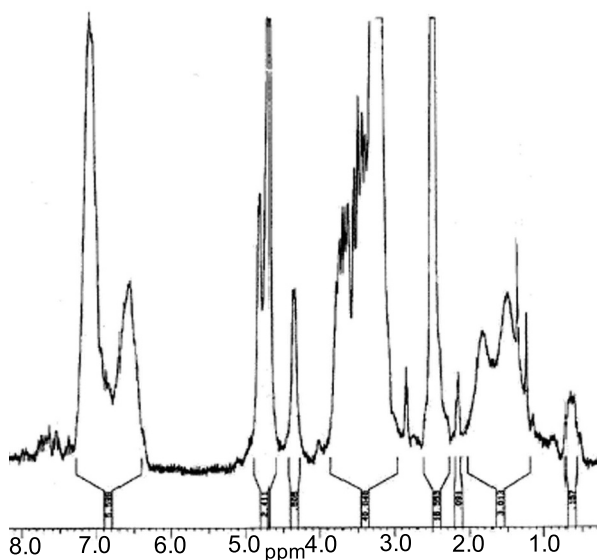


FIGURE 4.7. 200 MHz $^1\text{H-NMR}$ spectrum of PS(2100)-b-Dextran(6000) in DMSO-d_6 at 80°C .

unreacted DAH-linked dextran, the precipitate obtained after dialysis and filtration was purified by extensive washing with ultra pure water. Unreacted PS (both vinyl- and epoxide-terminated) was removed by suspending the precipitate in chloroform and sonication in an ultrasonic bath.

After filtration, the product was dried and analyzed by $^1\text{H-NMR}$ spectroscopy (figure 4.7 and figure 4.8). Both products (PS(2100)-b-Dextran(6000) and PS(2100)-b-Dextran(10000)) show the chemical shifts of the dextran hydrogens and PS hydrogens. Accordingly, it can be concluded that both PS and dextran are present in the products. However, the $^1\text{H-NMR}$ spectra do not allow confirmation of the presence of a C-N bond between epoxide-terminated PS and DAH-linked dextran. The reason is the great number of hydrogens present in the large PS-b-Dextran molecule, which screen the detection of the hydrogens of the -HN-CH₂- link between DAH-linked dextran and PS with $^1\text{H-NMR}$. No signals corresponding to geminal protons of vinyl-terminated PS between 5.2-6.0 ppm were observed, indicating that all vinyl-terminated PS had been washed out.

IR spectra of both PS(2100)-b-Dextran(6000) block copolymer and the starting materials, are presented in figure 4.9. The broad peak between 3600 and 3100 cm^{-1}

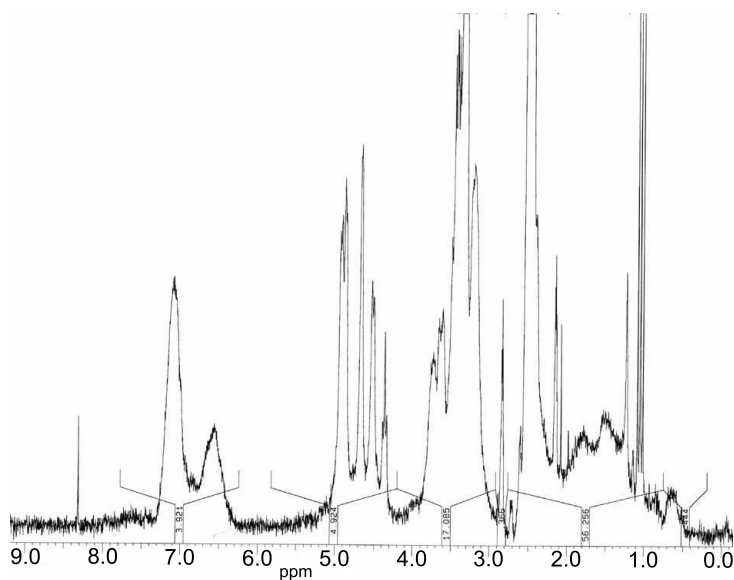


FIGURE 4.8. 200 MHz $^1\text{H-NMR}$ spectrum of PS(2100)-b-Dextran(10000) in DMSO-d^6 at $80\text{ }^\circ\text{C}$.

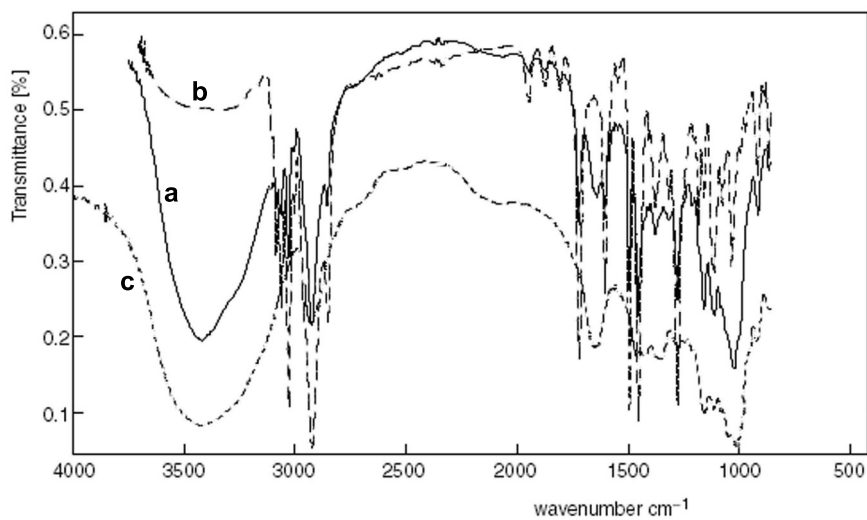


FIGURE 4.9. Transmission IR spectra (KBr, $700\text{-}4000\text{ cm}^{-1}$ region) of **a)** PS(2100)-b-Dextran(6000) - full line, **b)** epoxide-terminated PS - dashed line and **c)** DAH-linked Dextran(6000) - dotted line.

for DAH-linked Dextran(6000) in figure 4.9 illustrates the OH-vibration of the OH-groups of dextran. The sharp peaks round 1500 cm^{-1} for epoxide-terminated PS mark the C=C-vibrations of the aromatic ring. Both OH- and C=C-vibration peaks can be found in the IR spectrum of PS(2100)-b-Dextran(6000), proving the presence of dextran and PS in the product. Hence, IR and $^1\text{H-NMR}$ indicate a successful coupling reaction between epoxide-terminated PS and DAH-linked Dextran(6000). In the next section, the interfacial behaviour of the synthesized PS(2100)-b-Dextran(6000) will provide more evidence for a successful coupling. The yield of coupling is low, 11 Mol% for PS(2100)-b-Dextran(6000) and 5 Mol% for PS(2100)-b-Dextran(10000). One possible reason for the low yield is hydrolysis of the epoxide-terminated PS into PS-ethylene-diol. Even small traces of water in the reaction mixture can cause this hydrolysis. Another reason for the low yield is the very low reaction rate, due to the small probability that the reactive end-groups of both polymers meet. This will be discussed in more detail in the next section.

4.3.2. Interfacial Behaviour

PS(2100)-b-Dextran(6000). In figure 4.10 the recorded $\Pi - \sigma^{-1}$ isotherms for the newly synthesized PS(2100)-b-Dextran(6000) at the air–water interface are displayed. Several successive compression and expansion cycles are shown. The observed interfacial behaviour of PS(2100)-b-Dextran(6000) is typical for amphiphilic diblock copolymers (*e.g.* PS-b-PEO¹¹) and confirms the successful synthesis of the block copolymer.

For comparison, the $\Pi - \sigma^{-1}$ isotherms of PS(12300)-b-Dextran(6000) are shown in figure 4.11 (data from the previous chapter). The isotherms in figure 4.11A are for the air–water surface and those in figure 4.11B for the air–water+glycerol interface.

From the first compression isotherm of PS(2100)-b-Dextran(6000) and PS(12300)-b-Dextran(6000) the orientations and conformations of the block copolymers at the air–water interface, at different area per molecule, can be interpreted. This is illustrated by means of cartoons in figure 4.12, corresponding to the regions **a-d** in figures 4.10 and 4.11A. Both side views and top views are presented.

The PS coil is collapsed at the air–water surface (PS does not spread on water) and serves as an anchor for the dextran chains at the air–water interface. PS is not forced into solution upon compression, which is plausible because of the insolubility of PS in water. At large area per molecule (**a** in figures 4.10 and 4.11A) surface micelles are formed, similar to the surface micelles described by Israelachvili⁸⁷ and by

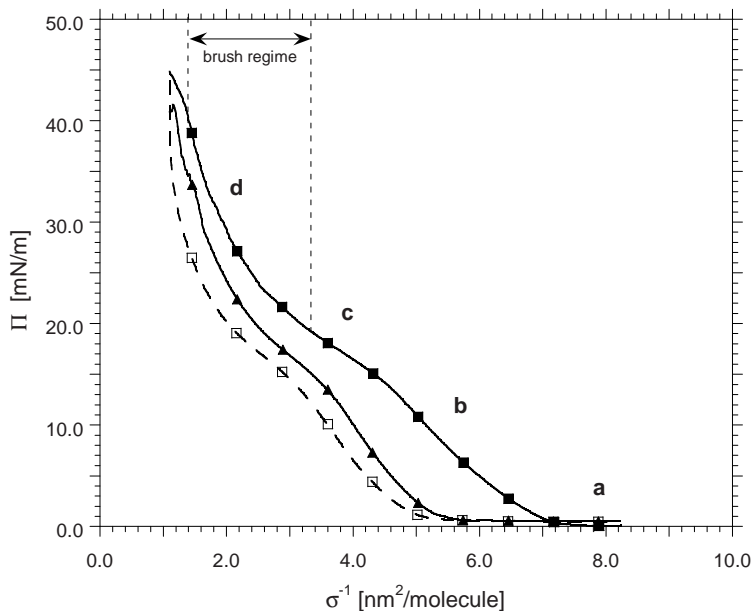


FIGURE 4.10. Interfacial pressure – area per molecule isotherms for PS(2100)-b-Dextran(6000) at room temperature. Successive compression and expansion curves: first compression (—■—), first expansion (—□—), second compression (—▲—). Dextran brush regime is indicated.

Eisenberg *et al.*^{32,33,104} for different amphiphilic block copolymers. This is illustrated in figure 4.12a. Self-assembly into surface micelles is favourable because of hydrophobic attraction of the PS blocks.^{86,88} The surface micelles remain isolated (see figure 4.12a, top view) because the dextran chains, adsorbed at the air–water surface, repel each other. In this range we have in a zero surface pressure. When the copolymer layer is compressed, the surface micelles start to interact, causing the dextran chains to desorb (figure 4.12b); ‘loops’ and ‘tails’ are formed.⁵⁶ This results in an increase in interfacial pressure (b in figures 4.10 and 4.11A). Upon further compression dextran chains become gradually desorbed from the air–water surface due to excluded volume interactions (figure 4.12c). More dextran chains desorb completely with increasing compression. In figures 4.10 and 4.11A this is reflected as a region of weaker increase in surface pressure, the ‘desorption region’ (c). In case of PS(12300)-b-Dextran(6000) a (quasi-)plateau regime is attained. This can be explained in the following way: due to the desorption of dextran, the water layer close to the air–water interface can be considered as a saturated

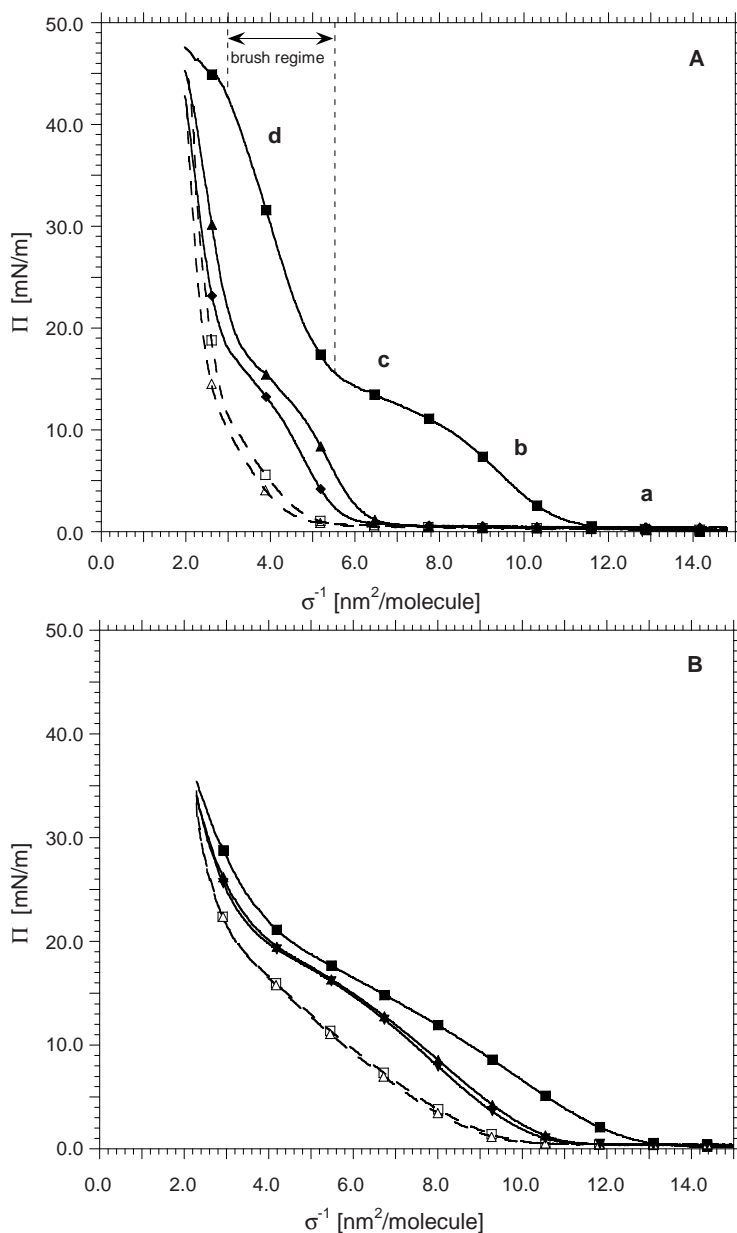


FIGURE 4.11. Interfacial pressure – area per molecule isotherms for PS(12300)-b-Dextran(6000)(A) and PS(12300)-b-Dextran(6000) with 2.5 wt% glycerol in water phase (B) at room temperature. Consecutive compression and expansion curves: first compression (–■–), first expansion (–□–), second compression (–▲–), second expansion (–△–) and third compression (–◆–). Dextran brush regime is indicated.

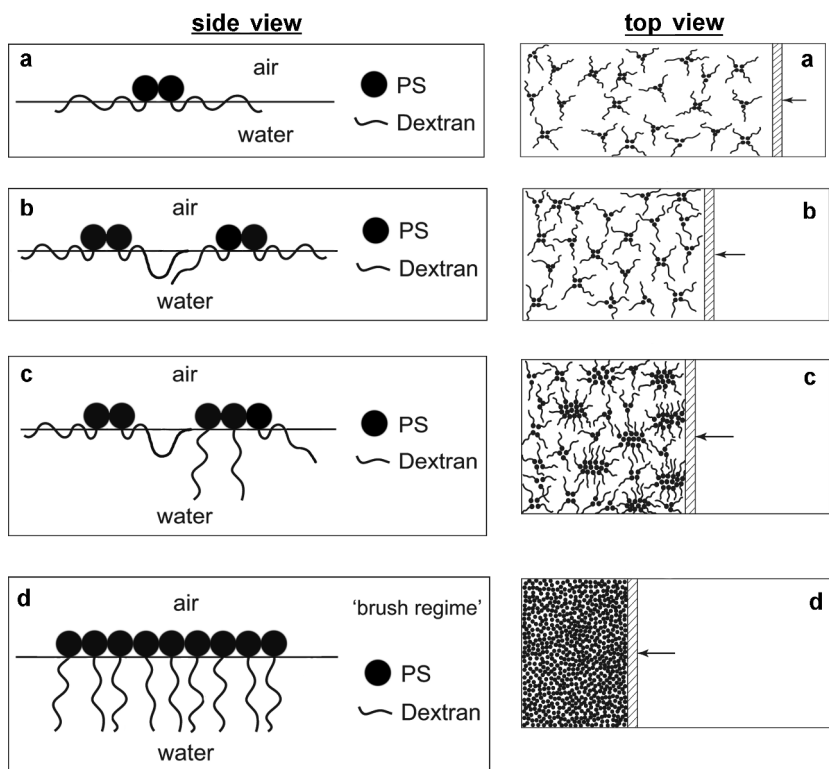


FIGURE 4.12. Conformations of PS-Dextran at different stages of compression (a-d), corresponding to stages indicated in figure 4.10 and figure 4.11A.

surface of a dextran solution. Therefore, the interfacial pressure in this region of the isotherm (c) is similar to the surface pressure of a saturated air–water surface of a dextran solution (approximately 16 mN/m, see figures 3.3 in the previous chapter). The continuous increase in Π with a decreasing area per molecule in the 'desorption region' indicates a continuous adsorption–desorption transition.³⁶

During desorption of the dextran chains, the PS blocks of the surface micelles aggregate into larger patches due to hydrophobic attraction, illustrated in figure 4.12c (top view). Moreover, the stability of the larger (quasi-) 2D aggregates may be enforced by intermolecular H-bonds between hydroxyl groups of the desorbed dextran chains.^{27,42} The presence of the large aggregates are demonstrated in the AFM section.

Eventually all dextran chains are desorbed from the air–water interface, stretching out into the water phase. For PS(2100)-b-Dextran(6000) this occurs at an area of $3.3 \text{ nm}^2/\text{molecule}$ and for PS(12300)-b-Dextran(6000) at an area of $5.5 \text{ nm}^2/\text{molecule}$. This marks the onset of the formation of a dextran brush (figure 4.12d). A steep increase of Π is observed upon further compression (**d** in figures 4.10 and 4.11A), which reflects repulsion between dextran chains due to excluded volume interactions. Region **d** is called the ‘brush regime’ and is indicated in figures 4.10 and 4.11A. For PS(2100)-b-Dextran(6000) it covers the range $1.4 \text{ nm}^2/\text{molecule} \leq \sigma^{-1} \leq 3.3 \text{ nm}^2/\text{molecule}$ and for PS(12300)-b-Dextran(6000) this is $3.0 \text{ nm}^2/\text{molecule} \leq \sigma^{-1} \leq 5.5 \text{ nm}^2/\text{molecule}$. In the brush regime the interfacial pressure is considered to consist of two contributions: a constant pressure $\Pi_{plateau}$ (approximately 16 mN/m) resulting from a monolayer of dextran segments of constant density and an increasing interfacial pressure Π_b due to the formation of a brush.³⁶

Hysteresis: dextran chain interactions and time dependency

We see that for both copolymers the curves for compression (filled symbols) and expansion (open symbols) do not coincide (hysteresis). This means that the recorded isotherms do not represent equilibrium. Reducing the compression/expansion speed resulted in less hysteresis for compression of PS(12300)-b-Dextran(6000) (figure 3.9, chapter 3), indicating that the hysteresis is time-dependent and indicative of a slow relaxation process. In chapter 3 the hysteresis of the PS(12300)-b-Dextran(6000) copolymer was partly attributed to the slow adsorption/desorption of dextran chains at the air–water surface, due to its relative stiffness, as well as aggregation of dextran chains in the brush regime. Experiments in this chapter will prove the contribution of slow adsorption/desorption to be of minor importance. The aggregation of dextran chains is most likely caused by intra- and intermolecular H-bond formation between hydroxyl groups of the desorbed dextran chains.^{27,42} Moreover, water molecules can form H-bonds with hydroxyl groups of dextran, within the same chain or between adjacent chains.^{27,42} The lifespan of a H-bond of a polysaccharide chain in water is 10^{-6}s , orders of magnitude longer than the lifespan of a H-bond in pure water: 10^{-10}s .⁴² Taking into account that each dextran chain in the brush regime is involved in multiple intra- and intermolecular H-bonding, this might explain the strong aggregation within the brush layer. By adding glycerol to the water phase, we tested this hypothesis: glycerol is known to form H-bonds with carbohydrates like starch, thereby preventing the formation of intra- and intermolecular H-bonds in the carbohydrates (referred to

as a plasticizing effect),^{58, 150, 151} so that we expect a reduced hysteresis. The result is presented in figure 4.11B (data from the previous chapter). Indeed, a strong decrease in hysteresis is observed when glycerol is added to the water phase. Another experiment supports this view of strong aggregation of dextran chains in the brush regime: when a PS(12300)-b-Dextran(6000) film was compressed down to the beginning of the 'desorption region', at $8.0 \text{ nm}^2/\text{molecule}$ (see 4.11A), and then expanded, no hysteresis was observed.

The experimental data suggest the following scenario. Upon expansion the compressed film breaks up, first into large aggregates and eventually, into small aggregates. This break up process is slow. Cracks are formed in the aggregated layer, causing the surface pressure to drop dramatically (see figures 4.10 and particularly 4.11A). However, after full expansion to the starting surface area, the initial stage of only surface micelles is likely not attained until much later; small aggregates are preserved. This is reflected in the shift of the second and third compression isotherm to lower values of σ^{-1} (compression of small aggregates instead of surface micelles). Increasing the time interval between an expansion and a compression or reducing the compression and expansion rates reduces the observed hysteresis (see figure 3.8 and figure 3.9 in chapter 3). This implies that, because of the increased relaxation time, more aggregates break up into smaller aggregates during the expansion and might even break up into surface micelles.

Hysteresis: PS aggregation

In spite of the qualitative similarities, there are a few quantitative differences between the compression and expansion isotherms of PS(2100)-b-Dextran(6000) and PS(12300)-b-Dextran(6000). These differences can be attributed to the difference in PS block length, which means that the PS block also takes part in the dynamic behaviour of the film. First, the area per molecule at which the surface micelles start to interact upon compression and, hence, Π increases (**a** in figures 4.10 and 4.11A) is larger for the block copolymer with the large PS block: approximately $12.0 \text{ nm}^2/\text{molecule}$ for the large and about $7.5 \text{ nm}^2/\text{molecule}$ in case of the short PS. We ascribe this to the fact that the large PS block occupies a larger surface area than the small PS block, accordingly forming bigger surface micelles. Second, PS(2100)-b-Dextran(6000) shows a much less pronounced 'desorption region' (**c**) than PS(12300)-b-Dextran(6000). In previous research on amphiphilic block copolymers (*e.g.* PS-b-PEO by Bijsterbosch *et al.*¹¹) the range of the 'desorption region' was associated with the length of the hydrophilic block of the copolymer:

the longer the hydrophilic block length, the more time it takes to completely desorb the polymer chain from the air–water interface upon compression, and the broader the ‘desorption region’. However, the PS block of the copolymers used was small compared to the PEO block. In case of PS-b-Dextrans the hydrophilic block length is the same for both copolymers and the PS is relatively large. Therefore, the PS of PS-b-Dextran occupies a large fraction of the surface area, especially in case of PS(12300)-b-Dextran(6000), and consequently, contributes to the range of the ‘desorption region’, besides the contribution of the dextran chains. Upon compression in the ‘desorption region’, the PS(12300) parts ‘meet’ more easily than the PS(2100) parts, because of their larger surface area and therefore form bigger (quasi-) 2D aggregates. The surface area in between the aggregated PS is filled with (partly) adsorbed dextran chains (see figure 4.12c). In order to completely desorb all dextran chains the PS-b-Dextran(6000) films need to be compressed to a low area per molecule, causing more aggregation of the PS. This strong aggregation, being more pronounced for PS(12300)-b-Dextran(6000), is demonstrated in the more extreme hysteresis observed for PS(12300)-b-Dextran(6000).

This brings us to the third quantitative difference: PS(2100)-b-Dextran(6000) displays much less hysteresis than PS(12300)-b-Dextran(6000). Upon expansion a dramatic drop of the interfacial pressure is observed for PS(12300)-b-Dextran(6000), much more than for PS(2100)-b-Dextran(6000). The PS(12300)-b-Dextran(6000) film breaks up and large patches are formed with cracks in between. These cracks grow upon expansion. Hence, the PS-b-Dextran film has become inhomogeneous and the interfacial tension measured by the Wilhelmy plate is that of the lowest density of the film, *i.e.* the interfacial tension of a pure air–water interface. This results in a vanishing surface pressure as can be seen in figure 4.11A. Attempts to demonstrate the cracks in the copolymer film using Brewster Angle Microscopy were unsuccessful. Because of the strong aggregation of PS(12300)-b-Dextran(6000), the patches formed upon expansion very gradually fall apart into smaller aggregates and the original situation of surface micelles is not attained. This break-up process is so slow, that the interfacial pressure measured during the expansion cycle is 0 mN/m over almost the complete σ^{-1} range. In the case of PS(2100)-b-Dextran(6000) the aggregation is less strong, which is reflected in a more gradual decrease of Π upon expansion. Nevertheless, in the final stage of expansion (right-hand side of figure 4.10) Π is 0 mN/m, indicative of the presence of (large) aggregates. The difference between the first and second compression is much larger for the copolymer with the larger PS block. This reflects the stronger

aggregation in case of PS(12300)-b-Dextran(6000): the second compression of the PS(12300)-b-Dextran(6000) film is a compression of large aggregates (larger than in case of PS(2100)-b-Dextran(6000)) and not of surface micelles. These large aggregates start to interact, displayed as an increase of Π , at a much lower value of the area per molecule than the original surface micelles (first compression). In other words, the relaxation of the compressed monolayer is very slow.

The aggregation of the PS blocks in the copolymer film upon compression is affirmed by compression/expansion experiments on a PS film, see figure 3.4 in chapter 3 and the study by Kumaki.¹⁰⁰ In figure 3.4 hysteresis is observed, indicating that the PS aggregates formed upon compression do not easily fall apart during expansion. The second and third compression isotherm are shifted to lower grafting densities, implying strong aggregation as well. This is supported by the research of Kumaki: surface balance experiments conducted on PS monolayers of different M_w displayed hysteresis. Direct evidence of PS aggregates at the air–water surface was obtained from transmission electron microscopy (TEM).¹⁰⁰ Recorded TEM pictures of compressed PS monolayers at different compression states show that the PS particles are already aggregated before compression and the aggregated structure is forced to rearrange during compression, resulting in an increasingly dense PS monolayer; large aggregates are formed that do not decompose upon expansion (because there is no repulsive driving force between the PS particles). The interfacial pressure measured is not a true interfacial pressure (as PS has no hydrophilic group), but corresponds to the mechanical resistance against these rearrangements.

Fourth difference is the difference in brush regime, which is for short PS $1.4 \text{ nm}^2/\text{molecule} \leq \sigma^{-1} \leq 3.3 \text{ nm}^2/\text{molecule}$ and for long PS $3.0 \text{ nm}^2/\text{molecule} \leq \sigma^{-1} \leq 5.5 \text{ nm}^2/\text{molecule}$. The difference can be assigned to the area of the PS block occupied at the air–water surface, being larger for PS(12300)-b-Dextran(6000).

Based on figures 4.10 and 4.11 it can be concluded that there are two major contributions to the formation of (quasi-) 2D PS-Dextran aggregates at the air–water surface, resulting in the observed hysteresis: aggregation of the PS blocks due to hydrophobic interaction, already starting at large area per molecule (in the ‘desorption regime’), and aggregation of dextran chains due to H-bonding (in the brush regime), when the monolayer is more compressed. A third, minor, contribution to the hysteresis is the slow adsorption/desorption of dextran chains at the air–water interface. The observed time-dependent hysteresis of PS-b-Dextran at the air–water interface has implications for the preparation of dextran brushes at a

solid surface using the Langmuir-Blodgett deposition. We adopted as a procedure that a freshly added PS-b-Dextran monolayer is compressed once to the objected σ , and then left to relax prior to the LB transfer.

PS(2100)-b-Dextran(10000). In figure 4.13a consecutive compression and expansion $\Pi - \sigma^{-1}$ isotherms for the synthesized PS(2100)-b-Dextran(10000) at the air-water interface are shown. There is no recognizable 'desorption region', no sharp increase of Π at low values of σ^{-1} (indicating the absence of a 'brush regime') and no pronounced hysteresis. Compared to the PS(2100)-b-Dextran(6000) copolymer a 'desorption regime' over a broader σ^{-1} range was expected, because of the longer dextran chains. All these observations suggest that the interfacial pattern in figure 4.13a does not resemble the interfacial behaviour of amphiphilic block copolymers. It resembles more to the $\Pi - \sigma^{-1}$ isotherms of a compressed PS monolayer,¹⁰⁰ as illustrated in figure 3.4. Based on the observed interfacial behaviour it is concluded that the coupling reaction between epoxide-terminated PS(2100) and DAH-linked Dextran(10000) failed. Most likely, the product consists mainly of PS(2100), in the form of PS-ethylene-diol, as explained in section 4.3.1. To check this supposition the first compression isotherm of PS(2100)-b-Dextran(10000) was replotted in figure 4.13b. The area per molecule was recalculated assuming only PS(2100)-ethylene-diol was present. A recorded first compression isotherm of PS(2100)-ethylene-diol is plotted for comparison. The isotherms do not coincide. Therefore, it can be concluded that the product does not consist of pure PS-ethylene-diol. The increase of Π of the replotted 'PS(2100)-b-Dextran(10000)' isotherm starts at 2.0 nm²/molecule, much higher than for the PS-ethylene-diol isotherm, 0.35 nm²/molecule. This means that some other surface active material is present in the obtained product (and adsorbed at the air-water surface).

Our attempts to synthesize copolymers with a long dextran block, described in this chapter and in chapter 3, proved to be unsuccessful. It turns out that the block coupling method is not suitable to synthesize PS-b-Dextrans with a dextran block $M_w \geq 10000$ Da. This is probably due to the small chance that the reactive end-groups of the PS and dextran blocks meet, in order to undergo a coupling reaction. The reason for this may be that the PS and dextran coils cannot inter penetrate, due to excluded volume interactions. The probability that the reactive end-groups meet ($P_{PS \leftrightarrow dextran}$) is a function of the number of polymer segments in both blocks. This can be calculated with an overlap integral using the probability functions of both reactive end-groups and provided that the PS and

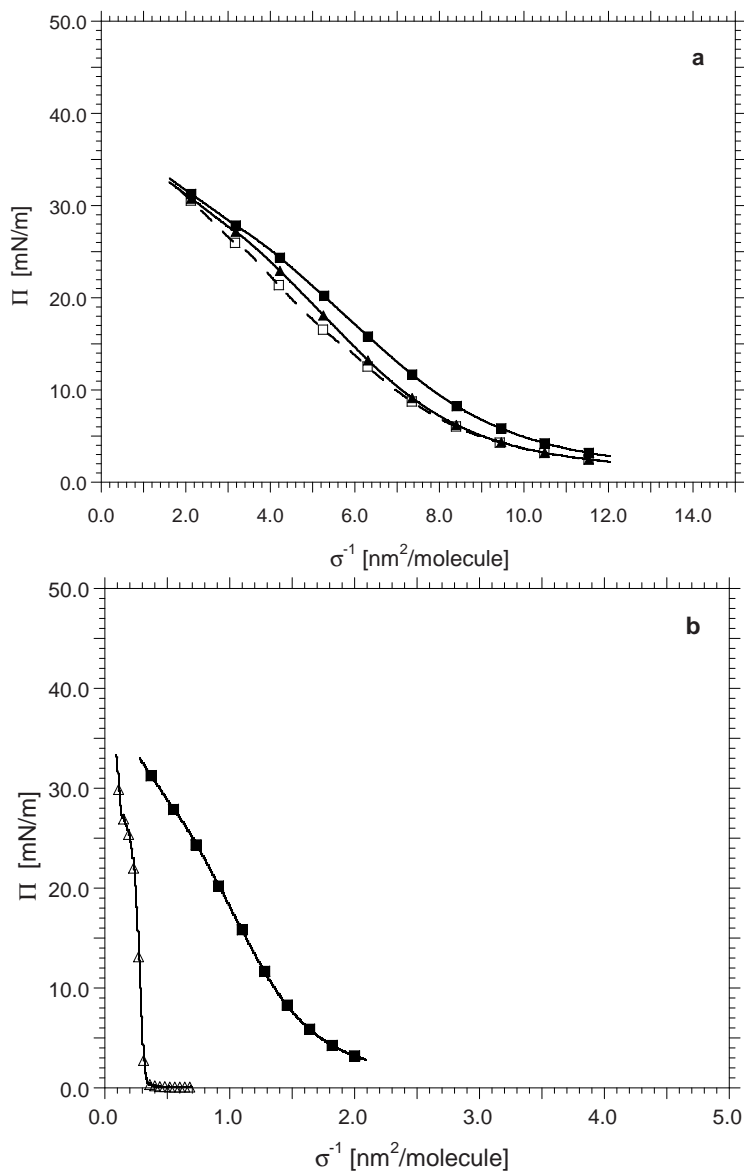


FIGURE 4.13. Interfacial pressure – area per molecule isotherms for PS(2100)-b-Dextran(10000) (a) at room temperature. Successive compression and expansion curves: first compression (—■—), first expansion (—□—), second compression (—▲—). And first compression isotherm of PS(2100)-b-Dextran(10000) (—■—) and PS-ethylene-diol (—Δ—) (b) at room temperature (see text).

dextran coils do not inter penetrate (closest contact is at the sum of the mean-end-to-end distances of both coils). In terms of the number of polymer segments N and the second virial coefficient ν , the following scaling arguments were deduced:

$$P_{PS \leftrightarrow dextran} \sim (N_{PS} + N_{dextran})^{-3/2} \quad (\text{theta solvent})$$

$$P_{PS \leftrightarrow dextran} \sim (\nu_{PS}^{0.34} N_{PS}^{1.20} + \nu_{dextran}^{0.34} N_{dextran}^{1.20})^{-3/2} \quad (\text{good solvent})$$

DMSO is used as solvent for the coupling reaction. It is a good solvent for dextran, but not for PS (still, PS does dissolve in DMSO at 60 °C, the reaction temperature used) Therefore, we assume that theta conditions are valid for the coupling reaction, so the $P_{PS \leftrightarrow dextran}$ for a theta solvent is applied. With increasing chain length of the dextran block $P_{PS \leftrightarrow dextran}$ becomes much smaller. This apparently results in hardly any or no coupling reaction in case of PS(2100) and dextran(10000). Most likely, the epoxide-terminated PS is hydrolyzed to PS-ethylene-diol. Consequently, choosing more reactive coupling mechanisms (like using the DAH spacer) will not help to synthesize copolymers with long dextran blocks, because the chance that the reactive end-groups meet is too low. A different approach would be needed to synthesize long PS-b-Dextran. One may think of a polymerization of glucose to dextran, starting from end-functionalized PS as a macro-initiator. Loos¹⁰⁶⁻¹⁰⁸ already proved this is a successful way to synthesize long PS-amylose block copolymers using an enzymatic polymerization procedure.

4.3.3. AFM

Tapping mode AFM images were captured of PS(12300)-b-Dextran(6000) LB depositions, on PS-coated silicon wafers, immersed in water. They are presented in figures 4.14b–e for different areas per molecule. A cross section of the image is shown as well. For comparison, a contact mode AFM image and cross section of a PS-coated silicon wafer in air is displayed in figure 4.14a. It shows that the spincoated PS surfaces, used for LB deposition, are smooth. At $\sigma_{LB} = 0.12 \text{ nm}^{-2}$ ($\sigma^{-1} = 8.3 \text{ nm}^2/\text{molecule}$) the surface is inhomogeneous (figure 4.14b). Large patches of PS-b-Dextran are observed and interstices without block copolymer. On a scale of 500 nm (figure 4.14c) patches of 50–150 nm can be distinguished, demonstrating the presence of large aggregates of PS(12300)-b-Dextran(6000) at the surface. The LB deposition was performed at $\sigma^{-1} = 8.3 \text{ nm}^2/\text{molecule}$, in region **c** of figure 4.11A. Consequently, the AFM images confirm our interpretation of the $\Pi - \sigma^{-1}$ isotherms of the block copolymers and the time-dependent hysteresis: in the 'desorption region' small surface micelles of the block copolymer are pushed together to form large aggregates (50-150 nm as observed by AFM).

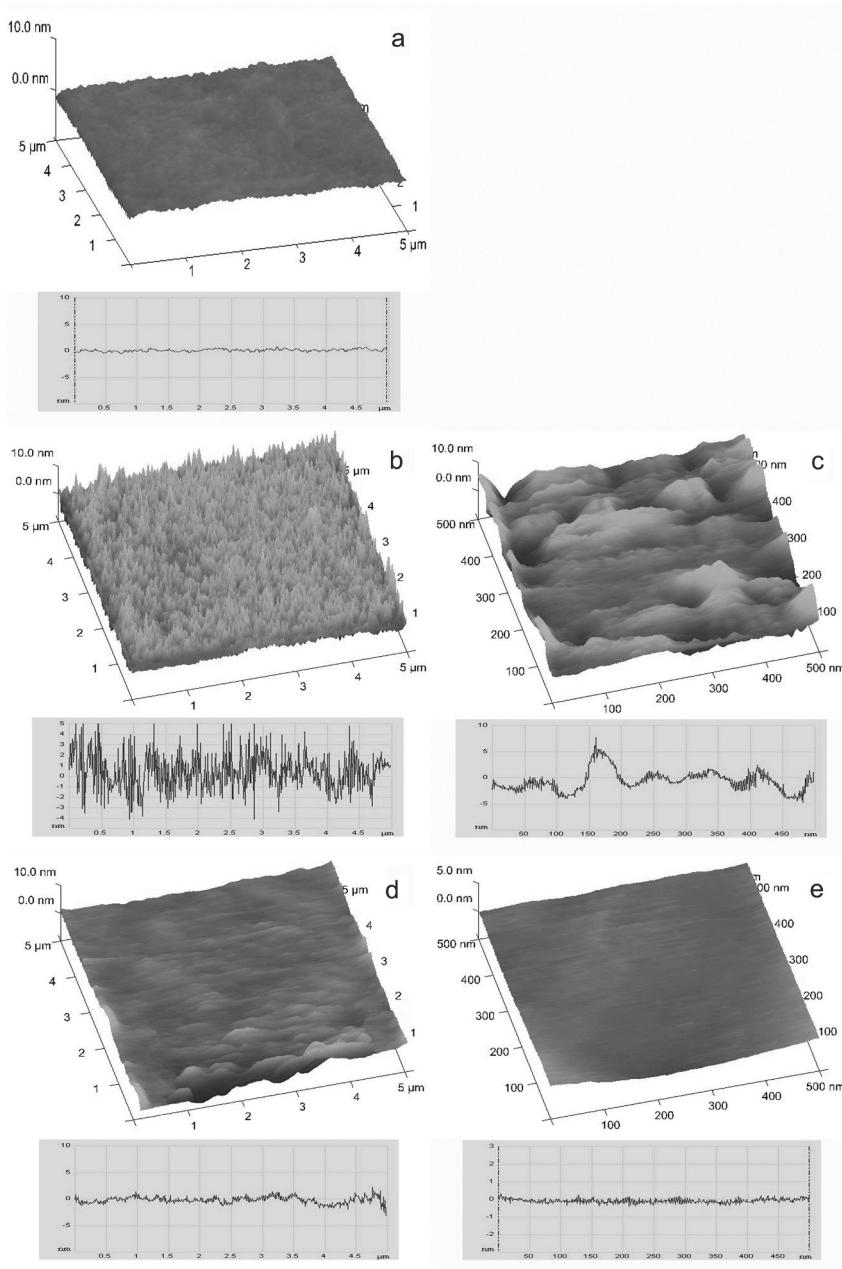


FIGURE 4.14. AFM images (3D and cross section): PS-coated silicon wafer (a) and grafted dextran $\sigma_{LB} = 0.12 \text{ nm}^{-2}$, scale 5 μm (b) and 500 nm (c), and $\sigma_{LB} = 0.26 \text{ nm}^{-2}$, scale 5 μm (d) and 500 nm (e).

At $\sigma_{LB} = 0.26 \text{ nm}^{-2}$ ($\sigma^{-1} = 3.8 \text{ nm}^2/\text{molecule}$) a homogeneous layer is captured with tapping mode AFM (figure 4.14d). On a scale of 500 nm (figure 4.14e) the surface is still smooth. Considering the observed layer lies within the brush regime (region **d** of figure 4.11A), the dextran brush must be homogeneous. Apparently, the observed PS-b-Dextran patches at intermediate σ^{-1} are pushed together upon compression, forming a homogeneous layer, whereby the closely packed dextran chains are stretched out into the solution to form a homogeneous brush (as illustrated in figure 4.12d).

4.4. Conclusions

We used a novel method to prepare PS-b-Dextran copolymers, applying a block coupling method with a DAH spacer. We successfully coupled DAH to several maltodextrins and dextrans, up to a M_w of 10.000 Da, as confirmed by ^1H - and ^{13}C -NMR and mass spectrometry. Moreover, under mild conditions we converted vinyl-terminated PS into epoxide-terminated PS, as proven by ^1H -NMR spectroscopy. DAH-linked dextran 6000 was coupled to epoxide-terminated PS, verified by ^1H -NMR and IR. The yield of coupling was low, which might be due to hydrolysis of the epoxide-terminated PS. The surface pressure isotherms of PS(2100)-b-Dextran(6000) showed behaviour typical of amphiphilic copolymers, thereby confirming the successful coupling. The PS(2100)-b-Dextran(10000) product showed a different interfacial behaviour, thereby indicating that the coupling was unsuccessful, even though the ^1H -NMR spectrum indicated the presence of PS- as well as dextran-fragments.

The interfacial pressure measurement turned out to be the conclusive test for the coupling reaction. Synthesis of 'small' PS-b-Dextran (dextran $M_w = 6000 \text{ Da}$) using a block coupling method as described in this chapter, proved to be effective. Attempts to synthesize large PS-b-Dextran (dextran $M_w \geq 10000 \text{ Da}$) were failing. Apparently, block coupling methods as described in this chapter and in chapter 3 are not suitable to produce large PS-b-Dextran. The plausible reason for this failed coupling is the insufficient inter penetration of the PS and dextran coils. We reasoned, with scaling arguments, that the probability for reactive end-groups to meet in the reaction mixture drops dramatically with increasing block lengths of PS and dextran.

Interfacial pressure measurements and AFM imaging demonstrated aggregation of the PS - b - Dextran copolymers at the air-water interface. Comparison of PS(2100) - b - Dextran(6000) and PS(12300)-b-Dextran(6000) revealed that there are two contributions to this aggregation: hydrophobic attraction between

PS blocks and hydrogen bonding between dextran blocks. The hydrophobic interactions between PS blocks already starts at a large area per molecule, resulting in surface micelles. These surface micelles grow into larger aggregates at intermediate area per molecule. When the area per molecule is small, a dense, homogeneous layer is formed, in which the dextran chains stretch out into the water to form a molecular brush. In this region multiple intra- and intermolecular hydrogen bonds are formed between the dextran chains. Aggregation of PS-b-Dextran has implications for the preparation of dextran brushes at a solid surface and for the use of these surfaces in protein adsorption experiments, as will be discussed in the next chapter.

Acknowledgement

The syntheses described in this chapter were performed by Eugen Sisu. I thank him for all the work he has done and all the effort to synthesize long PS-b-Dextrans. I enjoyed our collaboration. Ted Slaghek and Johan Timmermans from TNO Food are thanked for their help and fruitful discussions concerning the synthesis of PS-b-Dextran. I am very grateful to the people of the Laboratory of Organic Chemistry of Wageningen University for their time and help on the syntheses and characterizations. I thank Gerard Fleer for suggesting an approach to estimating the probability that reactive end-groups of polymers meet.

CHAPTER 5

Sweet Brushes and Dirty Proteins

Published in: *Soft Matter*, 3 (2007), 754–762

5.1. Introduction

Proteins at interfaces may lead to hazardous situations. Proteins tend to adsorb at solid surfaces and can thereby initiate the formation of an undesired biofilm at the surface (biofouling) - the adsorbed proteins form a conditioning film to which (bacterial) cells adhere that grow into a mature biofilm.^{31, 68, 69, 71, 125} In the (human) body biofilms cause serious problems - artificial implants can induce thrombosis or microbial infections.^{31, 68, 69, 71, 75} Ultimately, reoperation may be necessary, however, inflammation could also result in osteomyelitis, amputation, or even death.⁷¹ Other examples of biofouling can be found in diagnostics and therapeutics,⁸¹ the food industry and water purification plants (fouling of process equipment)¹²⁵ and the shipping industry, where algae and shellfish stick to ship hulls enhancing drag forces.⁷⁵ Microorganisms in biofilms are resistant to antibiotics,^{31, 69, 71} consequently prevention of biofilm formation may be the only solution to prevent the problems mentioned. Two ways of prevention may be distinguished: (1) modification of the material surface and (2) the use of biomimetic materials. Progress in biomaterial research with respect to biofilm formation has been reported, *e.g.*, in the review by Ratner and Bryant.¹³⁶ A specific way of modification of the surface is coating with a protective polymer layer to prevent proteins adsorbing at the surface, thereby inhibiting the formation of a conditioning film to which (bacterial) cells can adhere. Research over the past decade has shown that polymer coatings, especially of PEO (poly(ethylene oxide)) in a brush conformation, are most successful in reducing or preventing the adsorption of proteins and/or adhesion of bacteria at a solid surface.³⁷ However, under certain conditions attraction between PEO (or oligo(ethylene oxide)) and proteins was observed.^{2, 39, 51, 75, 138, 145} This attraction is explained by a change in conformation of the EO segments from a protein repellent, polar conformation into a protein attractive, apolar conformation.^{51, 75, 168} In a commentary Israelachvili touched on the 'different faces' of PEO, including PEO-protein attraction.⁸⁵ He suggested that hydrophobic patches on the protein could be responsible for the short-range attraction, by inducing intramolecular rearrangements within the PEO layer.

Polysaccharides may be a good alternative for PEO to form an antifouling brush. They are natural polymers and may therefore be more appropriate for use as an antifouling agent in biomedical applications. Amylose brushes have been manufactured before,^{16, 109} though, without testing the protein repellency of these brushes. In nature oligosaccharides are found in the extracellular matrix and glycocalyx of living cells; these coatings have the function to specifically bind proteins and cells,

while preventing non-specific adsorption.^{5,61,130} These oligosaccharides consist of a broad variety of glycosylic units, charged and non-charged, and their sequence determines the recognition of proteins and cells in biological fluids.^{61,130} To mimic such a layer is quite a task. Successful attempts have been made to unravel and/or express glycosylation sequences^{61,130} or prepare self-assembled monolayers (SAMs) of glycopolymers grafted phospholipids.⁵⁴

In the present work, we aimed at preparing polysaccharide brushes using a simpler approach, namely using neutral polysaccharides consisting of only one kind of glycosyl unit. We focused on dextran, a (relatively) flexible, neutral polysaccharide. At the low molecular weight used in our research, dextran can be considered linear.⁸⁴ It (mainly) consists of $\alpha(1 \rightarrow 6)$ -linked glycosyl units¹⁴⁶ and shows good solubility in water, where it adopts an open coil conformation.^{27,127} Because dextran is neutral it has no electrostatic interactions with proteins. Proteins and neutral polysaccharides in solution repel each other, due to excluded volume interactions, as demonstrated in partitioning studies of protein–dextran and protein–pullulan solutions.^{1,25,48,83,111,144,169} Over the past decades dextran gels (Sephadex) for protein chromatography and electrophoresis demonstrated relatively weak protein interactions.⁸ Dextran (and other polysaccharides like cellulose, maltose, agarose and heparin^{8,43,94,128,134}) has been employed in several ways to cover surfaces, and its protein-repelling capacity at a surface has been studied. Applying a physically adsorbed dextran layer does not suppress protein adsorption, because the dextran at the surface is displaced by protein molecules.^{43,116} In a considerable number of studies, dextran was grafted to surfaces, in most cases in a side-on configuration, so that loops and tails are formed at the surface.^{43,44,59,60,115,117,132,133,152} The adsorption suppression of different proteins at such dextran-grafted surfaces is 30–95% of the adsorbed amount at the uncovered surface, depending on the number of anchoring points of the dextran and also on the type of protein. For bovine serum albumin the suppression of adsorption by side-on grafted dextran is 65–90%.^{59,117} Marchant *et al.* used SAMs of comb-like surfactants containing end-grafted dextran side-chains that exhibited a protein repellence of 90%.^{80,128} Österberg and coworkers studied the fibrinogen adsorption at dextran grafted end-on (dextran brush) and compared it to dextran grafted side-on.⁴⁴ They concluded that dextran grafted side-on is more effective in preventing protein adsorption. However, they only studied adsorption on a dilute brush and at one grafting density only. Altogether, no solid conclusions could be drawn about the protein-repelling efficiency of dextran brushes. Shortcomings of

most studies cited are the *ex situ* measurement of the adsorbed amount and the use of a washing step prior to the determination of the adsorbed amount, by which weakly adsorbed protein may be washed off. Consequently, the protein-repellency capacity of the dextran layers is probably overestimated in these investigations.

A more recent study by Razatos and coworkers showed that dextran coated surfaces resist Bovine Serum Albumin (BSA) adsorption.¹⁵⁵ They used Atomic Force Microscopy (AFM) with a BSA-coated cantilever tip and immobilized dextran on gold, that showed no adhesion on approach and no pull-off force. Rixman *et al.* performed force measurements between Human Serum Albumin and SAMs of various materials, including oligo(ethylene oxide) and oligomannose-9, with High Resolution Force Spectroscopy.¹³⁷ They reported that the oligosaccharide exhibits superior resistance to protein adsorption.

In the current study, we present data on protein adsorption for a wide range of dextran-grafting densities, demonstrating the protein repellency of dextran brushes. In order to control the grafting density of dextran at the solid surface we applied polystyrene(PS)-b-Dextran copolymers that were transferred from an air–water interface to a PS surface by using the Langmuir-Blodgett (LB) deposition technique.¹³⁹ In a previous studies (see chapters 3 and 4) the interfacial pressure (Π) *versus* grafting density (σ) isotherms of PS-b-Dextran demonstrated the formation of a dextran brush at the air–water interface. To study the protein rejecting capacity of the brushes, we used two different proteins, BSA and trypsin. BSA is a main constituent of bovine blood. Its structure and physical-chemical characteristics are well known.²⁶ In previous studies, it proved to be a 'sticky' protein, especially at hydrophobic surfaces like PS.^{77,124} Furthermore, in various studies, BSA was used to test the resistance to protein adsorption at modified surfaces.^{39,59,79,117,126,138,155} Trypsin is an enzyme excreted by the pancreas and takes part in the digestive degradation of food proteins. It may be immobilized in bioreactors and biosensors, and in that context we have previously investigated the adsorption behaviour and conformational changes of trypsin at silica and PS surfaces.⁹⁹ Applying a positively (trypsin) and a negatively (BSA) charged protein allows us to study the influence of charge on the interaction between proteins and dextran brushes. The grafted dextran layers were characterized with ellipsometry (to determine the efficiency of the LB transfer), contact-angle measurements (to measure the wettability) and AFM (to determine the homogeneity). The adsorption of proteins at the dextran layers was measured *in situ* with optical reflectometry.

5.2. Materials and Methods

5.2.1. Materials

All solvents used were pro analysis grade (Sigma-Aldrich). Ultra pure water was processed using Seralpur Pro 90C (conductivity $< 0.055 \mu\text{S}/\text{cm}$, pH 6). Two types of PS-b-Dextran copolymers were utilized, both with dextran weight-average molecular mass $M_w = 6000 \text{ Da}$ ($M_w/M_n = 1.65$ (M_n is number-average molecular mass, M_w/M_n is a measure of polydispersity)) and with different PS block lengths ($M_w = 12300 \text{ Da}$ ($M_w/M_n = 1.02$) and 2100 Da ($M_w/M_n = 1.11$), respectively). Synthesis and interfacial behaviour of these block copolymers is described in chapters 3 and 4.

Two proteins, BSA (Sigma, A3912, minimum 96%, $M_w = 66 \text{ kDa}$) and trypsin (Sigma, from bovine pancreas, T1426, saltfree, $M_w = 24 \text{ kDa}$) were used to test the protein repellency of dextran brushes. BSA is a heart-shaped protein; its dimensions in solution (pH 4.5–8.0) can be approximated by a triangle with sides of 8.0 nm and a depth of 3.0 nm and the isoelectric point is at pH 4.7.²⁶ Based on crystallographic information (Protein Data Bank entry 2PTN), the native conformation of bovine trypsin can be approximated as an ellipsoid with axes of 4.8 nm \times 3.7 nm \times 3.2 nm.¹⁶⁶ It is isoelectric at pH 10.5.¹⁹ BSA solutions of 50 mg/l in phosphate buffer (Merck, 52 mM, pH = 7.0) were applied. Trypsin was dissolved in freshly prepared phosphate buffer (55 mM, pH = 7.6), from K_2HPO_4 and KH_2PO_4 (Merck), at 50 mg/l.

5.2.2. Preparation of the Brushes

The amount of adsorbed proteins on dextran brushes was measured using optical reflectometry.^{45,46} As substrates reflecting silicon wafers (Wafernet GmbH, Si(100) with a SiO_2 -layer of 2-3 nm) were used, cut in slides of 1 cm wide and 6 cm long. Prior to grafting the dextran, the wafers were coated with a polystyrene (PS) film (approximate thickness 70 nm) as reported in chapter 2. The dextran brushes were applied by transferring a compressed PS-b-Dextran copolymer monolayer from an air–water interface in a Langmuir trough to the PS-coated wafer, using the LB deposition technique,¹³⁹ as previously described for PS-b-PEO copolymers^{39,126} (see chapter 2 as well) and PS-b-PAA copolymer.³⁸

The PS(12300) - b - Dextran(6000) copolymer was dissolved in chloroform and spread on a clean air–water surface with a micro syringe. The PS(2100) - b - Dextran(6000) copolymer was dissolved in DMSO at 70 °C and introduced to the air–water interface using the Trurnit method.¹⁶⁰

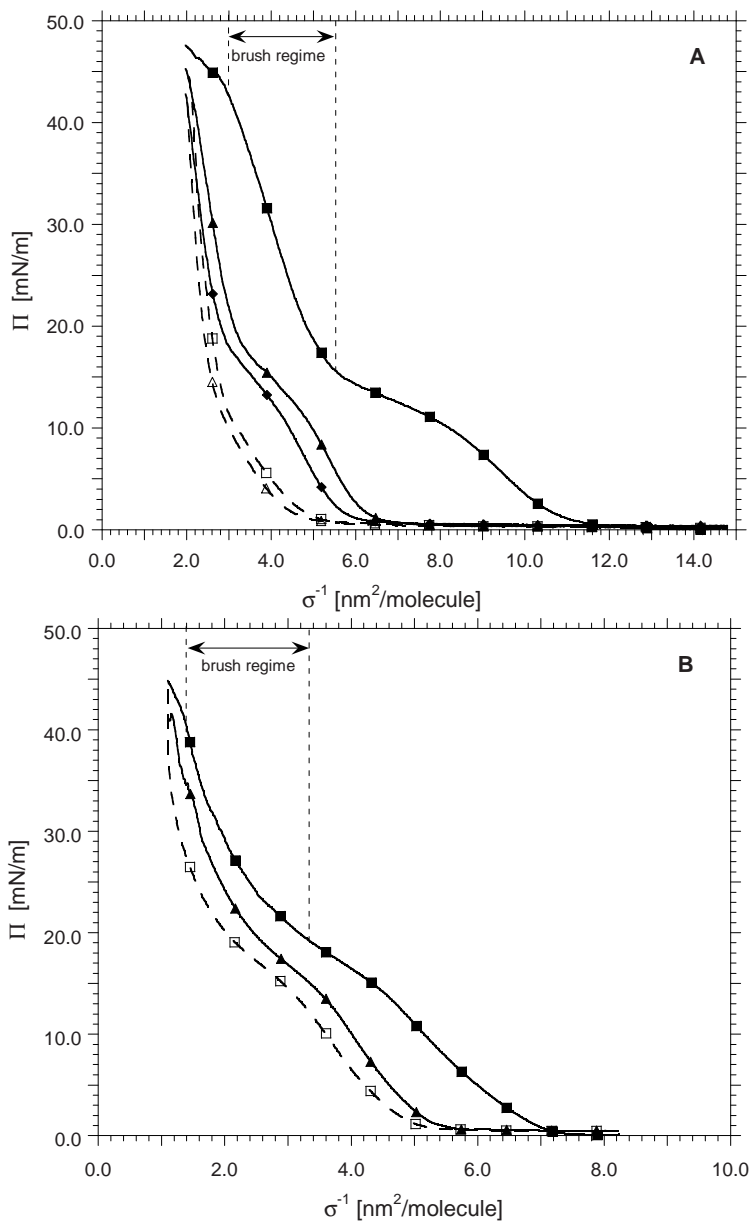


FIGURE 5.1. Interfacial pressure – area per molecule isotherms for PS(12300)-b-Dextran(6000)(A) and PS(2100)-b-Dextran(6000)(B) at room temperature. Successive compression and expansion curves: first compression (—■—), first expansion (—□—), second compression (—▲—), second expansion (—△—) and third compression (—◆—). Dextran brush regime is indicated.

Figure 5.1A and figure 5.1B show the $\Pi - \sigma^{-1}$ isotherms for both block copolymers for successive compression and expansion cycles (σ^{-1} is the area per molecule). The brush regime is indicated. For explanation of the isotherms in figure 5.1, see chapter 4. The copolymer with the smaller PS block is used to prepare dextran brushes at high grafting densities; $\sigma > 0.30 \text{ nm}^{-2}$. The recorded interfacial pressure isotherms do not represent an equilibrium situation. There is appreciable time-dependent hysteresis, having consequences for the LB deposition. For each σ , a freshly added PS-b-Dextran monolayer was compressed to the desired grafting density and left to relax until a stable, constant Π was reached. At high grafting density, a relaxation period up to 24 hr was needed. After relaxation, the LB deposition to the PS-coated wafers was performed with two wafers at a time, to produce duplicates. A dipping 'speed' of $1 \text{ mm}^2/\text{s}$ was used.

The dextran-grafting density (σ_{LB}) was calculated from the amount of copolymer added to the air-water interface ($V \times C$, V is the volume added, C is the copolymer concentration) and the area of the (compressed) monolayer in the Langmuir trough at the start of LB transfer (A_0): $\sigma_{LB} = \frac{V \times C \times N_{Av}}{M \times A_0}$ (M is the molar mass of the copolymer, N_{Av} is Avogadro's number). At high grafting densities ($\sigma \geq 0.28 \text{ nm}^{-2}$), a vertical transfer was not possible, probably due to a strongly aggregated monolayer. At these high grafting densities, the monolayer was transferred horizontally, according to the Langmuir-Schaefer (LS) method.¹⁰² After deposition of the PS-b-Dextran, the wafers were annealed for 10 min. at $120 \text{ }^\circ\text{C}$ (above the glass-transition temperature of PS) in an oven, allowing diffusion of the PS block of the copolymer into the PS sublayer. After cooling to room temperature, the PS layer becomes glassy and the block copolymers are irreversibly attached to the surface.

5.2.3. Ellipsometry

The thickness of the transferred PS-b-Dextran layer was determined with ellipsometry (Sentech Instruments GmbH, $\lambda = 632.8 \text{ nm}$, $\theta = 70.00^\circ$). The ellipsometry measurements were performed in air (implying that the dextran brush is collapsed), at 3 different spots on the wafer. At each spot the thickness was measured 3 times and the lowest value was used. The values at the 3 different spots were averaged. The thickness of the PS-b-Dextran layer (d) is the difference between the measured thickness of the PS-coating + PS-b-Dextran and the thickness of the PS layer, measured beforehand. From the d values the grafting density of the dextran brush at the wafer (σ_{ell}) can be calculated with $\sigma_{ell} = \rho d N_{av} / M$,

where ρ is the density of the PS-b-Dextran layer, N_{Av} Avogadro's number and M the molar mass of the PS-b-Dextran.

5.2.4. Contact-angle Measurements

The water wettability of the LB wafers was tested by advancing contact angles of a sessile drop of ultra pure water at room temperature in air, using a Krüss microscope and a digital camera setup. For each wafer, contact angles were determined at 4 different spots of the wafer and averaged. For comparison, the contact angle on a PS-coated wafer was measured.

5.2.5. AFM

Tapping mode AFM was applied to investigate the structure of the dextran brushes in water, at different grafting densities. A Digital Instruments Nanoscope III Multimode Scanning Probe Microscope was used, equipped with a fluid cell filled with ultra pure water. Veeco TESP silicon cantilevers were used with length of 125 μm and tip radius of 10 nm. A 1 x 1 cm^2 piece was cut from the LB wafers, placed in the fluid cell and covered with ultra pure water. The surface was scanned in tapping mode at a scan rate of 0.5–1 Hz and with a cantilever driving frequency of about 130 kHz. 3D AFM images are displayed, as well as a cross section perpendicular to the scanning direction. The smoothness of the spin-coated PS layer was investigated with contact mode AFM in air, using a Veeco DNP silicon nitride cantilever with a tip radius of 20 nm. A scan rate of 2 Hz was applied.

5.2.6. Reflectometry

We made use of an optical reflectometry set-up described in detail by Dijt^{45,46} and, more recently, by Cohen Stuart and de Keizer.²⁹ Detector sampling time was 1 second; the flow of protein solution was set at 1 ml/min. All experiments were performed in duplicate or triplicate at room temperature and average values are displayed, including error bars.

5.3. Results and Discussion

5.3.1. Characterization of Dextran Brushes

Ellipsometry and Contact-angle Measurements. Average ellipsometric PS-b-Dextran layer thicknesses (d) are listed in table 5.1, together with Π values at LB transfer, σ_{LB} and σ_{ell} values. The d value from ellipsometry at each spot on the wafer is calculated as the difference between the measured thicknesses of the PS-layer +

Π [mN/m]	σ_{LB} [nm ⁻²] ^a	d [nm] ^b	σ_{ell} [nm ⁻²] ^c
PS(12300)-b-Dextran(6000)			
10	0.12±0.007 (4.6%)	2.7±0.4 (16.8%)	0.09±0.02 (16.8%)
12	0.13±0.006 (4.6%)	3.4±1.3 (38.3%)	0.12±0.04 (38.3%)
20	0.20±0.012 (6.1%)	5.8±0.7 (12.6%)	0.20±0.03 (12.6%)
27	0.23±0.011 (5.1%)	8.1±0.3 (3.6%)	0.28±0.01 (3.6%)
31	0.26±0.012 (4.6%)	6.1±1.1 (18.3%)	0.21±0.04 (18.3%)
39	0.30±0.020 (6.7%)	11.2±1.7 (14.9%)	0.39±0.06 (14.9%)
PS(2100)-b-Dextran(6000)			
29	0.53±0.031 (4.6%)	4.5±0.6 (14.2%)	0.37±0.05 (14.2%)

^a Error calculated with: $\Delta\sigma_{LB}/\sigma_{LB} = \Delta V/V + \Delta C/C + \Delta A_0/A_0$.

V is the volume and C the concentration of the PS-b-Dextran solution, A_0 is the area of the compressed monolayer.

^b Average value from 3 measured d values at different spots of the wafer, including calculated error from these 3 values.

^c Error calculated with: $\Delta\sigma_{ell}/\sigma_{ell} = \Delta d/d$.

TABLE 5.1. LB interfacial pressure (after compression) (Π), LB grafting density (σ_{LB}), average ellipsometric thickness of transferred PS-b-Dextran layer (d) and calculated grafting density from ellipsometry (σ_{ell}).

PS-b-Dextran and that of the PS layer. The latter being relatively thick compared to d ; one expects an considerable scattering in the d values at each wafer. This contributes to the observed errors of the d values in table 5.1 and, consequently, of σ_{ell} .

In figure 5.2 σ_{ell} values are plotted against σ_{LB} values, to check the efficiency of the LB and LS transfer. For the majority of samples, the data in figure 5.2 confirm a successful transfer of PS-b-Dextran copolymer. Only at $\sigma_{LB} = 0.53$ nm⁻², is a significant difference between σ_{ell} and σ_{LB} observed. Those wafers were prepared with the LS method, which is less controllable than the LB method. Furthermore, at such a high grafting density the PS-b-Dextran monolayer is strongly aggregated at the air–water surface in the Langmuir trough, which probably reduces the transfer of the monolayer. In the contact-angle and adsorption results the grafting density value of $\sigma_{LB} = 0.53$ nm⁻² was corrected to the actual σ_{ell} value of 0.37 nm⁻².

The advancing contact angles (θ_{adv}) of water on the brushes are presented in figure 5.3 as a function of σ (including a trend-line). The contact angle for all the brushes is lower than the values measured on a pure PS film ($88.8^\circ \pm 0.8^\circ$), confirming the presence of a dextran layer. θ_{adv} decreases with increasing σ and levels off at high σ to a finite contact angle of approximately 70° . The θ_{adv}

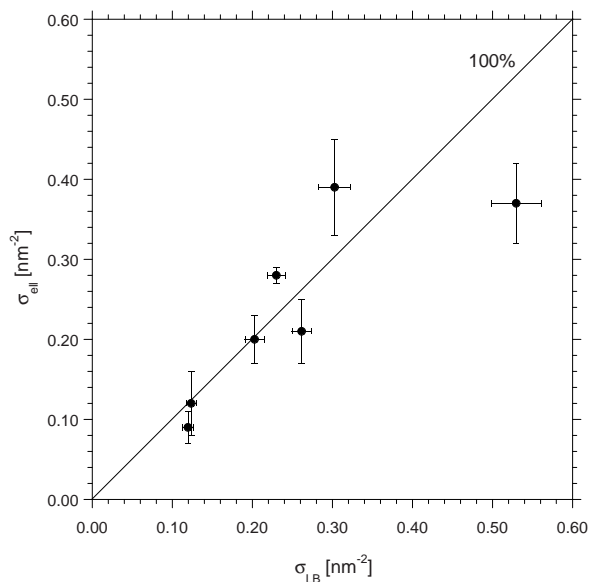


FIGURE 5.2. Efficiency of LB and LS transfer: grafting densities calculated from ellipsometry data (σ_{ell}) versus grafting density from LB (σ_{LB}). Line represents 100% transfer in LB or LS deposition.

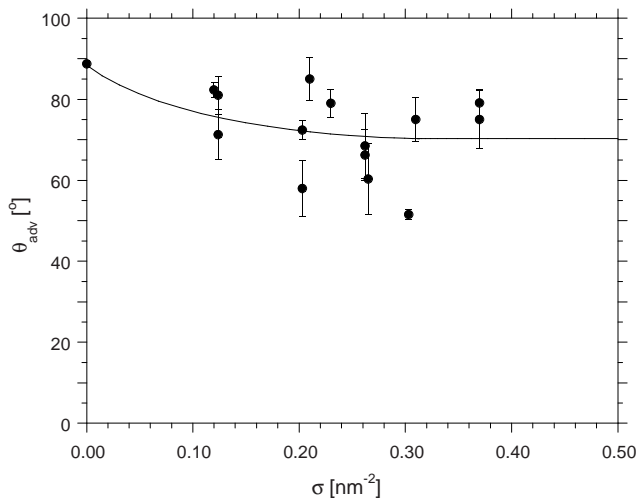


FIGURE 5.3. Advancing contact angles of water (θ_{adv}) on the dextran-grafted wafers as a function of the grafting density (σ) (including trend-line).

values are higher than might be expected for a coating of a hydrophilic polymer such as dextran. Yet, this is typical behaviour for wetting of a polymer brush by a good solvent, as explained by SCF calculations and experiments for PEO brushes by Cohen Stuart *et al.*³⁰ Grafted chains adsorb at the solvent–air interface, forming a bridge between the solid surface and the solvent–air interface, thereby preventing the droplet from spreading. Therefore, even at high grafting densities of a hydrophilic polymer, a finite contact angle for water is observed. Accordingly, the data in figure 5.3 do indicate the presence of a dextran brush at the solid surface.

AFM. Figure 5.4a shows a 3D AFM image and cross section of a spin-coated PS surface in air, displaying a smooth surface onto which the PS-b-Dextran layers are transferred. Figures 5.4b–e show AFM images of grafted dextran immersed in water, at different grafting densities, captured with tapping mode AFM. The images in figure 5.4 are the same as those in figure 4.14 in chapter 4. At $\sigma_{LB} = 0.26 \text{ nm}^{-2}$ the grafted dextran chains form a homogeneous layer (see figure 5.4d). On a scale of 500 nm (figure 5.4e) the dextran-covered surface is smooth. This is the region where the dextran chains are in the 'brush regime' ($\sigma \geq 0.18 \text{ nm}^{-2}$, see figure 5.1). However at $\sigma_{LB} = 0.12 \text{ nm}^{-2}$ the surface is inhomogeneous (see figure 5.4b and figure 5.4c). On a scale of 500 nm (figure 5.4c) patches of 50–150 nm can be distinguished, indicating the presence of aggregates at the surface, which were formed during the compression of the PS-b-Dextran monolayer at the air–water interface. Thus, the AFM images confirm our interpretation of the $\Pi - \sigma$ isotherms, including the time-dependent hysteresis, in terms of aggregation of the PS-b-Dextran copolymer, explained in chapter 4. As will be discussed in the next section, the existence of patches of PS-b-Dextran at low σ has large implications to the effect of the dextran coating on the adsorption of proteins.

5.3.2. Protein Adsorption

Two proteins were used to challenge the (brushed) surfaces, namely BSA and trypsin. The average charge of BSA is negative and of trypsin is positive at the pH applied. In figure 5.5 results of a few reflectometry experiments are shown, exemplary for BSA adsorption at dextran brushes at different grafting densities. Depending on the substrate, a steady-state adsorption is reached in 20 to 100 minutes. At low grafting densities ($\sigma \leq 0.20 \text{ nm}^{-2}$) the initial adsorption is fast, comparable to the initial adsorption on PS. With increasing grafting densities, the initial adsorption is slower and the steady-state adsorption values are lower.

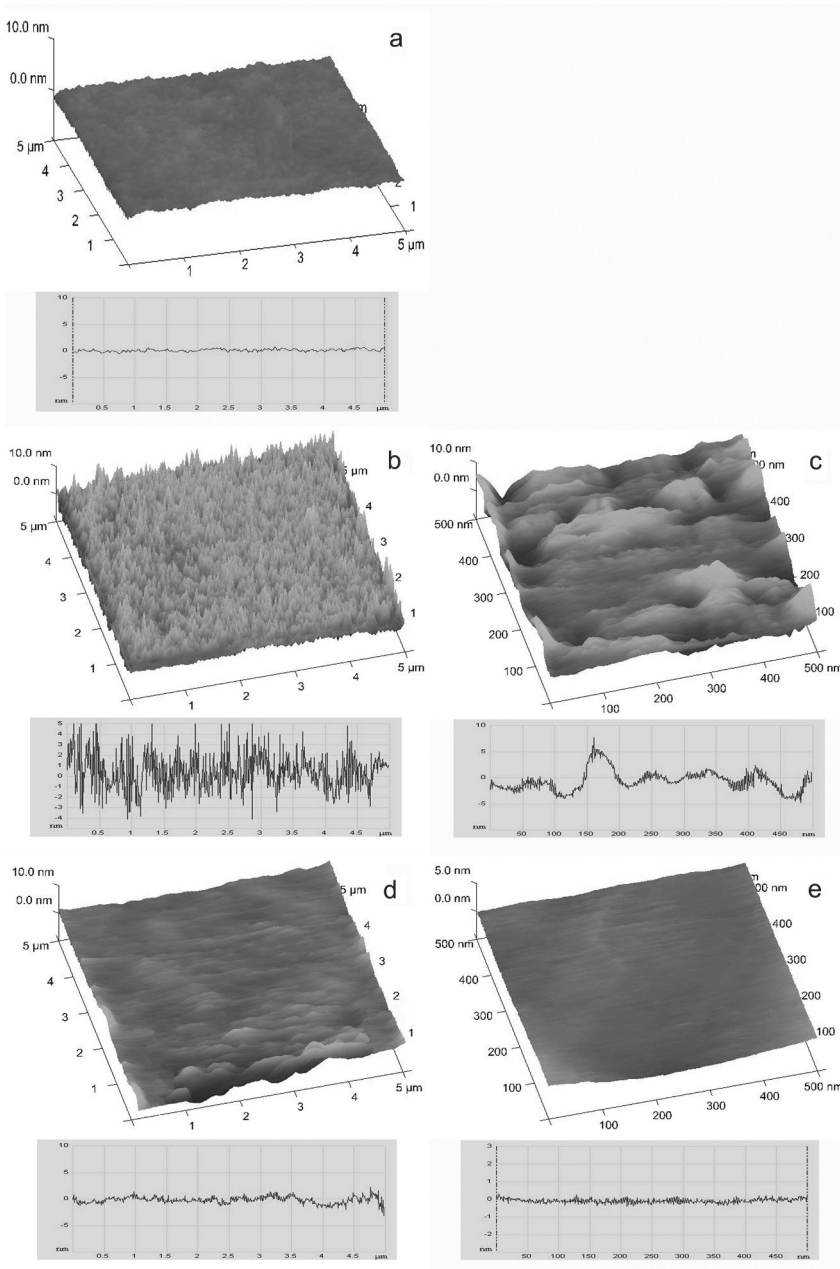


FIGURE 5.4. AFM images (3D and cross section): PS-coated silicon wafer (a) and grafted dextran $\sigma_{LB} = 0.12 \text{ nm}^{-2}$, scale $5 \mu\text{m}$ (b) and 500 nm (c), and $\sigma_{LB} = 0.26 \text{ nm}^{-2}$, scale $5 \mu\text{m}$ (d) and 500 nm (e).

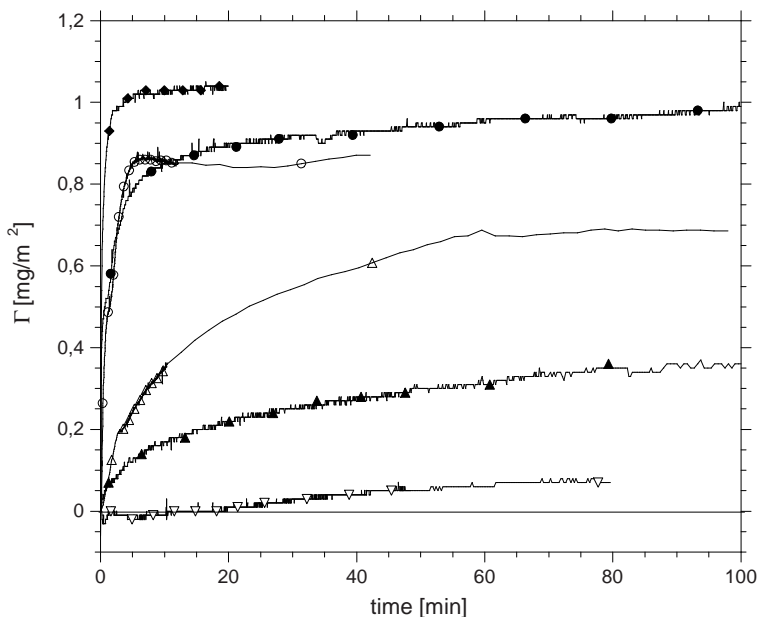


FIGURE 5.5. Some reflectometry experiments for BSA adsorption at dextran brushes with different grafting densities (adsorbed amount Γ versus time): PS ($-\blacklozenge-$), $\sigma = 0.12 \text{ nm}^{-2}$ ($-\circ-$), $\sigma = 0.20 \text{ nm}^{-2}$ ($-\bullet-$), $\sigma = 0.26 \text{ nm}^{-2}$ ($-\triangle-$), $\sigma = 0.30 \text{ nm}^{-2}$ ($-\blacktriangle-$), $\sigma = 0.37 \text{ nm}^{-2}$ ($-\nabla-$).

The averaged steady-state adsorbed amounts for BSA and trypsin from the reflectometry experiments are displayed in figure 5.6 as a function of the grafting density. At $\sigma \leq 0.20 \text{ nm}^{-2}$, the adsorbed amount is almost constant and similar to the adsorbed amount on a bare PS surface. At grafting densities $> 0.20 \text{ nm}^{-2}$ the adsorption drops steeply with increasing grafting density until nearly complete suppression of protein adsorption is attained at a grafting density as high as 0.37 nm^{-2} .

This adsorption behaviour may be understood with the help of the AFM images in figure 5.4. At $\sigma \leq 0.20 \text{ nm}^{-2}$, islands of block copolymer aggregates are found, leaving room for protein molecules to adsorb at areas of the PS surface that are not covered with dextran. It is known that protein molecules tend to spread on a hydrophobic surface like PS, reducing the adsorbed mass per unit surface area.¹²⁵ The small dextran-free interstices probably do not allow for full protein spreading, which could explain the almost constant adsorbed amount of protein for $0 \leq \sigma \leq 0.20 \text{ nm}^{-2}$. At $\sigma > 0.18 \text{ nm}^{-2}$ a homogeneous brush is formed, as

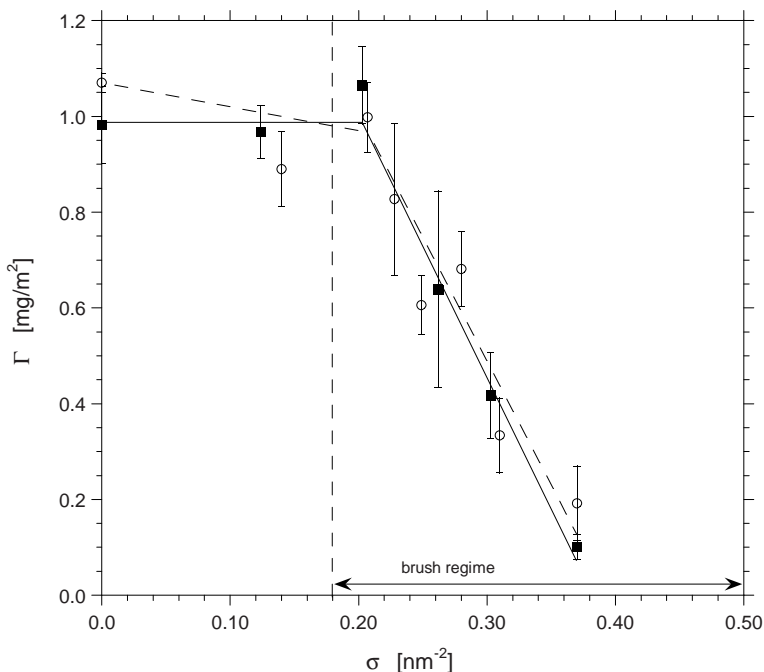


FIGURE 5.6. Adsorbed amount (Γ) as a function of grafting density (σ) for BSA (—■—) and trypsin (—○—). Lines shown are curve fits.

shown in AFM images 5.4d and 5.4e. Protein molecules trying to adsorb at the PS surface have to penetrate the brush. Excluded volume interactions between the protein and dextran chains oppose this penetration. This 'squeezing out' effect increases with increasing grafting density of the dextran chains, resulting in the observed reduction of adsorbed amount of protein.

There is hardly any difference between the adsorption patterns for the negatively charged BSA and the positively charged trypsin. This indicates that there is no significant contribution of electrostatic interaction to the adsorption at the electrically neutral dextran brush, as anticipated. Although BSA and trypsin are different in size (molecular volume of BSA is 88.2 nm³²⁶ and of trypsin is 29.8 nm³, based on molecular dimensions), the adsorptions, at different grafting densities, are similar. This might be due to the fact that BSA is heart-shaped and probably penetrates the dextran brush in a preferential orientation ('point-down'). With increasing grafting density, it is likely less immersed in the brush.

After reaching a steady-state adsorption in the reflectometry experiments, the protein solution was replaced by a buffer solution and the dextran-grafted wafers were rinsed to test a possible desorption of protein. No desorption of BSA was observed up to 120 minutes of rinsing. However, as for trypsin a desorption of 0–20% was detected during 120 minutes of rinsing, for wafers with $0 \leq \sigma \leq 0.25 \text{ nm}^{-2}$. Densely dextran-grafted wafers ($\sigma > 0.25 \text{ nm}^{-2}$) showed no desorption of trypsin upon rinsing. This can be explained as follows. At low grafting density the trypsin adsorbs at the dextran-free area of the PS surface, where part of the trypsin is only loosely bound to the surface and can be rinsed off with buffer. This is in accordance with research by Koutsopoulos and coworkers, who found 8–14% desorption of trypsin by flushing with buffer, after adsorption of trypsin at a PS surface.⁹⁹ BSA that adsorbs at wafers with low grafting density ($\sigma \leq 0.20 \text{ nm}^{-2}$) cannot be flushed off, because BSA is a 'sticky' protein that, once adsorbed at the PS areas of the wafer, cannot be removed with buffer, as previous results of BSA adsorption at PS surfaces reported.^{77, 124}

The adsorption of BSA on brushes of dextran and of PEO are compared for similar grafting densities and presented in figure 5.7. Dextran and PEO brushes of similar molecular weight are displayed. Normalized adsorption is shown: Γ/Γ_0 , Γ_0 being the adsorption at the bare PS surface. The data for the PEO brushes are taken from Currie and coworkers.³⁹ They used PS(4000)-b-PEO(6500) copolymer, LB to prepare the PEO brushes at PS surfaces and reflectometry to measure BSA adsorption. In the case of PEO, there is a substantial decrease of adsorbed amount at low grafting densities and a more gradual decrease at higher grafting densities, whereas in the case of dextran, adsorption suppression starts beyond a critical grafting density. There are a few possible reasons for this difference. First, in the case of PS-Dextran, large aggregates are formed at low grafting densities during the brush preparation, resulting in dextran-free areas at the surface where proteins can easily adsorb. This PS-b-Dextran aggregation on the air–water interface is promoted by the relatively large PS block of PS-b-Dextran ($M_w = 12300 \text{ Da}$) (see chapter 4). Second, at low σ , PEO forms a larger barrier against adsorption than dextran of similar molecular weight, due to the larger excluded volume of PEO in water, reflected in the reported lower χ -parameter (at room temperature); 0.44–0.46⁴⁷ for PEO-water as compared to 0.49–0.51 for dextran-water.²⁸ This is supported by calculations by Szleifer *et al.*²⁴ who showed that flexible grafted polymers are more effective in preventing protein adsorption than rigid grafted polymers (the bulky glycosylic units make dextran less flexible than PEO). Despite

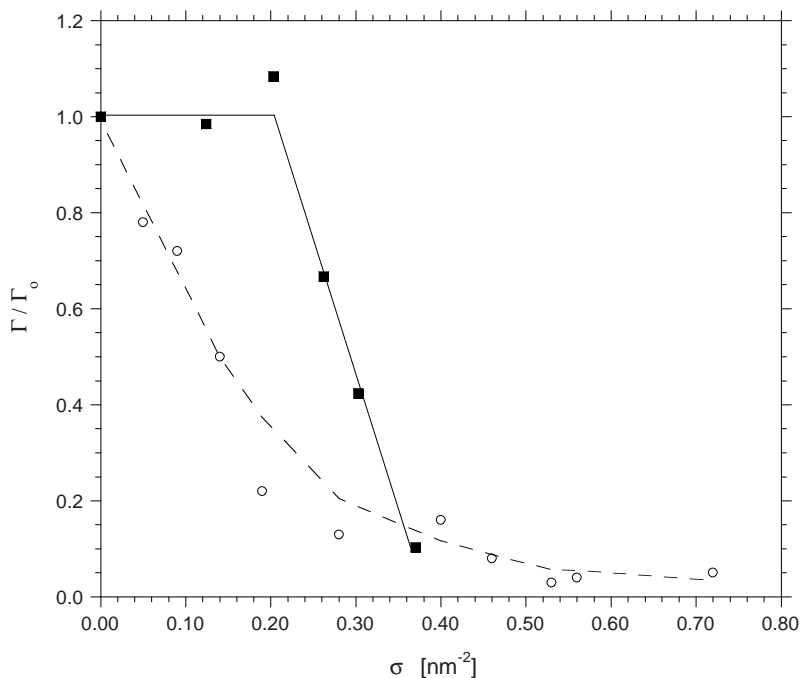


FIGURE 5.7. Normalized BSA adsorption (Γ/Γ_0) for dextran brushes ($M_w = 6000$ Da) (—■—) and PEO brushes ($M_w = 6500$ Da) (-○-) as a function of the grafting density. Lines shown are curve fits

the difference between PEO and dextran, laid out in figure 5.7, it can be concluded that at high grafting densities dextran brushes can reach the same level of protein repellency as PEO brushes (of comparable molecular weight).

Dextran brushes do not outperform PEO brushes as oligomannose-9 SAMs outperformed oligo(ethylene oxide) SAMs in surface force experiments with Human Serum Albumin.¹³⁷ Oligomannose-9 is a branched, neutral oligosaccharide. It is one of the oligosaccharides found at numerous blood-contacting surfaces throughout the human body that are likely evolutionarily selected because of superior anti-adhesive properties. Accordingly, it might form better protein rejecting surfaces than dextran-grafted surfaces. However, no protein-adsorption measurements at oligomannose-9 grafted surfaces have been reported yet.

5.4. Conclusions

We successfully prepared dextran brushes at a solid surface of PS at various grafting densities in a controlled way. The brushes were characterized by ellipsometry and water contact-angle measurements. Tapping mode AFM imaging showed that a homogeneous dextran brush is formed at $\sigma \geq 0.18 \text{ nm}^{-2}$. At lower grafting densities, aggregates of PS-b-Dextran are observed. This inhomogeneity can explain the relatively high amounts of adsorption of BSA and trypsin at $\sigma \leq 0.20 \text{ nm}^{-2}$. Beyond this value of 0.20 nm^{-2} adsorption of these proteins is suppressed because of the presence of a homogeneous dextran brush. Adsorption decreases with increasing grafting density due to increasing excluded volume interactions between the brush and the proteins. Almost complete adsorption suppression is reached at high grafting density, up to levels comparable to PEO brushes (of similar molecular weight). However, at low grafting densities PEO brushes seem to block protein adsorption better than dextran brushes.

Using PS-b-Dextran copolymers and the LB method to prepare dextran brushes in a 'real life' application is likely to be unsuitable, because of the aggregation and long relaxation times of the PS-b-Dextran monolayer and the fact that only flat surfaces can be coated in this way. Other preparation techniques, 'grafting from'⁴ (using *e.g.* the enzymatic method of¹⁰⁶) or the adsorption of complex coacervate core micelles^{18,20,162} are promising in that case.

What can be concluded from this research is that dense dextran brushes perform well in preventing BSA and trypsin to adsorb at a solid surface. Because the resistance of polymer brushes to protein adsorption is governed by generic physicochemical interactions, the observed adsorption pattern may apply to other proteins as well. Therefore, dense dextran brushes could be used for *e.g.* biomedical antifouling purposes. Moreover, the dextran brushes could be functionalized to bind specific proteins or enzymes while blocking the non-specific adsorption of other proteins. This could be applied to biosensors, separation technology and controlled release devices. Preparation of even more effective antifouling surfaces is likely accomplished using biomimetic oligo- or polysaccharides instead of dextran.

Acknowledgement

I thank Katja Patzsch for performing the trypsin adsorption experiments. I enjoyed our pleasant collaboration and useful discussions.

Part III

General Discussion

CHAPTER 6

General Discussion

In this General Discussion two phenomena will be elaborated, encountered during my research. First, some complications of preparing polymer brushes using Langmuir-Blodgett deposition will be reported. Second, some characteristics of the interaction of proteins with polymer brushes will be outlined, with special emphasis on the nature of the polymer used.

6.1. Langmuir-Blodgett Deposition and (Quasi-) 2D Aggregation

Over the last decade, Langmuir-Blodgett (LB) deposition of amphiphilic diblock copolymers was believed to be an excellent technique to produce well-defined, homogeneous, and reproducible polymer brushes at solid surfaces with tunable grafting densities.^{37,39,126} From the results in this thesis, it can be concluded that LB still is an adequate technique. However, there are some complications that need to be considered and under certain conditions the preparation of homogeneous brushes is not possible with LB.

The first complication was discovered by De Vos,¹⁶⁴ preparing PEO brushes at a PS surface with LB applying PS-*b*-PEO with various PEO chain lengths, in the same way as mentioned in chapter 2. The transfer of PS-*b*-PEO to the PS surface proved to be incomplete; the longer the PEO chain, the less the transfer. This imperfection is due to a competition for the PS surface between the PEO block and the PS block. Nonetheless, homogeneous PEO brushes were obtained with LB.¹⁶⁴

This incomplete transfer illustrates that the film deposition principle of LB is not as straightforward as depicted in textbooks, like *Langmuir-Blodgett Films*.¹³⁹ In fact, although the LB technique has been used extensively since the first publication of Blodgett in 1934,¹² a comprehensive mechanism explaining the transfer of floating monolayers to solid substrates on a molecular level is still lacking. This was previously questioned by Gaines and is still unresolved.⁶³

Another complication encountered, using amphiphilic diblock copolymers as applied in this thesis, is (quasi-) 2D aggregation. In chapters 3 and 4 the interfacial

behaviour of PS-b-Dextran was outlined, as well as the LB deposition of monolayers of PS-b-Dextran to PS coated surfaces. (Quasi-) 2D aggregation of these copolymers at the air–water interface was fully explained, including precautions needed for LB deposition of these layers.

Chapter 2 showed some strange interfacial behaviour of monomodal and bimodal PS-b-PEO, especially $\Pi(\sigma)$ hysteresis, suggesting a kind of 2D-aggregation. It was assumed that, for the purpose of preparing brushes at a solid surface, the obtained isotherms were adequate. We performed some additional experiments to check this assumption and to investigate the nature of the observed interfacial behaviour. As a starting point we used figure 2.5 in chapter 2 that presents the $\Pi - \sigma^{-1}$ isotherms of PS₂₉-b-PEO₄₈. It demonstrates hysteresis, as well as a minimum at low σ^{-1} upon expansion. This observation was first reported by Gonçalves da Silva *et al.*^{66,67} for PS-b-PEO_x with different PEO chain lengths ($x = 90 - 445$), however without a satisfactory explanation. They attributed the hysteresis to entanglements of the PEO chains. Our additional experiments on PS₂₉-b-PEO₄₈ monolayers proved this interpretation to be wrong. Gonçalves da Silva and coworkers showed that the hysteresis and the minimum gradually disappeared with PEO chain length increasing from 90 to 445.⁶⁶ In case of PS₃₇-b-PEO₇₇₀ we also did not record any hysteresis (see figure 2.4, chapter 2, except for high area per molecule). Consequently, it can be concluded that the hysteresis is maximal when the PS and PEO blocks are of similar size.

Fresh PS₂₉-b-PEO₄₈ monolayers were compressed to different values of Π and left to relax. Furthermore, PS₂₉-b-PEO₄₈ monolayers were compressed and immediately slightly expanded, up to the minimum in the interfacial pressure. From these experiments it appears that there are two types of relaxations of the monolayer, one from the maximal pressure (after compression) and one from the pressure at the minimum (after expansion), as can be seen in figure 6.1a. Besides, concerning the relaxation from the maximal pressure, a trigger pressure of 15 mN/m exists (see in figure 6.1b). Below a maximal pressure of 15 mN/m no relaxation is recorded, which indicates that the monolayer is stable at lower pressures. In comparison, PS₃₇-b-PEO₇₇₀ monolayers are stable even at high interfacial pressures; no relaxation is observed. Figure 6.1b also shows that, beyond 15 mN/m, the relaxation increases with increasing compression of the layer (increasing Π). The relaxation times of the PS₂₉-b-PEO₄₈ monolayer in figure 6.1b are relatively short. Relaxation is (almost) completed within 12 min. much less than the relaxation

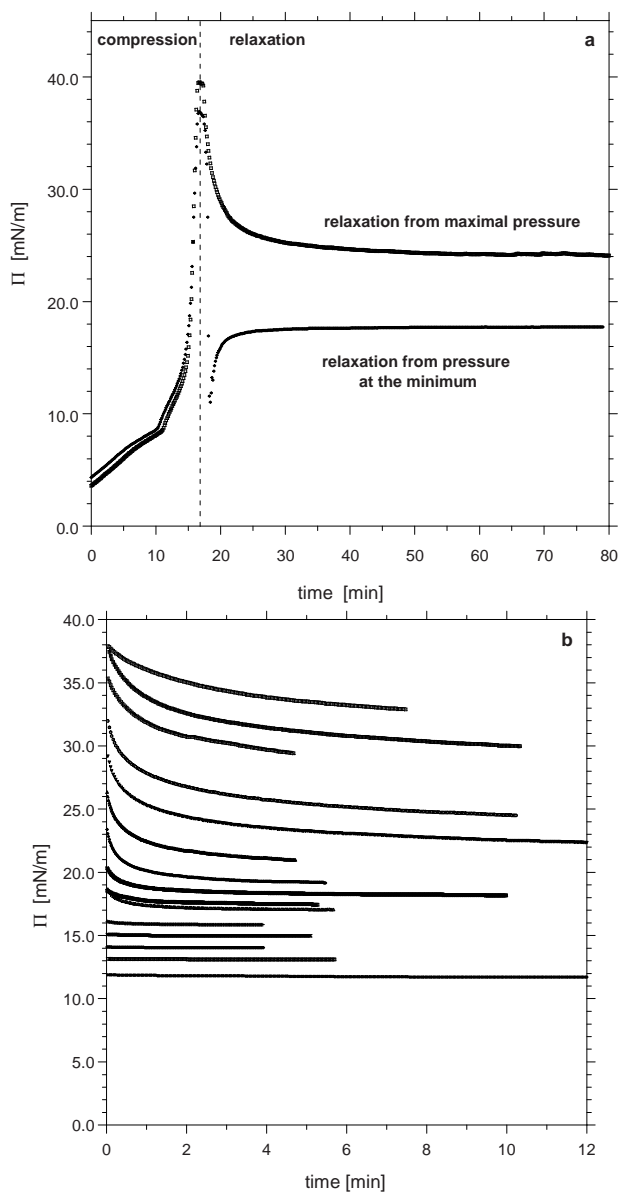


FIGURE 6.1. Interfacial pressure relaxation of $\text{PS}_{29}\text{-b-PEO}_{48}$ monolayers from two different compression states (a): Relaxation from maximal pressure (upper curve) and relaxation from pressure at the minimum (lower curve). Trigger pressure for relaxation of $\text{PS}_{29}\text{-b-PEO}_{48}$ monolayer (from maximal pressure) (b).

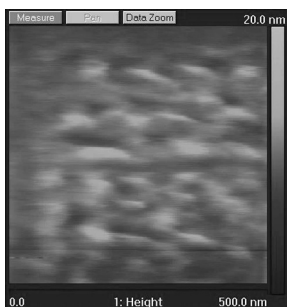


FIGURE 6.2. Contact mode AFM image of $\text{PS}_{29}\text{-b-PEO}_{48}$ compressed to $\Pi = 10$ mN/m.

times for the PS-b-Dextran layers described in chapters 3 and 4. This denotes a relatively short time scale process causing the pressure relaxation.

Subsequently, monolayers of $\text{PS}_{29}\text{-b-PEO}_{48}$ at different states of compression and expansion, and after relaxation as well, were transferred to a PS-coated silicon wafer using the Langmuir-Schaefer (LS) deposition method. This horizontal deposition technique was chosen to be able to transfer the $\text{PS}_{29}\text{-b-PEO}_{48}$ monolayer without distorting it. The time in between completion of compression and the actual LS deposition was kept as minimal as possible, to be able to 'capture' the state of the monolayer at the completion of compression. Subsequently, the transferred layers were investigated with contact mode AFM in air. Figure 6.2 presents the contact mode AFM image of an $\text{PS}_{29}\text{-b-PEO}_{48}$ monolayer compressed to $\Pi = 10$ mN/m. At this pressure there is no relaxation. The image demonstrates that the $\text{PS}_{29}\text{-b-PEO}_{48}$ layer is inhomogeneous at this pressure. There is some structure visible, although vague, indicating some height differences in the layer. Most likely, the thicker patches are composed of large $\text{PS}_{29}\text{-b-PEO}_{48}$ aggregates, formed during compression, according to the following scenario: at large area per molecule ($\Pi = 0$) the $\text{PS}_{29}\text{-b-PEO}_{48}$ self assembles into surface micelles, as reported by Eisenberg *et al.*. Upon compression, the PEO is forced to desorb into the water sub phase, reflected in an increase in Π . At a pressure of 10 mN/m the monolayer is within the (quasi-)plateau regime (see figure 2.5), where the PEO chains start to desorb completely into the water sub phase, as described in chapter 2. Because the PS and PEO blocks are of similar size, and the PEO is desorbed from the air-water surface, the PS blocks can meet and stick together through hydrophobic attraction, in a similar way as described for PS-b-Dextran in the plateau regime in

chapter 4. Thereby, large PS₂₉-b-PEO₄₈ aggregates are formed that coexist with dilute regions of PS₂₉-b-PEO₄₈ surface micelles.

In figure 6.3 a series of AFM images is collected, showing compressed PS₂₉-b-PEO₄₈ layers at different stages: compressed to $\Pi = 30$ mN/m (a1 and a2), compressed to $\Pi = 30$ mN/m and left to relax for 15 min. (b1 and b2), expanded to $\Pi = 9$ mN/m after relaxation (c1 and c2) and left to relax for 15 min. after expansion (d1 and d2). The AFM images clearly prove that the PS₂₉-b-PEO₄₈ monolayer is inhomogeneous at high interfacial pressures (above the trigger pressure of 15 mN/m). A pronounced structure is displayed, with high and low patches. Comparing figures 6.3a1 and 6.3a2 with figures 6.3b1 and 6.3b2, respectively, shows that the high and low patches grow significantly during relaxation. This resembles spinodal decomposition. The question arises: what are the different patches that get separated? Figure 6.3b1 and figure 6.3b2 represent a fully relaxed layer (compared to the relaxation times in figure 6.1b) and the high patches have sizes in the order of 100 nm. From figure 6.3b2 a height difference of ± 5 nm between the high and low patches can be deduced. This approximately equals the (average) thickness d of the PS₂₉-b-PEO₄₈ monolayer in air, $d = \sigma M / \rho N_{av}$. At $\Pi = 30$ mN/m, $\sigma^{-1} = 1.75$ nm² (from figure 2.5), therefore the average $\sigma = 0.57$ nm⁻². Consequently, the calculated $d = 4.5$ nm. This indicates that the observed height difference of ± 5 nm in AFM at $\Pi = 30$ mN/m might originate from multilayers of PS₂₉-b-PEO₄₈ present.

When the relaxed monolayer was slightly expanded, Π dropped to 9 mN/m, implying the formation of cracks at the air–water interface. Figure 6.3c1 confirms the presence of large cracks. Crack formation upon expansion was also affirmed by Brewster Angle Microscopy (BAM) experiments (data not shown). The fact that cracks are formed upon expansion, points out that the compressed layer is aggregated on a macroscopic level. It can be argued that this is due to PS aggregation, because of the relatively large size of the PS block of the copolymer. According to Kumaki, who studied the compression of PS particles of various molecular weights at the water surface, PS particles strongly aggregate at the air-water surface, forming an extensive network that does not decompose upon expansion.¹⁰⁰ The area occupied by PS₂₉ particles ($M_n \approx 3000$ g/mol) at the water surface is 1.0 nm².¹⁰⁰ At a Π of 30 mN/m, the average σ^{-1} of PS₂₉-b-PEO₄₈ is 1.75 nm². Therefore, it can be concluded that the water surface is largely covered with PS blocks, that strongly aggregate. From the cross section in figure 6.3c2 the thickness of the different patches can be obtained. The high

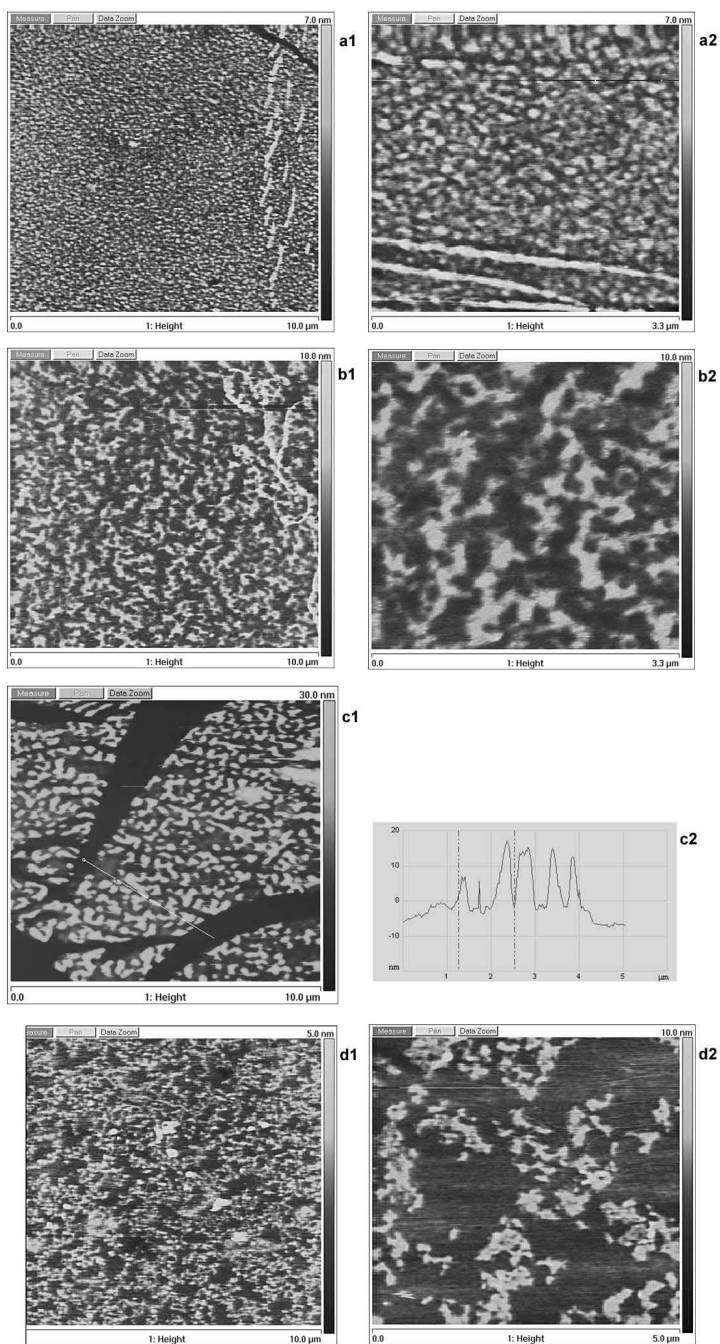


FIGURE 6.3. Contact mode AFM images of PS₂₉-b-PEO₄₈ compressed to $\Pi = 30$ mN/m (a1 and a2), left to relax for 15 min. (Π dropped to 23 mN/m) (b1 and b2), expanded to $\Pi = 9$ mN/m (c1 and c2) and left to relax for 15 min. (Π rose to 17 mN/m) (d1 and d2).

patches have a thickness of about 15-20 nm (compared to the crack/water phase), the low patches approximately 5 nm (compared to the crack/water phase). Again, this is a proof of the presence of multilayers. When compared to the calculated monolayer thickness of 4.5 nm, the high patches in figure 6.3 presumably consist of three layers of PS₂₉-b-PEO₄₈, the low patches of one layer. This points to the following scenario for the compression of a PS₂₉-b-PEO₄₈ monolayer. Starting from surface micelles, the PS₂₉-b-PEO₄₈ starts to form bigger aggregates in the (quasi-)plateau regime around 10 mN/m, where the PEO chains desorb into the water. When the monolayer is compressed to high pressures (above the trigger pressure of 15 mN/m), the lateral pressure in the monolayer is so high that the layer becomes unstable. Parts of the monolayer are budded off as a bilayer of PS₂₉-b-PEO₄₈ into the water sub phase, forced by the high interfacial pressure within the monolayer. The PS parts face each other, the PEO chains are stretched out into the water, forming the exterior of the bilayer. As a result of this 'budding off', the grafting density at the air-water surface is reduced and, consequently, the interfacial pressure relaxes. Eventually an equilibrium is attained, the relaxation process terminates within approximately 12 min. as mentioned before. The bilayer probably does not fold towards the interface, but dangles in the water phase, because the bilayer will be repelled by the PEO layer at the air-water interface. When the layers are transferred to the PS-coated surface and examined with AFM, the layers have dried and the bilayer covers the PS₂₉-b-PEO₄₈ monolayer, forming a tri-layer. The relative speed of the bilayer formation process is also illustrated by figure 6.3c1 and figures 6.3d1 and d2, respectively. The cracks that are formed upon expansion are filled with PS₂₉-b-PEO₄₈ from the bilayer in the water sub phase, that folds back towards the interface. The recovery is completed within 15 min. and a structure similar to the one prior to the expansion is regained. This PS-b-PEO interfacial behaviour is most pronounced when the PS and PEO blocks are of the same size. In case of relatively long PEO blocks, *e.g.* PS₃₇-b-PEO₇₇₀, the monolayer is stable upon compression and expansion.

A final peculiarity of the PS₂₉-b-PEO₄₈ layer exhibited in figure 2.5, is the disappearing of the minimum upon expansion with increasing number of compressions and expansions. Apparently, the layer becomes less rigid (although still aggregated) through some reorganization. Eventually, no more cracks are formed upon expansion, because the PS₂₉-b-PEO₄₈ layer responds to the expansion in a more flexible way by (partly) folding back of the bilayer to the air-water surface instead of breaking up.

The AFM images in figure 6.3 clearly demonstrate that monolayers of PS₂₉-b-PEO₄₈, compressed up to the 'brush regime', are inhomogeneous and, therefore, the wafers used in chapter 2 did not comprise of homogeneous PEO₄₈ brushes. Though, the wafers did contain a layer of PEO chains at the surface and, when in water, the bilayer present probably stretched out into the water phase. These wafers repel proteins from the surface, as observed in the adsorption experiments in chapter 2. However, because of the inhomogeneity, it is hard to draw solid conclusions based on the adsorption experiments.

6.2. Brushes and Proteins

The main objective of this PhD research was to investigate whether polysaccharide brushes were capable of preventing protein adsorption at a solid surface. The results in chapter 5 clearly showed that a polysaccharide brush consisting of dextran chains can reduce the protein adsorbed amount considerably. Almost complete suppression of protein adsorption is attained at high grafting densities. The performance of dense dextran brushes is identical to that of dense PEO brushes of similar molecular weight and grafting density. In a way, this is not surprising, if one considers the theoretical models of the 1990's.^{72,90,91,118} These models describe the interaction of colloidal particles, like proteins, with grafted polymer chains at a solid surface. According to these models, any flexible, water soluble polymer of a specific chain length will perform in a similar way, irrespective of the type of monomer. The main polymer brush parameters in these models, determining the adsorbed amount of protein, are the grafting density, the chain length and the solvent quality. The reason the type of monomer has no influence is the major assumption in these models that no attraction between the polymer (forming the brush) and the proteins exists. Several researchers over the past decades have proven this assumption to be wrong. Neutron scattering,² light scattering and fluorescence spectroscopy,¹⁰ force measurements^{51,138,145} and adsorption experiments^{39,50,126} demonstrated an attraction between proteins and PEO, the polymer mostly used as brush material in antifouling studies. In a recent review on PEO in drug delivery, Schubert and coworkers summarized some drawbacks of the use of PEO in the biomedical field.⁹⁷ One of the disadvantages is an immunological response. When intravenous administrated, PEO can cause blood clotting, indicating non-specific interaction with blood. Moreover, a hypersensitivity reaction is observed in 5–10% of the patients administrated with PEO-containing carriers, that can only be explained by some non-specific interaction with the immune

system. More sophisticated theories were proposed in the past decade, that include attraction between EO units and proteins.^{36,37,51,73,74} However, most of these theories only describe the attraction in terms of an attraction energy, the nature of the attraction is not explained. It is evidential that PEO is not a 'simple' polymer as considered for years. More 'complex' models for PEO were proposed, allowing for multiple and interconverting monomeric states of PEO.⁷⁵ In one of these models, Leckband *et al.* suggest that the hydrophobic parts of the protein are attracted to apolar EO segments, the apolar segments being induced by the advancing protein.⁵¹ This seems plausible, although incomplete. Dehydration of the hydrophobic parts of the protein might contribute to the attraction as well. Additionally, PEO is known to form hydrogen bonds in water. It might also form hydrogen bonds with proteins in water, directly or through water molecules. Multiple hydrogen bonds between EO units in the brush and proteins can add to the attraction. A study on complexation of Human Serum Albumin and PEO in aqueous solutions confirms the suggested hydrogen bonding between proteins and PEO.¹⁰ Apart from that, Morra emphasized the role of hydrogen bonds and hydration forces in a review on fouling resistant surfaces.¹²¹ Yet, a comprehensive model for protein-polymer brush interaction, including all contributions mentioned, is still lacking. Concerning the adsorption of proteins at dextran brushes, the theoretical models used so far cannot be applied, because of hydrogen bonding within the brush (see chapters 3 and 4). More sophisticated models are needed, including dextran-dextran and dextran-protein hydrogen bonding. Because glycerol prevents the formation of hydrogen bonds, as illustrated in chapter 3, protein adsorption experiments at dextran brushes using glycerol can be performed to test these models and to highlight the role of hydrogen bonds in the adsorption process.

The focus in theory and experiments of protein adsorption at brushes is mainly on the brush characteristics and how to control them and less on the proteins and their aspects related to adsorption. Proteins are mostly treated as spheres or ellipsoids with some interaction energy with the surface and, in some cases, with some interaction energy with the polymer in the brush. However, proteins are much more complicated and should be treated likewise. This oversimplification of proteins was previously remarked by Halperin and Leckband.⁷⁵ Theory depicting protein adsorption at brushes needs to be more realistic, *e.g.* by incorporating the contributions to adsorption mentioned above. Appropriate measurements should be performed to test these contributions.

Adsorption experiments of BSA at PEO₇₇₀ brushes display ternary adsorption, as discussed in chapter 2. This means that BSA is captured inside the PEO brush where attraction between BSA and PEO occurs. As yet, there is no experimental evidence that reveals the position of the protein inside the brush. Neutron Reflectivity (NR) is a technique that may provide this information. We performed a preliminary NR experiment with silica particle adsorption at a PEO₇₇₀ brush, as a model system for colloid-brush interaction. The result is promising, because it clearly demonstrates the position of the silica particles inside the brush.

Until now, PEO has been considered the ideal candidate for antifouling applications. For good reasons, because PEO is a very flexible, water soluble polymer that has a large excluded volume in water, has shown to reduce protein adsorption and is nontoxic. Yet, there is substantial evidence of attraction between PEO and proteins, that makes PEO less suitable. Based on force measurements,^{137, 155} neutral oligo- or polysaccharides, *e.g.* dextran, are probably more appropriate candidates for protein rejection, because no attraction occurs. Especially biomimetic saccharides seem to be very effective, like oligomannose-9 studied by Rixman.¹³⁷ Even more sophisticated oligo- or polysaccharide coatings, with neutral and charged monomers, can be manufactured for *e.g.* biosensors, blocking non-specific adsorption, while binding specific proteins or enzymes. An important aspect of polysaccharides in aqueous solutions is hydrogen bonding, intra- and intermolecular, as well as with water molecules.^{27, 42, 121} This was clearly demonstrated for dextran brushes at the air-water surface in chapters 3 and 4. Most likely, hydrogen bonding and hydration^{89, 135} also play an important role in the interaction of oligo- and polysaccharide coated surfaces with biocolloids. To which extent is not yet known.

Using amphiphilic PS-b-polysaccharide copolymers and the LB method to prepare polysaccharide brushes, as outlined in this thesis, in a 'real life' application is inappropriate, because of the complications with diblock copolymers in LB (aggregation, long relaxation times) and the fact that only flat surfaces can be coated in this way. Furthermore, the use of PS in the biomedical field on a nanoscale may not be safe.^{57, 123} Research shows that, although PS is considered a low-toxic material,¹⁷ PS nanoparticles cause inflammatory effects as a consequence of their large surface area.^{17, 57} Useful preparation techniques for dextran or other polysaccharide brushes may be 'grafting from'⁴ (using *e.g.* the enzymatic method of Loos¹⁰⁶), the adsorption of complex coacervate core micelles^{18, 20, 162} or the 'zipper brush' technique (ultra dense brushes through adsorption) of de Vos and coworkers.¹⁶⁵

Acknowledgement

I thank Martijn Hendriksen for performing the additional interfacial pressure, AFM and BAM experiments on PS₂₉-b-PEO₄₈ layers. I am grateful to Petya Iakovlev and Frans Leermakers for the enlightening discussions on the behaviour of PS₂₉-b-PEO₄₈ at the air-water interface. I also want to thank Ad van Well from TU Delft for the pleasant collaboration on the NR experiments at ISIS.

Bibliography

- [1] N.L. Abbott, D. Blankschtein, and T.A. Hatton. Protein partitioning in two-phase aqueous polymer systems. 1. novel physical pictures and a scaling-thermodynamic formulation. *Macromolecules*, 24:4334–4348, 1991.
- [2] N.L. Abbott, D. Blankschtein, and T.A. Hatton. Protein partitioning in two-phase aqueous polymer systems. 3. a neutron scattering investigation of the polymer solution structure and protein-polymer interactions. *Macromolecules*, 25:3932–3941, 1992.
- [3] W. Adam, C.R. Saha-Möller, and C. Zhao. *Organic Reactions*, volume 61. Wiley, 2002.
- [4] R.C. Advincula, W.J. Brittain, K.C. Caster, and J. Rühle. *Polymer Brushes. Synthesis, Characterization, Applications*. Wiley-VCH, Weinheim, Germany, 2004.
- [5] B. Alberts, D. Bray, J. Lewis, M. Raff, K. Roberts, and J.D. Watson. *Molecular Biology of the Cell*. Garland Publishing, New York, USA, 1994.
- [6] S. Alexander. Adsorption of chain molecules with a polar head. a scaling description. *J. Phys. (France)*, 38:983–987, 1977.
- [7] J.D. Andrade. *Surface and Interfacial Aspects of Biomedical Polymers. Protein Adsorption*. Plenum Press, New York, USA, 1985.
- [8] J.D. Andrade, V. Hlady, L. Feng, and K. Tingey. *Interfacial Phenomena and Bioproducts*. Marcel Dekker, New York, USA, 1996.
- [9] D. Appelhans, H. Komber, M.A. Quadir, S. Richter, S. Schwarz, J. van der Vlist, A. Aigner, M. Müller, K. Loos, J. Seidel, K.-F. Arndt, R. Haag, and B. Voit. Hyperbranched pei with various oligosaccharide architectures: Synthesis, characterization, atp complexation, and cellular uptake properties. *Biomacromolecules*, 10:1114–1124, 2009.
- [10] S. Azegami, A. Tsuboi, T. Izumi, M. Hirata, P.L. Dubin, B. Wang, and E. Kokufuta. Formation of an intrapolymer complex from human serum albumin and poly(ethylene glycol). *Langmuir*, 15:940–947, 1999.
- [11] H.D. Bijsterbosch, V.O. de Haan, A.W. de Graaf, M. Mellema, F.A.M. Leermakers, M.A. Cohen Stuart, and A.A. van Well. Tethered adsorbing chains: Neutron reflectivity and surface pressure of spread diblock copolymer monolayers. *Langmuir*, 11:4467–4473, 1995.
- [12] K.B. Blodgett. Monomolecular films of fatty acids on glass. *J. Am. Chem. Soc.*, 56:495, 1934.
- [13] K.B. Blodgett. Films built by depositing successive monomolecular layers on a solid surface. *J. Am. Chem. Soc.*, 57:1007–1022, 1935.
- [14] K.B. Blodgett and I. Langmuir. Built-up films of barium stearate and their optical properties. *Phys. Rev.*, 51:964–982, 1937.
- [15] R.F. Borch, M.D. Bernstein, and H.D. Durst. Cyanohydrinborate anion as a selective reducing agent. *J. Am. Chem. Soc.*, 93:2897–2904, 1971.

- [16] H.G. Breitinger. Synthesis of silica-bound amylose by phosphorolytic elongation of immobilised maltoheptaosyl hydrazides. *Tetrahedron Lett.*, 43:6127–6131, 2002.
- [17] D.M. Brown, M.R. Wilson, W. MacNee, V. Stone, and K. Donaldson. Size-dependent proinflammatory effects of ultrafine polystyrene particles: A role for surface area and oxidative stress in the enhanced activity of ultrafines. *Toxicology Appl. Pharmacology.*, 175:191–199, 2001.
- [18] A.M. Brzozowska, B. Hofs, A. de Keizer, R. Fokkink, M.A. Cohen Stuart, and W. Norde. Reduction of protein adsorption on silica and polystyrene surfaces due to coating with complex coacervate core micelles. *Colloids Surfaces A*, 347:146–155, 2009.
- [19] F.F. Buck, A.J. Vithayathil, M. Bier, and F.F. Nord. On the mechanism of enzyme action. lxxiii. studies on trypsin from beef, sheep and pig pancreas. *Arch. Biochem. Biophys.*, 97:417–424, 1962.
- [20] S. van der Burgh, R. Fokkink, A. de Keizer, and M.A. Cohen Stuart. Complex coacervation core micelles as anti-fouling agents on silica and polystyrene surfaces. *Colloids Surfaces A*, 242:167–174, 2004.
- [21] H.J. Busscher, R.J. Ploeg, and H.C. van der Mei. Snapshot: Biofilms and biomaterials; mechanisms of medical device related infections. *Biomaterials*, 30:4247–4248, 2009.
- [22] H.J. Busscher and A.H. Weerkamp. Specific and non-specific interactions in bacterial adhesion to solid substrata. *FEMS Microbiol. Rev.*, 46:165–173, 1987.
- [23] B.H. Cao and M.W. Kim. Molecular weight dependence of the surface tension of aqueous poly(ethylene oxide) solutions. *Faraday Discuss.*, 98:245–252, 1994.
- [24] M.A. Carignano and I. Szeifer. Prevention of protein adsorption by flexible and rigid chain molecules. *Colloids Surfaces B*, 18:169–182, 2000.
- [25] M. Carlsson, P. Linse, and F. Tjerneld. Temperature-dependent protein partitioning in two-phase aqueous polymer systems. *Macromolecules*, 26:1546–1554, 1993.
- [26] D.C. Carter and J.X. Ho. Structure of serum albumin. *Adv. Protein Chem.*, 45:153–203, 1994.
- [27] P.M. Claesson. *Biopolymers at Interfaces*. Marcel Dekker, New York, USA, 1998.
- [28] A.H. Clark. Direct analysis of experimental tie line data (two polymer-one solvent systems) using flory-huggins theory. *Carbohydrate Polymers*, 42:337–351, 2000.
- [29] M.A. Cohen Stuart and A. de Keizer. *Oxide Surfaces*. Marcel Dekker, New York, USA, 2001.
- [30] M.A. Cohen Stuart, W.M. de Vos, and F.A.M. Leermakers. Why surfaces modified by flexible polymers often have a finite contact angle for good solvents. *Langmuir*, 22:1722–1728, 2006.
- [31] J.W. Costerton, P.S. Stewart, and E.P. Greenberg. Bacterial biofilms: A common cause of persistent infections. *Science*, 284:1318–1322, 1999.
- [32] J.K. Cox, A. Eisenberg, and R.B. Lennox. Patterned surfaces via self-assembly. *Cur. Op. Colloid Interface Sci.*, 4:52–59, 1999.
- [33] J.K. Cox, K. Yu, B. Constantine, A. Eisenberg, and R.B. Lennox. Polystyrene-poly(ethylene oxide) diblock copolymers form well-defined surface aggregates at the air/water interface. *Langmuir*, 15:7714–7718, 1999.

- [34] J.K. Cox, K. Yu, A. Eisenberg, and R.B. Lennox. Compression of polystyrene-poly(ethylene oxide) surface aggregates at the air/water interface. *Phys. Chem. Chem. Phys.*, 1:4417–4421, 1999.
- [35] E.P.K. Currie. *Brushes and Soap*. Wageningen Universiteit, 2000.
- [36] E.P.K. Currie, F.A.M. Leermakers, M.A. Cohen Stuart, and G.J. Fleer. Grafted adsorbing polymers: Scaling behavior and phase transitions. *Macromolecules*, 32:487–498, 1999.
- [37] E.P.K. Currie, W. Norde, and M.A. Cohen Stuart. Tethered polymer chains: surface chemistry and their impact on colloidal and surface properties. *Adv. Colloid Interface Sci.*, 100–102:205–265, 2003.
- [38] E.P.K. Currie, A.B. Sieval, M. Avena, H. Zuilhof, E.J.R. Sudhölter, and M.A. Cohen Stuart. Weak polyacid brushes: Preparation by lb deposition and optically detected titrations. *Langmuir*, 15:7116–7118, 1999.
- [39] E.P.K. Currie, J. van der Gucht, O.V. Borisov, and M.A. Cohen Stuart. Stuffed brushes: theory and experiment. *Pure Appl. Chem.*, 71:1227–1241, 1999.
- [40] E.P.K. Currie, M. Wagemaker, M.A. Cohen Stuart, and A.A. van Well. Structure of monodisperse and bimodal brushes. *Macromolecules*, 32:9041–9050, 1999.
- [41] E.P.K. Currie, M. Wagemaker, M.A. Cohen Stuart, and A.A. van Well. Structure of grafted polymers, investigated with neutron reflectometry. *Physica B*, 283:17–21, 2000.
- [42] S. David. *The molecular and supramolecular chemistry of carbohydrates: chemical introduction to the glycosciences*. Oxford University Press, Oxford, UK, 1997.
- [43] E. Österberg, K. Bergström, K. Holmberg, J.A. Riggs, J.M. Van Alstine, T.P. Schuman, N.L. Burns, and J. Milton Harris. Comparison of polysaccharide and poly(ethylene glycol) coatings for reduction of protein adsorption on polystyrene surfaces. *Colloids Surfaces A*, 77:159–169, 1993.
- [44] E. Österberg, K. Bergström, K. Holmberg, T.P. Schuman, J.A. Riggs, N.L. Burns, J.M. Van Alstine, and J. Milton Harris. Protein-rejecting ability of surface-bound dextran in end-on and side-on configurations: Comparison to peg. *J. Biomed. Mat. Res.*, 29:741–747, 1995.
- [45] J.C. Dijt, M.A. Cohen Stuart, and G.J. Fleer. Reflectometry as a tool for adsorption studies. *Adv. Colloid Interface Sci.*, 50:79–101, 1994.
- [46] J.C. Dijt, M.A. Cohen Stuart, J.E. Hofman, and G.J. Fleer. Kinetics of polymer adsorption in stagnation point flow. *Colloids Surfaces*, 51:141–158, 1990.
- [47] E.E. Dormidontova. Role of competitive peo-water and water-water hydrogen bonding in aqueous solution peo behavior. *Macromolecules*, 35:987–1001, 2002.
- [48] J.-L. Doublier, C. Garnier, D. Renard, and C. Sanchez. Protein-polysaccharide interactions. *Cur. Op. Colloid Interface Sci.*, 5:202–214, 2000.
- [49] P.D. Drumheller, C.B. Herbert, and J.A. Hubbel. *Interfacial Phenomena and Bioproducts*. Marcel Dekker, New York, USA, 1996.
- [50] N.V. Efremova, B. Bondurant, D.F. O’Brien, , and D.E. Leckband. Measurements of interbilayer forces and protein adsorption on uncharged lipid bilayers displaying poly(ethylene glycol) chains. *Biochemistry*, 39:3441–3451, 2000.

- [51] N.V. Efremova, S.R. Sheth, and D.E. Leckband. Protein-induced changes in poly(ethylene glycol) brushes: Molecular weight and temperature dependence. *Langmuir*, 17:7628–7636, 2001.
- [52] C. von Eiff, W. Kohnen, K. Becker, and B. Jansen. Modern strategies in the prevention of implant-associated infections. *Int. J. Artificial Organs*, 28:1146–1156, 2005.
- [53] A. Escher and W.G. Characklis. *Biofilms*. John Wiley & Sons, New York, USA, 1990.
- [54] K.M. Faucher, X.-L. Sun, and E.L. Chaikof. Fabrication and characterization of glycocalyx-mimetic surfaces. *Langmuir*, 19:1664–1670, 2003.
- [55] M.C. Fauré, P. Bassereau, L.T. Lee, A. Menelle, and C. Lheveder. Phase transitions in monolayers of ps-peo copolymer at the air-water interface. *Macromolecules*, 32:8538–8550, 1999.
- [56] G.J. Fleer, M.A. Cohen Stuart, J.M.H.M. Scheutjens, T. Cosgrove, and B. Vincent. *Polymers at Interfaces*. Chapman & Hall, London, UK, 1993.
- [57] U.S. Food and Drug Administration. Nanotechnology Task Force. *Nanotechnology*. 2007.
- [58] P.M. Forssell, J.M. Mikkilä, G.K. Moates, and R. Parker. Phase and glass transition behaviour of concentrated barley starch-glycerol-water mixtures, a model for thermoplastic starch. *Carbohydrate Polymers*, 34:275–282, 1997.
- [59] C. Fournier, M. Leonard, I. Coq-Leonard, and E. Dellacherie. Coating polystyrene particles by adsorption of hydrophobically modified dextran. *Langmuir*, 11:2344–2347, 1995.
- [60] R.A. Frazier, G. Matthijs, M.C. Davies, C.J. Roberts, E. Schacht, and S.J.B. Tendler. Characterization of protein-resistant dextran monolayers. *Biomaterials*, 21:957–966, 2000.
- [61] M. Fukuda and O. Hindsgaul. *Molecular Glycobiology*. IRL Press, Oxford, UK, 1994.
- [62] I Fundeanu, H.C. van der Mei, A.J. Schouten, and H.J. Busscher. Microbial adhesion to surface-grafted polyacrylamide brushes after long-term exposure to pbs and reconstituted freeze-dried saliva. *J. Biomed. Mat. Res. A*, 94, 2010.
- [63] G.L. Gaines Jr. From monolayer to multilayer: Some unanswered questions. *Thin Solid Films*, 68:1–5, 1980.
- [64] P.-G. de Gennes. Conformations of polymers attached to an interface. *Macromolecules*, 13:1069–1075, 1980.
- [65] W.R. Gombotz, W. Guanghui, T.A. Horbett, and A.S. Hoffman. Protein adsorption to poly(ethylene oxide) surfaces. *J. Biomed. Mat. Res.*, 25:1547–1562, 1991.
- [66] A.M. Gonçalves da Silva, E.J.M. Filipe, J.M.R. d’Oliveira, and J.M.G. Martinho. Interfacial behavior of poly(styrene)-poly(ethylene oxide) diblock copolymer monolayers at the air-water interface. hydrophilic block chain length and temperature influence. *Langmuir*, 12:6547–6553, 1996.
- [67] A.M. Gonçalves da Silva, A.L. Simões Gamboa, and J.M.G. Martinho. Aggregation of poly(styrene)-poly(ethylene oxide) diblock copolymer monolayers at the air-water interface. *Langmuir*, 14:5327–5330, 1998.
- [68] B. Gottenbos, H.J. Busscher, H.C. van der Mei, and P. Nieuwhuis. Pathogenesis and prevention of biomaterial centered infections. *J. Mat. Sci. Mat. Med.*, 13:717–722, 2002.
- [69] B. Gottenbos, H.C. van der Mei, and H.J. Busscher. Models for studying initial adhesion and surface growth in biofilm formation on surfaces. *Methods Enzymology*, 310:523–534, 1999.

- [70] E. Grill, C. Huber, P.J. Oefner, A.E. Vorndran, and G.K. Bonn. Capillary zone electrophoresis of *p*-aminobenzoic acid derivatives of aldoses, ketoses and uronic acids. *Electrophoresis*, 14:1004–1010, 1993.
- [71] A.G. Gristina. Biomaterial-centered infection: Microbial adhesion versus tissue integration. *Science*, 237:1588–1595, 1987.
- [72] A. Halperin. Polymer brushes that resist adsorption of model proteins: Design parameters. *Langmuir*, 15:2525–2533, 1999.
- [73] A. Halperin, G. Fragneto, A. Schollier, and M. Sferrazza. Primary versus ternary adsorption of proteins onto peg brushes. *Langmuir*, 23:10603–10617, 2007.
- [74] A. Halperin and M. Kröger. Ternary protein adsorption onto brushes: Strong versus weak. *Langmuir*, 25:11621–11634, 2009.
- [75] A. Halperin and D.E. Leckband. From ship hulls to contact lenses: repression of protein adsorption and the puzzle of peo. *C. R. Acad. Sci. Paris*, 1:1171–1178, 2000.
- [76] P. Harder, M. Grunze, R. Dahint, G.M. Whitesides, and P.E. Laibinis. Molecular conformation in oligo(ethylene glycol)-terminated self-assembled monolayers on gold and silver surfaces determines their ability to resist protein adsorption. *J. Phys. Chem. B*, 102:426–436, 1998.
- [77] C.A. Haynes and W. Norde. Globular proteins at solid/liquid interfaces. *Colloids Surfaces B*, 2:517–566, 1994.
- [78] G. T. Hermanson. *Bioconjugate Techniques*. Academic Press, San Diego, USA, 1996.
- [79] J.F. Hester, P. Banerjee, and A.M. Mayes. Preparation of protein-resistant surfaces on poly(vinylidene fluoride) membranes via surface segregation. *Macromolecules*, 32:1643–1650, 1999.
- [80] N.B. Holland, Y. Qiu, M. Ruegsegger, and R.E. Marchant. Biomimetic engineering of non-adhesive glycocalyx-like surfaces using oligosaccharide surfactant polymers. *Nature*, 392:799–801, 1998.
- [81] K. Holmberg and G. Quash. *Biopolymers at Interfaces*. Marcel Dekker, New York, USA, 2003.
- [82] S. Honda, S. Iwase, A. Makino, and S. Fujiwara. Simultaneous determination of reducing monosaccharides by capillary zone electrophoresis as the borate complexes of *n*-2-pyridylglycamines. *Anal. Biochem.*, 176:72–77, 1989.
- [83] A.R. Hoskins, I.D. Robb, and P.A. Williams. Selective separation of proteins from mixtures using polysaccharides. *Biopolymers*, 45:97–104, 1998.
- [84] C.E. Ioan, T. Aberle, and W. Burchard. Structure properties of dextran. 2. dilute solution. *Macromolecules*, 33:5730–5739, 2000.
- [85] J. Israelachvili. The different faces of poly(ethylene glycol). *Proc. Natl. Acad. Sci. USA*, 94:8378–8379, 1997.
- [86] J. N. Israelachvili. *Intermolecular and Surface Forces*. Academic Press, London, UK, 1991.
- [87] J.N. Israelachvili. Self-assembly in two dimensions: Surface micelles and domain formation in monolayers. *Langmuir*, 10:3774–3781, 1994.
- [88] J.N. Israelachvili and R.M. Pashley. The hydrophobic interaction is long range, decaying exponentially with distance. *Nature*, 300:341–342, 1982.

- [89] J.N. Israelachvili and H. Wennerström. Role of hydration and water structure in biological and colloidal interactions. *Nature*, 379:219–225, 1996.
- [90] S.I. Jeon, J.H. Lee, J.D. Andrade, and P.-G. de Gennes. Protein-surface interactions in the presence of polyethylene oxide. i. simplified theory. *J. Colloid Interface Sci.*, 142:149–158, 1991.
- [91] S.I. Jeon, J.H. Lee, J.D. Andrade, and P.-G. de Gennes. Protein-surface interactions in the presence of polyethylene oxide. ii. effect of protein size. *J. Colloid Interface Sci.*, 142:159–166, 1991.
- [92] H.J. Kaper, H.J. Busscher, and W. Norde. Characterization of poly(ethylene oxide) brushes on glass surfaces and adhesion of staphylococcus epidermidis. *J. Biomat. Sci. Polymer Edn*, 14:313–324, 2003.
- [93] K. Kawasaki, M. Kambara, H. Matsumura, and W. Norde. Protein adsorption at polymer-grafted surfaces: Comparison between a mixture of saliva proteins and some well-defined model proteins. *Biofouling*, 19:355–363, 2003.
- [94] J.F.W. Keuren, S.J.H. Wielders, G.M. Willems, M. Morra, L. Cahalan, P. Cahalan, and T. Lindhout. Thrombogenicity of polysaccharide-coated surfaces. *Biomaterials*, 24:1917–1924, 2003.
- [95] B. Klajnert, D. Appelhans, H. Komber, N. Morgner, S. Schwarz, S. Richter, B. Brutschy, M. Ionov, A.K. Tonkikh, M. Bryszewska, and B. Voit. The influence of densely organized maltose shells on the biological properties of poly(propylene imine) dendrimers: New effects dependent on hydrogen bonding. *Chem. Eur. J.*, 14:7030–7041, 2008.
- [96] M. Klawonn, S. Bohr, G. Mehlretter, C. Dobler, C. Fischer, and M. Beller. A simple and convenient method for epoxidation of olefins without metal catalysts. *Adv. Synth. Catal.*, 345:389–392, 2003.
- [97] K. Knop, R. Hoogenboom, D. Fischer, and U.S. Schubert. Poly(ethylene glycol) in drug delivery: Pros and cons as well as potential alternatives. *Angew. Chem. Int. Ed.*, 49:6288–6308, 2010.
- [98] K. Kobayashi, S. Kamiya, and Enomoto N. Amylose-carrying styrene macromonomer and its homo- and copolymers: Synthesis via enzyme-catalyzed polymerization and complex formation with iodine. *Macromolecules*, 29:8670–8676, 1996.
- [99] S. Koutsopoulos, K. Patzsch, W.T.E. Bosker, and W. Norde. Adsorption of trypsin on hydrophilic and hydrophobic surfaces. *Langmuir*, 23:2000–2006, 2007.
- [100] J. Kumaki. Monolayer of polystyrene monomolecular particles on a water surface studied by langmuir-type through film balance and transmission electron microscopy. *Macromolecules*, 21:749–755, 1988.
- [101] B.S. Lane and K. Burgess. A cheap, catalytic, scalable, and environmentally benign method for alkene epoxidations. *J. Am. Chem. Soc.*, 123:2933–2934, 2001.
- [102] I. Langmuir and V.J. Schaefer. Activities of urease and pepsin monolayers. *J. Am. Chem. Soc.*, 60:1351–1360, 1938.
- [103] D. E. Leckband, S.R. Sheth, and A. Halperin. Grafted poly(ethylene oxide) brushes as nonfouling surface coatings. *J. Biomat. Sci. Polymer Edn*, 10:1125–1147, 1999.

- [104] S. Li, C.J. Clarke, R.B. Lennox, and A. Eisenberg. Two-dimensional self assembly of polystyrene-*b*-poly(butyl-methacrylate) diblock copolymers. *Colloids Surfaces A*, 133:191–203, 1998.
- [105] J. Liu, O. Shirota, and M. Novotny. Sensitive, laser-assisted determination of complex oligosaccharide mixtures separated by capillary gel electrophoresis at high resolution. *Anal. Chem.*, 64:973–975, 1992.
- [106] K. Loos. *Hybridmaterialien mit Amylose durch enzymatische grafting from Polymerisation*. Universität Bayreuth, 2001.
- [107] K. Loos and A.H.E. Müller. New routes to the synthesis of amylose-block-polystyrene rod-coil block copolymers. *Biomacromolecules*, 3:368–373, 2002.
- [108] K. Loos and R. Stadler. Synthesis of amylose-block-polystyrene rod-coil block copolymers. *Macromolecules*, 30:7641–7643, 1997.
- [109] K. Loos, V. von Braunmühl, and R. Stadler. Saccharide modified silica particles by enzymatic grafting. *Macromol. Rapid Commun.*, 18:927–938, 1997.
- [110] M.C.M. van Loosdrecht, J. Lyklema, W. Norde, and A.J.B. Zehnder. Influence of interfaces on microbial activity. *Microbiol. Rev.*, 54:75–87, 1990.
- [111] M. Lu, G. Johansson, P.-Å. Albertsson, and F. Tjerneld. Partitioning of proteins in dextran/hydrophobically modified dextran aqueous two-phase systems. *Bioseparations*, 5:351–358, 1995.
- [112] J. Lyklema. *Fundamentals of interface and colloid science, Liquid–fluid interfaces*, volume III. Academic Press, London, UK, 2000.
- [113] J.H. Maas, M.A. Cohen Stuart, A.B. Sieval, H. Zuilhof, and E.J.R. Sudhölter. Preparation of polystyrene brushes by reaction of terminal vinyl groups on silicon and silica surfaces. *Thin Solid Films*, 426:135–139, 2003.
- [114] F. MacRitchie. *Chemistry at Interfaces*. Academic Press, San Diego, USA, 1990.
- [115] R.E. Marchant, S. Yuan, and G. Szakalas-Gratzl. Interaction of plasma proteins with a novel polysaccharide surfactant physisorbed to polyethylene. *J. Biomat. Sci. Polymer Edn*, 6:549–564, 1994.
- [116] B. Matuszewska, W. Norde, and J. Lyklema. Competitive adsorption of human plasma albumin and dextran on silver iodide. *J. Colloid Interface Sci.*, 84:403–408, 1981.
- [117] S.L. McArthur, K.M. McLean, P. Kingshott, H.A.W. St John, R.C. Chatelier, and H.J. Griesser. Effect of polysaccharide structure on protein adsorption. *Colloids Surfaces B*, 17:37–48, 2000.
- [118] T. McPherson, A. Kidane, I. Szleifer, and K. Park. Prevention of protein adsorption by tethered poly(ethylene oxide) layers: Experiments and single-chain mean-field analysis. *Langmuir*, 14:176–186, 1998.
- [119] S.T. Milner, T.A. Witten, and M.E. Cates. Theory of the grafted polymer brush. *Macromolecules*, 21:2610–2619, 1988.
- [120] J. Milton Harris. *Poly(Ethylene Glycol) Chemistry. Biotechnological and Biomedical Applications*. Plenum Press, New York, USA, 1992.
- [121] M. Morra. On the molecular basis of fouling resistance. *J. Biomat. Sci. Polymer Edn*, 11:547–569, 2000.

- [122] M.R. Nejadnik, A.F. Engelsman, I.C. Saldarriaga Fernández, H.J. Busscher, W. Norde, and H.C. van der Mei. Bacterial colonization of polymer brush-coated and pristine silicone rubber implanted in infected pockets in mice. *J. Antimicrobial Chemotherapy*, 62:1323–1325, 2008.
- [123] A. Nel, T. Xia, L. Mädler, and N. Li. Toxic potential of materials at the nanolevel. *Science*, 311:622–627, 2006.
- [124] W. Norde. *Proteins at Interfaces: the Adsorption of Human Plasma Albumin and Bovine Pancreas Ribonuclease on Polystyrene Latices*. Landbouwhogeschool Wageningen, 1976.
- [125] W. Norde. *Colloids and Interfaces in Life Sciences*. Marcel Dekker, New York, USA, 2003.
- [126] W. Norde and D. Gage. Interactions of bovine serum albumin and human blood plasma with peo-tethered surfaces: Influence of peo chain length, grafting density and temperature. *Langmuir*, 20:4162–4167, 2004.
- [127] E. Nordmeier. Static and dynamic light-scattering solution behavior of pullulan and dextran in comparison. *J. Phys. Chem.*, 97:5770–5785, 1993.
- [128] Y. Oiu and R.E. Marchant. Protein resistant biomaterial surfaces derived from physically immobilized novel oligosaccharide surfactant molecules. *Annu. Me. Soc. Biom.*, 23:224, 1997.
- [129] K.D. Park, Y.S. Kim, D.K. Han, Y.H. Kim, E.H.B. Lee, H. Suh, and K.S. Choi. Bacterial adhesion on peg modified polyurethane surfaces. *Biomaterials*, 19:851–859, 1998.
- [130] J.C. Paulson. Glycoproteins: what are the sugar chains for? *Trends Biochem. Sci.*, 14:272–276, 1989.
- [131] A. Paulus and A. Klockow. Detection of carbohydrates in capillary electrophoresis. *J. Chromatogr. A*, 720:353–376, 1996.
- [132] J. Piehler, A. Brecht, K.E. Geckeler, and G. Gauglitz. Surface modification for direct immunoprobes. *Biosensors Bioelectronics*, 11:579–590, 1996.
- [133] J. Piehler, A. Brecht, K. Hehl, and G. Gauglitz. Protein interactions in covalently attached dextran layers. *Colloids Surfaces B*, 13:325–336, 1999.
- [134] K.L. Prime and G.M. Whitesides. Self-assembled organic monolayers: Model systems for studying adsorption of proteins at surfaces. *Science*, 252:1164–1167, 1991.
- [135] R.P. Rand. Raising water to new heights. *Science*, 256:618, 1992.
- [136] B.D. Ratner and S.J. Bryant. Biomaterials: Where we have been and where we are going. *Annu. Rev. Biomed. Eng.*, 6:41–75, 2004.
- [137] M.A. Rixman. *Investigating the Molecular Origins of Biocompatibility: Intermolecular Interactions between Human Serum Albumin and Various Chemically Modified Surfaces via High Resolution Force Spectroscopy*. Massachusetts Institute of Technology, Boston, 2004.
- [138] M.A. Rixman, D. Dean, and C. Ortiz. Nanoscale intermolecular interactions between human serum albumin and low grafting density surfaces of poly(ethylene oxide). *Langmuir*, 19:9357–9372, 2003.
- [139] G. Roberts. *Langmuir-Blodgett Films*. Plenum Press, New York, USA, 1990.
- [140] A. Roosjen. *The Use of Polymer Brush Coatings to Prevent Microbial Adhesion*. Rijksuniversiteit Groningen, 2005.

- [141] A. Roosjen, H.J. Kaper, H.C. van der Mei, W. Norde, and H.J. Busscher. Inhibition of adhesion of yeasts and bacteria by poly(ethylene oxide)-brushes on glass in a parallel plate flow chamber. *Microbiology*, 149:3239–3246, 2003.
- [142] I.C. Saldarriaga Fernández, H.C. van der Mei, S. Metzger, D.W. Grainger, A.F. Engelsman, M.R. Nejadnik, and H.J. Busscher. In vitro and in vivo comparisons of staphylococcal biofilm formation on a cross-linked poly(ethylene glycol)-based polymer coating. *Acta Biomaterialia*, 6:1119–1124, 2010.
- [143] H. Schwaiger, P.J. Oefner, C. Huber, E. Grill, and G.K. Bonn. Capillary zone electrophoresis and micellar electrokinetic chromatography of 4-aminobenzonitrile carbohydrate derivatives. *Electrophoresis*, 15:941–952, 1994.
- [144] M.G. Semenova and L.B. Saviolova. The role of biopolymer structure in interactions between unlike biopolymers in aqueous medium. *Food Hydrocolloids*, 12:65–75, 1998.
- [145] S.R. Sheth and D. Leckband. Measurements of attractive forces between proteins and end-grafted poly(ethylene glycol) chains. *Proc. Natl. Acad. Sci. USA*, 94:8399–8404, 1997.
- [146] R.L. Sidebotham. Dextran. *Adv. Carboh. Chem. Biochem.*, 30:371–444, 1974.
- [147] E. Sisu, W.T.E Bosker, W. Norde, T.M. Slaghek, J.W. Timmermans, J. Peter-Katalinić, M.A. Cohen Stuart, and A.D. Zamfir. Electrospray ionization quadrupole time-of-flight tandem mass spectrometric analysis of hexamethylenediamine-modified maltodextrin and dextran. *Rapid Comm. Mass Spectrom.*, 20:209–218, 2006.
- [148] L.C.P.M. de Smet, A.V. Pukin, Q.-Y. Sun, B.J. Eves, G.P. Lopinski, G.M. Visser, H. Zuilhof, and E.J.R. Sudhölter. Visible-light attachment of sic linked functionalized organic monolayers on silicon surfaces. *Appl. Surface Sci.*, 252:24–30, 2005.
- [149] L.C.P.M. de Smet, G.A. Stork, G.H.F. Hurenkamp, Q.-Y. Sun, H. Topal, P.J.E. Vronen, A.B. Sieval, A. Wright, G.M. Visser, H. Zuilhof, and E.J.R. Sudhölter. Covalently attached saccharides on silicon surfaces. *J. Am. Chem. Soc.*, 125:13916–13917, 2003.
- [150] A.L.M Smits, S.H.D. Hulleman, J.J.G. Van Soest, H. Feil, and J.F.G. Vliegthart. The influence of polyols on the molecular organization in starch-based plastics. *Polymers Adv. Technol.*, 10:570–573, 1999.
- [151] A.L.M Smits, P.H. Kruiskamp, J.J.G. Van Soest, and J.F.G. Vliegthart. Interaction between dry starch and plasticisers glycerol and ethylene glycol, measured by differential scanning calorimetry and solid state nmr spectroscopy. *Carbohydrate Polymers*, 53:409–416, 2003.
- [152] A. De Sousa Delgado, M. Léonard, and E. Dellacherie. Surface properties of polystyrene nanoparticles coated with dextrans and dextran-peo copolymers. effect of polymer architecture on protein adsorption. *Langmuir*, 17:4386–4391, 2001.
- [153] R. Srinivasan, M. Chandrasekharam, P.V.S.N. Vani, A.S. Chida, and A.K. Singh. Epoxidation of olefins at low temperature using m-chloroperbenzoic acid. *Synth. Commun.*, 32:1853, 2002.
- [154] M. Stefansson and M. Novotny. Resolution of the branched forms of oligosaccharides by high-performance capillary electrophoresis. *Carbohydrate Research*, 258:1–9, 1994.
- [155] M. Sze Wang, L.B. Palmer, J.D. Schwartz, and A. Razatos. Evaluating protein attraction and adhesion to biomaterials with the atomic force microscope. *Langmuir*, 20:7753–7759, 2004.

- [156] I. Szleifer. Protein adsorption on surfaces with grafted polymers: A theoretical approach. *Biophys. J.*, 72:595–612, 1997.
- [157] P.W. Tang and J.M. Williams. An improved method for the liquid chromatography of the 1-deoxy-1-(2-pyridylamino)alditol derivatives of oligosaccharides and its application to structural studies of the carbohydrate moieties of glycoproteins. *Carbohydrate Research*, 136:259, 1985.
- [158] S. Tangestaninejad, M.H. Habibi, V. Mirkhani, and M. Moghadam. Manganese(iii) porphyrin supported on polystyrene as a heterogeneous alkene epoxidation and alkane hydroxylation catalyst. *Synth. Commun.*, 32:3331, 2002.
- [159] K.H. Tong, K.Y. Wong, and T.H. Chan. Manganese/bicarbonate-catalyzed epoxidation of lipophilic alkenes with hydrogen peroxide in ionic liquids. *Org. Lett.*, 5:3423–3425, 2003.
- [160] H.J. Trurnit. A theory and method for the spreading of protein monolayers. *J. Colloid Sci.*, 15:1–13, 1960.
- [161] J. van der Vlist. *Polymerization of Hyperbranched Polysaccharides by Combined Biocatalysis*. Rijksuniversiteit Groningen, 2011.
- [162] I.K. Voets, W.M. de Vos, B. Hofs, A. de Keizer, M.A. Cohen Stuart, R. Steitz, and D. Lott. Internal structure of a thin film of mixed polymeric micelles on a solid/liquid interface. *J. Phys. Chem. B*, 112:6937–6945, 2008.
- [163] W.M. de Vos. *Brushes and Particles*. Wageningen Universiteit, 2009.
- [164] W.M. de Vos, A. de Keizer, J.M. Kleijn, and M.A. Cohen Stuart. The production of peo polymer brushes via langmuir-blodgett and langmuir-schaeffer methods: Incomplete transfer and its consequences. *Langmuir*, 25:4490–4497, 2009.
- [165] W.M. de Vos, J.M. Kleijn, A. de Keizer, and M.A. Cohen Stuart. Ultradense polymer brushes by adsorption. *Angew. Chem. Int. Ed.*, 48:5369–5371, 2009.
- [166] J. Walter, W. Steigemann, T.P. Singh, H. Bartunik, W. Bode, and R. Huber. On the disordered activation domain in trypsinogen. chemical labelling and low-temperature crystallography. *Acta Crystallogr. B*, 38:1462–1472, 1982.
- [167] R.L.C. Wang, H.J. Kreuzer, and M. Grunze. Molecular conformation and solvation of oligo(ethylene glycol)-terminated self-assembled monolayers and their resistance to protein adsorption. *J. Phys. Chem. B*, 101:9767–9773, 1997.
- [168] R.L.C. Wang, H.J. Kreuzer, and M. Grunze. The interaction of oligo(ethylene oxide) with water: a quantum mechanical study. *Phys. Chem. Chem. Phys.*, 2:3613–3622, 2000.
- [169] S. Wang, J.A.P.P. van Dijk, T. Odijk, and J.A.M. Smit. Depletion-induced demixing in aqueous protein-polysaccharide solutions. *Biomacromolecules*, 2:1080–1088, 2001.
- [170] M. Wengert, A.M. Sanseverino, and M.C.S. de Mattos. Trichloroisocyanuric acid: An alternate green route for the transformation of alkenes into epoxides. *J. Braz. Chem. Soc.*, 13:700–703, 2002.
- [171] H.Q. Xie and D. Xie. Molecular design, synthesis and properties of block and graft copolymers containing polyoxyethylene segments. *Prog. Polymer Sci.*, 24:275–313, 1999.
- [172] D. Yang, Y.C. Yip, G.S. Jioao, and M.K. Wong. *Organic Syntheses*. Wiley, 2002.
- [173] X. Yao, H. Chen, W. Lü, G. Pan, X. Hu, and Z. Zheng. Enantioselective epoxidation of olefins catalyzed by two novel chiral poly-salenmn(iii) complexes. *Tetrahedron Lett.*, 41:10267–10271, 2000.

- [174] E.B. Zhulina, O.V. Borisov, and V.A. Pryamitsyn. Theory of steric stabilization of colloid dispersions by grafted polymers. *J. Colloid Interface Sci.*, 137:495–511, 1990.
- [175] G. Ziegast and B. Pfannemüller. Phosphorolytic synthesis with di-, oligo- and multi-functional primers. *Carbohydrate Research*, 160:185–204, 1987.

Summary

Protein adsorption is the first step in the formation of a biofilm. Biofilms can cause serious problems, in technical equipment, but especially in medicine, where they induce infections at biomaterials used for implants. The best cure is prevention. This thesis presents research on the prevention of protein adsorption by polymer brushes. In a polymer brush, polymers are end-grafted to a surface and stretch out into the solution, thereby forming a barrier for the proteins to reach the surface. Most research concerns the use of synthetic polymers to prepare brushes from, particularly poly(ethylene oxide) (PEO). This thesis emphasizes the manufacturing of natural, polysaccharide brushes and their antifouling capacity, as well. In nature, oligosaccharides are found at the exterior of living cells, having the function to explicitly bind necessary proteins and cells, while preventing non-specific adsorption. Moreover, polysaccharides are natural polymers and may therefore be more appropriate for use in biomedical applications.

The first part, chapter 2, discusses protein adsorption at PEO brushes, highlighting the ternary adsorption of Bovine Serum Albumin (BSA) at relatively dilute brushes of long PEO chains. Preparation of bimodal PEO brushes, consisting of a dense layer of short PEO chains ($N=48$) and a variable grafting density of long PEO chains ($N=770$), by Langmuir-Blodgett (LB) deposition is described, using polystyrene(PS)-PEO diblock copolymers. With these bimodal brushes primary adsorption of BSA at low grafting densities (σ) of PEO(770) is suppressed. Results of BSA adsorption show that the observed maximum of the bimodal brush is similar to the observed maximum for the PEO(770) brush, indeed confirming ternary adsorption.

Moreover, the interfacial behaviour of compressed monolayers of PS-PEO(48) and the bimodal PS-PEO layers at the air-water interface showed $\Pi - \sigma^{-1}$ -hysteresis (Π is the interfacial pressure). This hysteresis is explained in more detail in the General Discussion. It originates from 2D aggregation of the PS-PEO(48) layer upon compression, due to hydrophobic attraction of the PS parts. It is followed by relaxation of the aggregated layer at high interfacial pressure by

budding off parts of the monolayer into the water sublayer. The hysteresis (and hence, the aggregation and relaxation) turned out to be dependent on the size of the PS block relative to the PEO block. When they are of comparable size the hysteresis is maximal. With increasing PEO size it eventually vanishes (at PEO(445)) and the PS-PEO monolayer is stable upon compression.

The second part, constituted of chapters 3 to 5, presents the results on polysaccharide brushes, in particular dextran brushes. In chapters 3 and 4 the synthesis and interfacial behaviour of PS-polysaccharide diblock copolymers is discussed, in the context of preparing brushes using the LB method. The LB method is chosen in order to control the grafting density. A coupling method of prefabricated blocks is employed to control the size of the copolymer, *i.e.*, the chain length in the brush. In chapter 3 reductive amination is applied to directly couple amino-terminated PS to dextrans and maltodextrins. In chapter 4 a different block coupling route was employed, using 1,6-diaminohexane (DAH) as a spacer between epoxide-terminated PS and dextran, aiming at synthesizing block copolymers with a long dextran block. However, this procedure appeared to be unsuccessful. Results of the syntheses described in chapters 3 and 4 show that, using a block coupling method, PS-b-Dextrans can be prepared with a maximum dextran M_w of 6000 Da. A plausible reason is an insufficient inter penetration of the PS and dextran coils, through which the reactive ends of the polymers cannot meet.

The synthesized PS-polysaccharide copolymers show air-water interfacial behaviour typical for amphiphilic diblock copolymers. The $\Pi - \sigma^{-1}$ isotherms can be explained by the changes in conformation of the block copolymers at the air-water surface. When a monolayer of the block copolymer is compressed, the polysaccharide chains are forced to desorb into the water phase, forming loops and tails. Upon further compression, a quasi-plateau regime is observed in the $\Pi - \sigma^{-1}$ isotherm. In this region the polysaccharide chains completely desorb into the water sub phase and the interfacial pressure corresponds to that of an air-water surface of a saturated polysaccharide solution. When all the polysaccharide chains are desorbed, the onset of a brush at the interface is reached. Continuing compression of the monolayer results in a sharp increase of Π , reflecting the repulsion between polysaccharide chains in the brush.

Successive compression and expansion $\Pi - \sigma^{-1}$ isotherms of PS(12300) - b - Dextran(6000) and PS(2100) - b - Dextran(6000) in chapters 3 and 4, respectively, show time-dependent hysteresis, unusual for amphiphilic block copolymers. There are two driving forces for this displayed hysteresis. The first, occurring at

intermediate area per molecule, is PS aggregation due to hydrophobic attraction of the PS blocks. This is similar to the observed aggregation of PS-PEO copolymers. Again, the aggregation is stronger the bigger the PS block is. The second contribution to the hysteresis is hydrogen bonding between the dextran chains in the brush regime.

In chapter 5 protein adsorption experiments are presented at dextran(6000) brushes of various σ , using BSA and trypsin as model proteins. BSA is negatively and trypsin is positively charged at the pH applied. The adsorption as function of the grafting density proved to be discontinuous. No adsorption suppression at low σ , inhibition up to 90% at high σ , comparable to protein adsorption suppression by PEO brushes of similar M_w . This discontinuity is caused by the aggregation of the PS-b-Dextran at low and intermediate grafting density, generating inhomogeneities (patches without dextran) at the wafers prepared with LB. These inhomogeneities at the surface are confirmed with AFM. At high σ a smooth surface is detected with AFM, indicating a homogeneous dextran brush. The adsorption of BSA and trypsin at different grafting densities are similar, which is evidence of a minor electrostatic contribution, if any, to the adsorption. The adsorption results show that dense dextran brushes have a good protein repellency and might therefore be used in antifouling applications. Because dextran is a natural polymer, it may be preferable for use in biomedical practice.

The final part, the General Discussion (chapter 6) reflects on the LB deposition technique to prepare polymer brushes and the existence of 2D aggregation of the block copolymers used. Furthermore, some general comments on the interaction of proteins with polymer brushes, stemming from theoretical and experimental observations, will be given, with special interest on the nature of the polymer used.

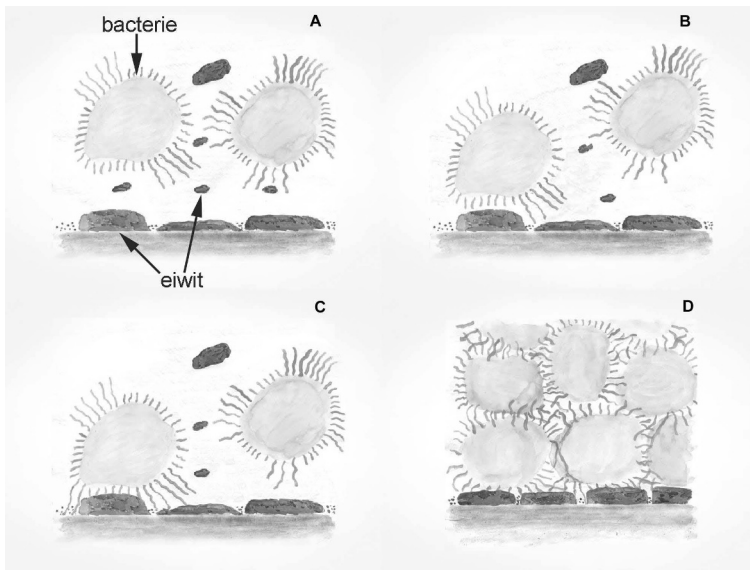
Samenvatting

Mijn proefschrift is getiteld 'Brushes and Proteins', oftewel 'Borstels en Eiwitten'. Het gaat over het voorkomen van eiwit hechting aan oppervlakken door het aanbrengen van een borstel aan dat oppervlak. In deze samenvatting zal ik proberen wat meer duidelijkheid te geven over mijn onderzoek van de afgelopen jaren, aan de hand van de titel.

Eiwitten

Eiwitten zijn alomtegenwoordig in alles wat leeft; in planten en bomen, in dieren en in mensen. Er zijn ontelbaar veel verschillende eiwitten, met ieder hun eigen functie. Ze zijn zeer belangrijk voor het leven op aarde. Ieder van u heeft wel eens van eiwitten gehoord, want ze vormen een belangrijk bestanddeel van ons voedsel. De eiwitten die u eet bevatten de bouwstenen waaruit weer de essentiële eiwitten worden gemaakt nodig voor uw lichaam. Eiwitten hebben vele bijzondere eigenschappen. Ik zal het hier beperken tot slechts één eigenschap die van belang is voor mijn onderzoek: eiwitten hebben de neiging zich te hechten aan oppervlakken, zowel vaste oppervlakken alsmede het lucht-water grensvlak. In de wetenschap wordt dat aangeduid met de term 'adsorptie'.

Deze hechting kan zeer vervelende gevolgen hebben. Ik zal een voorbeeld geven: mensen met een implantaat, bijvoorbeeld een kunstheup of kunststof hartklep, kunnen last krijgen van trombose, doordat eiwitten uit het bloed hechten aan het lichaams-vreemde materiaal. Er is nog een veel groter probleem. De hechting van eiwitten aan oppervlakken is namelijk de eerste stap in het proces dat 'biovervuiling' heet. Biovervuiling is de 'ongewenste hechting van eiwitten en bacteriën aan een oppervlak'. In figuur 1 zijn de vier stappen van biovervuiling weer-gegeven. In figuur 1A is te zien hoe eiwitten zich hechten aan het vaste oppervlak. Vervolgens maken bacteriën contact met deze eiwitlaag (figuur 1B) en gaan ze zich stevig hechten aan het oppervlak d.m.v. 'draden' (figuur 1C). Als de bacteriën zich eenmaal stevig hebben gehecht, gaan ze zich razendsnel vermenigvuldigen (figuur 1D). Dit proces kan uiteindelijk leiden tot infectie. Het vervelende van een infectie bij



FIGUUR 1. Het proces van biovervuiling: hechting van eiwitten (A), contact tussen bacterie en eiwitlaag (B), bacterie hechting aan het oppervlak (C) en groei van bacteriën (D). Met dank aan Willem Norde voor de plaatjes.

een implantaat is, dat het niet te behandelen is met antibiotica (het is onmogelijk alle bacteriën die zich aan het oppervlak hebben gehecht te verwijderen). Het is ook onmogelijk om te voorkomen dat er bacteriën op het implantaat komen tijdens het inbrengen in het ziekenhuis. Dit betekent dat mensen met een implantaat vaak opnieuw geopereerd moeten worden. In ernstige gevallen is amputatie nodig, soms kan de infectie zelfs leiden tot de dood. Ook meer alledaagse problemen worden veroorzaakt door biovervuiling. Denk bijvoorbeeld aan vervuiling van contactlenzen, maar ook tandbederf.

De enige manier om infectie te voorkomen, is het aanpassen van het oppervlak van het implantaat, zodat eiwitten niet meer kunnen hechten. Daar wordt veel onderzoek naar gedaan. Eén van de mogelijkheden is op zoek te gaan naar andere materialen om het implantaat van te maken. Een andere oplossing is, de implantaten te voorzien van een beschermende laag tegen eiwitten en bacteriën. Dat is wat ik heb onderzocht. Daarover straks meer.

Omdat hechting van eiwitten de eerste stap is in het proces van biovervuiling, is het logisch te kijken naar het voorkomen van die eerste stap en daarmee het hele



FIGUUR 2. Model van het eiwit BSA.

proces van biovervuiling te stoppen. Als eiwitten hechten aan een oppervlak, zoals weergegeven in figuur 1A, dan plakken ze met heel veel 'stukjes' aan het oppervlak. Bovendien past het eiwit zijn vorm vaak aan, zodat het optimaal kan hechten (het smeert vaak uit als een dikke pannenkoek). Het is dan ook heel moeilijk om een eiwit te verwijderen, als het eenmaal vast zit. Dus nogmaals: het is beter om de eiwit hechting te voorkomen. Bijvoorbeeld door het aanbrengen van een borstel aan het oppervlak, zoals ik heb onderzocht.

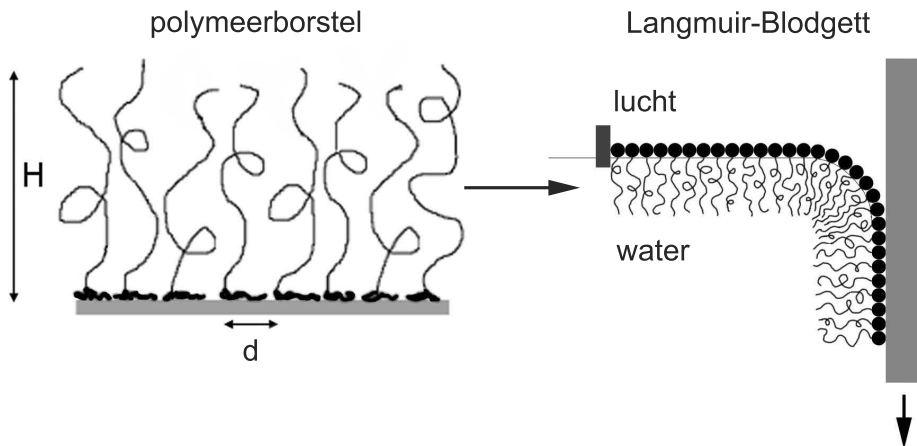
In mijn onderzoek heb ik voornamelijk gebruik gemaakt van het eiwit BSA (Bovine Serum Albumine). Het is een van de belangrijkste eiwitten in bloed. Het heeft een hartvormige structuur, zoals te zien is in figuur 2. Oplossingen met BSA vormden het modelsysteem dat ik gebruikte om de borstels te testen. Wat ik nog niet heb vermeld, is de zeer kleine afmeting van eiwitten, enkele nanometers groot (een nanometer is een miljardste van een meter). De eiwitten zijn dus niet met het blote oog te zien en ook niet met een microscoop. Ik heb speciale meetapparatuur gebruikt om de eiwit hechting te meten, gebaseerd op de eigenschappen van laserlicht. Ik zal daar verder niet op ingaan.

Borstels

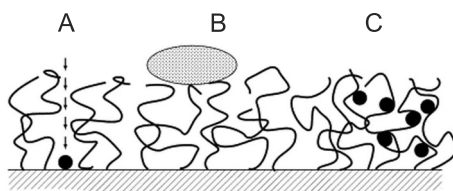
De borstels die ik heb gebruikt zijn zogenaamde 'polymeerborstels'. Allereerst, wat is een polymeer? 'Polymeer' is Grieks en betekent 'veel deeltjes'. Een polymeer is een lange keten bestaande uit veel deeltjes, als kralen aaneengeregen aan een ketting. Voorbeelden van polymeren zijn: alle plastics, maar ook veel natuurlijke stoffen zoals koolhydraten en eiwitten zijn polymeren. Net als DNA.

Als je zulke ketens dicht op elkaar vast maakt aan een oppervlak met een van de uiteinden, dan krijg je een polymeerborstel. Hoe dit werkt, kun je zien in figuur 3. De ketens zijn vastgemaakt op een afstand d van elkaar, de ketens strekken zich uit tot een hoogte H . Deze afstand d en hoogte H zijn bepalend voor de eigenschappen van de borstel. Om een borstel te kunnen vormen, moeten de ketens in een goed oplosmiddel zitten. In mijn onderzoek is dat water, aangezien ik metingen gedaan heb met eiwitten. Eiwitten lossen goed op in water. Daarom heb ik polymeren gebruikt die ook goed oplosbaar zijn in water. Een andere eigenschap van de polymeerborstels die ik heb gebruikt is hun flexibiliteit, waardoor ze zich aan kunnen passen aan hun omgeving.

Omdat de afstand d erg belangrijk is, heb ik gekozen voor een techniek waarmee deze afstand erg nauwkeurig te controleren is. Deze techniek heet 'Langmuir-Blodgett' (vernoemd naar de twee uitvinders ervan) en is ook schematisch weergegeven in figuur 3. Bij deze techniek wordt gebruik gemaakt van polymeren met een ankerblok, dat de ketens vastmaakt aan het vaste oppervlak (de zwarte bolletjes in figuur 3). De polymeren met ankerblok worden eerst aangebracht aan het lucht-water grensvlak. Vervolgens worden ze samengeperst. Hierbij ontstaat een polymeerborstel aan dat lucht-water grensvlak met de gewenste afstand d (zie figuur 3, borstel is op kop). Vervolgens wordt deze borstel overgebracht naar een vast oppervlak (verticaal weergegeven in figuur 3).



FIGUUR 3. Tekening van een polymeerborstel (links) en de gebruikte methode van borstels maken: de Langmuir-Blodgett techniek (rechts). Voor uitleg, zie tekst.



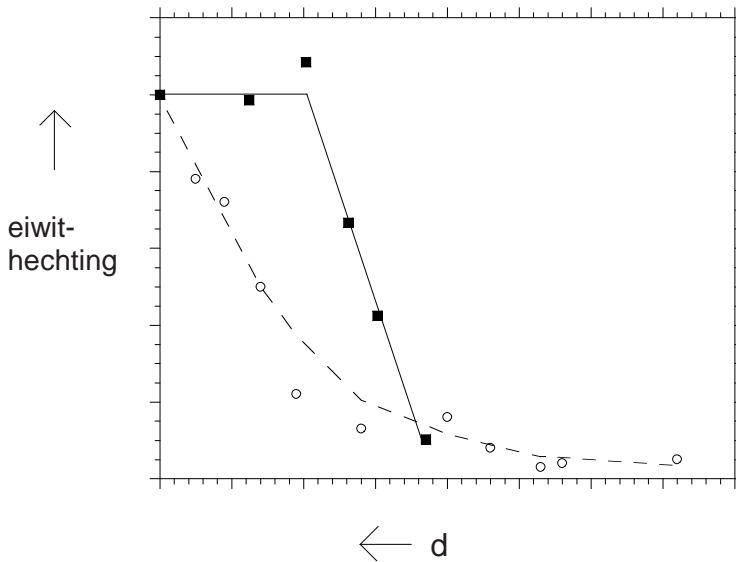
FIGUUR 4. Drie manieren van eiwit hechting aan een oppervlak met een borstel.

Uit mijn onderzoek blijkt dat hierbij soms complicaties optreden, wat het borstel maken bemoeilijkt. De ketens kunnen aan elkaar gaan klitten, doordat de ankerblokken vastplakken aan elkaar aan het lucht–water grensvlak. Ik zal hier niet verder op ingaan, maar het is een belangrijke conclusie van mijn onderzoek, verwoord in Stelling 2.

Borstels en Eiwitten

Nu zijn we aanbeland bij het eigenlijke doel van mijn onderzoek: nagaan hoe hechting van eiwitten aan een oppervlak kan worden voorkomen, door het aanbrengen van een (polymeer)borstel. Het komt er in wezen op neer, dat er een barrière wordt gevormd tegen de eiwitten, die daardoor het oppervlak niet meer kunnen bereiken. Het belangrijkste daarbij is de afstand tussen de ketens van de borstel. Dit bepaald voornamelijk óf en hoeveel eiwit hecht aan het oppervlak. Er worden drie manieren onderscheiden waarop eiwitten kunnen hechten aan een oppervlak met een borstel. Dit is weergegeven in figuur 4. Als de eiwitten klein zijn t.o.v. de afstand tussen de ketens, dan kunnen ze doordringen in de borstel en uiteindelijk hechten aan het oppervlak (zie **A** in figuur 4). Wanneer de eiwitten groot zijn t.o.v. de afstand tussen de ketens (**B**), kunnen de eiwitten niet doordringen en blijven ze aan de buitenkant van de borstel. In het derde geval (**C**) zijn de eiwitten ook klein en kunnen ze doordringen, maar hechten ze in de borstel aan de borstelharen. Dit is nog niet zo lang bekend, maar er is wel steeds meer bewijs dat dit gebeurt. Ik heb dit nader onderzocht in hoofdstuk 2.

Er is veel onderzoek gedaan naar het voorkomen van eiwit hechting m.b.v. borstels van synthetische polymeren (met name PEO). In het verleden bleken deze synthetische borstels vaak efficiënt te zijn. Er is echter steeds meer bewijs dat ze toch niet zo efficiënt zijn. Eiwitten blijken te hechten aan de borstelharen, zoals weergegeven in situatie **C** in figuur 4. Dit leidde tot de twee kernvragen in mijn onderzoek: 1. Is het mogelijk borstels te maken van natuurlijke polymeren,



FIGUUR 5. eiwit hechting aan dextraanborstels (—■—) en PEO-borstels (-○-). Voor uitleg, zie tekst.

namelijk polysachariden (lange koolhydraten)? 2. Kunnen deze natuurlijke borstels eiwit hechting tegengaan? Het antwoord op beide vragen is ja. De tweede, en belangrijkste, conclusie is gebaseerd op figuur 5 (deze komt overeen met figuur 5.7 in hoofdstuk 5). In deze figuur zie je de eiwit hechting weergegeven aan zowel dextraanborstels (de natuurlijke borstel, weergegeven met ■) als aan PEO-borstels (synthetische borstel, weergegeven met ○). Ik zal de details van de figuur buiten beschouwing laten. Het belangrijkste wat uit de figuur kan worden geconcludeerd, is het halverwege kruisen van de lijnen van de dextraanborstel en de PEO-borstel. Oftewel, de dextraanborstel en de PEO-borstel zijn net zo effectief bij deze afstand **d** (zie pijl in figuur 5). Deze belangrijke conclusie heb ik verwoord in Stelling 1. In dit kruispunt wordt ongeveer 90% van de eiwitten tegengehouden. Het is mogelijk nog dichtere dextraanborstels te maken. Bovendien blijkt uit onderzoek door anderen, dat eiwitten niet hechten aan de dextraanketens. Vandaar dat ik verwacht dat dextraanborstels, of andere natuurlijke borstels, uiteindelijk effectiever blijken te zijn dan synthetische borstels. Dat moet verder onderzoek uitwijzen.

List of Publications

- W.T.E Bosker, K. Ágoston, M.A. Cohen Stuart, W. Norde, J.W. Timmermans and T.M. Slaghek, Synthesis and Interfacial Behavior of Polystyrene-Polysaccharide Diblock Copolymers, *Macromolecules*, 36 (2003), 1982–1987. (Chapter 3)
- J.P. Pinheiro and W.T.E Bosker, Polystyrene Film-coated Glassware: a New Means of Reducing Metal Losses in Trace Metal Speciation, *Anal. Bioanal. Chem.*, 380 (2004), 964–968.
- W.T.E Bosker, P.A. Iakovlev, W. Norde and M.A. Cohen Stuart, BSA Adsorption on Bimodal PEO Brushes, *J. Colloid Interface Sci.*, 286 (2005), 496–503. (Chapter 2)
- E. Sisu, W.T.E Bosker, W. Norde, T.M. Slaghek, J.W. Timmermans, J. Peter-Katalinić, M.A. Cohen Stuart and A.D. Zamfir, Electrospray Ionization Quadrupole Time-of-flight Tandem Mass Spectrometric Analysis of Hexamethylenediamine-modified Maltodextrin and Dextran, *Rapid Comm. Mass Spectrom.*, 20 (2006), 209–218.
- S. Koutsopoulos, K. Patzsch, W.T.E Bosker and W. Norde, Adsorption of Trypsin on Hydrophilic and Hydrophobic Surfaces, *Langmuir*, 23 (2007), 2000–2006.
- W.T.E Bosker, K. Patzsch, M.A. Cohen Stuart and W. Norde, Sweet Brushes and Dirty Proteins, *Soft Matter*, 3 (2007), 754–762. (Chapter 5)
- W.T.E Bosker, W. Norde and M.A. Cohen Stuart, (Quasi-) 2D Aggregation of Polystyrene-b-Dextran at the Air–Water Interface, *in preparation*. (Chapter 4)

Levensloop

Ik ben geboren op 13 juli 1969 te Groenlo, in de Achterhoek. Ik ging naar de Canisius lagere school, gevolgd door de R.K. Scholengemeenschap Marianum (VWO), beiden te Groenlo. Aangezien Scheikunde een van mijn favoriete vakken was op het VWO, ging ik Chemische Technologie studeren aan de Universiteit Twente te Enschede. Mijn afstudeer onderzoek deed ik bij de vakgroep Membraantechnologie. Ik verhuisde naar Utrecht voor mijn eerste baan, als consultant bij Polysep Industrial Consultants. Daarna heb ik diverse dingen gedaan, o.a. als vrijwilliger voor Milieudefensie en als barcoördinator bij Theater Kikker te Utrecht. Onderzoeken kreeg weer mijn interesse en ik ging werken bij ATO-DLO te Wageningen (tegenwoordig Food & Biobased Research, onderdeel van de kenniseenheid AFSG van WUR). Mijn volgende baan was bij Koninklijke De Ruijter te Maarsse, als kwaliteitsmedewerker. Mijn interesse in onderzoek bleef en ik besloot promotieonderzoek te gaan doen. Na een korte zoektocht, vond ik een leuk onderzoeksproject bij het Laboratorium voor Fysische chemie en Kolloïdkunde (Fysko) aan de Universiteit Wageningen. Dit proefschrift is de weergave van het onderzoek dat ik daar heb uitgevoerd.

Overview of Training Activities

Courses

- Physical Chemistry of Macromolecules, Wageningen, 2001
- Physical Chemistry Winterschool, Han-sur-Lesse, 2002
- Physical Chemistry Winterschool, Han-sur-Lesse, 2003
- RPK-course Polymer Physics, Utrecht, 2003
- Molecular Modeling, Wageningen, 2003
- Kolloïdkunde, Wageningen, 2003
- Bio-Nanotechnology, Wageningen, 2005

Conferences

- Vloeistoffen en Grensvlakken, Lunteren, 2001
- Macromoleculen, Lunteren, 2002
- Vloeistoffen en Grensvlakken, Lunteren, 2002
- Polymers at Interfaces, Rhodia conference, Bristol, 2002
- Autumn meeting on Macroscopic Physical Chemistry, Schiermonnikoog, 2002
- Vloeistoffen en Grensvlakken, Lunteren, 2003
- European Student Colloid Conference, Bristol, 2003
- Autumn meeting on Macroscopic Physical Chemistry, Schiermonnikoog, 2003
- Scientific Meeting DSM, Geleen, 2003
- Macromoleculen, Lunteren, 2004
- Vloeistoffen en Grensvlakken, Lunteren, 2004
- ECIS, Almeria, 2004
- Autumn meeting on Macroscopic Physical Chemistry, Schiermonnikoog, 2004
- Macromoleculen, Lunteren, 2005
- Molecular Order and Mobility in Polymer Systems, St. Petersburg, 2005

Other Activities

- Weekly discussion group Fysko, 2001–2005
- Colloquia, 2001–2011
- Visit BASF, Ludwigshafen, 2006

The research described in this thesis was financially supported by NWO, Project 'Brush Surfaces', NWO CW project 700.99.304.

Printing: GVO drukkers & vormgevers B.V. — Ponsen & Looijen, Ede